Title	Development of Liquid Scintillation α/SF Detection System for Aqueous Chemical Studies of Element 106, Seaborgium
Author(s)	Komori, Yukiko
Citation	大阪大学, 2013, 博士論文
Version Type	VoR
URL	https://doi.org/10.18910/26248
rights	
Note	

Development of Liquid Scintillation α/SF Detection System for Aqueous Chemical Studies of Element 106, Seaborgium

By Yukiko Komori

Thesis submitted to Graduate School of Science,

Osaka University

2013

Summary

An on-line liquid scintillation detection system to detect α particles and spontaneous fission (SF) fragments in solution samples has been developed for aqueous chemical studies of transactinide elements, especially for element 106, seaborgium (Sg). A liquid scintillation detection chamber which consists of a photomultiplier tube, a cell, and a reflector was newly fabricated and the detection performance of α particles and SF fragments was investigated. The developed system allows to detect α particles and SF fragments in aqueous solution samples with a detection efficiency of almost 100%. The aqueous solution sample can be subjected to α/SF spectrometry in a few seconds after the end of the chemical separation. Finally, the developed system was applied to the on-line liquid scintillation measurement of short-lived α-emitting nuclide, ^{213}Fr ($T_{1/2} =$ 34.6 s) as a granddaughter nuclide produced in the ^{209}Bi(^{16}O, $4n$)^{221}Pa reaction as a practical application. In the on-line measurement of the isotope ^{213}Fr, procedures of the collection, dissolution into the aqueous solution, mixing with the liquid scintillator and liquid scintillation detection were automatically repeated with good stability. Start of the measurement of the reaction products was approximately 15 s after the end of collection, which is applicable time scale for the detection of 14-s ^{265}Sg^{b}.

To detect the α and SF events originating from the transactinide elements by liquid scintillation, low background condition is necessary due to some problems in liquid scintillation spectrometry such as relatively poor energy resolution and high sensitivity to β particles and γ rays as well as α particles. We are planning to remove radioactive by-products using GARIS gas-jet system to attain the low background condition in liquid scintillation measurement. We attempted on-line liquid scintillation measurement

of preseparated ^{262}Db with the GARIS gas-jet system to evaluate the background count rate for the detection of ^{262}Db and the daughter nuclide ^{258}Lr ($T_{1/2} = 3.8$ s). To evaluate background count rate derived from the fast neutrons and γ rays generated by beam irradiation, blank samples were measured under the beam on and off conditions. The detection chambers were shielded with polyethylene blocks against fast neutrons which are observable as recoil protons in α-event region. It was found that background count rates increased by approximately ten times under the beam on condition compared with those of under beam off condition, which is attributed to the fast neutrons and γ rays. Further reduction of background count rates in α- and SF-event regions is necessary.

In parallel to the development of the liquid scintillation detection system, experimental conditions applicable to Sg were investigated using the lighter homologues, Mo and W. Extraction behavior of carrier-free radiotracers Mo and W onto Aliquat 336-loaded resin from HF and HCl solutions was investigated by a batch method. It was found that extraction reaction kinetics in both HF and HCl solutions is fast enough to reach the equilibrium state within approximately 10 s under the studied conditions. The distribution coefficients (K_d) of Mo and W were obtained as functions of HF and HCl concentrations. On-line extraction chromatography of Mo and W in 2–8 M HCl solutions was also performed with a liquid chromatography apparatus, ARCA. It was found that the order of extractability was Mo > W in 2–8 M HCl solutions, which is consistent with the of order of the K_d values obtained in the batch experiment in HCl system.

Table of Contents

7

Chapter 1
General Introduction

1-1.   Chemical Studies of Transactinide Elements

Elements with atomic numbers $Z \geq 104$ are called transactinide elements. These elements are placed beyond actinides in the 7th row of the periodic table as shown in Fig. 1-1. These elements are synthesized only by the nuclear fusion reaction. These heavy elements are all radioactive and decay mainly by α-particle emission or spontaneous fission (SF). Since the discovery of the first transactinide element, rutherfordium (Rf, Z = 104), in 1960's [1], much heavier elements up to element 118 have been produced [2, 3]. Chemical characterization of these newly synthesized elements is an important and challenging subject in modern nuclear and radiochemistry. In addition, it is expected that these heavy elements have chemical properties which cannot be simply deduced from the periodicity of the lighter homologues due to the large relativistic effects on the valence electron configurations [2]. According to electronic structure calculations, relativistic effects increase with Z^2 and it leads to a large spin-orbit splitting of electron orbitals and a strong energetic stabilization of spherical s and $p_{1/2}$ orbitals, which is equivalent to spatial contraction of the s and $p_{1/2}$ orbitals. In contrast, $p_{3/2}$, d, and f orbitals are energetically destabilized and spatially expanded.

The transactinide elements are produced in heavy-ion-induced nuclear reactions using the accelerator. Because of extremely low production rates and short half-lives of these elements, chemical experiments of these elements must be performed rapidly and efficiently on a single atom scale. Partition experiments in a two-phase system are usually employed to investigate the chemical properties of the transactinide elements. In "one-atom-at-a-time" situation, if fast equilibrium in chemical reactions is achieved, finding probabilities of a single atom in one phase or in the other one are considered to

provide distribution probabilities of macro amounts of atoms between the two phases [4, 5]. Prior to experiments with the transactinide elements, the experimental systems and conditions are selected with the lighter homologues at the tracer scale. The results with the lighter homologues are compared those with the transactinide elements to discuss similarity or deviation from the periodicity of the chemical properties among the transactinide elements and the lighter homologues.

The chemical studies of the transactinide elements have been performed in some accelerator facilities in the world such as the Lawrence Berkeley National Research Institute (LBNL) and the Lawrence Livermore National Laboratory (LLNL) in the United States, the Flerov Laboratory of Nuclear Reactions (FLNR) in Russia, the Gesellschaft für Schwerionenforschung (GSI) in Germany, the Paul Scherrer Institute (PSI) in Switzerland, and Japan Atomic Energy Agency (JAEA) in Japan under worldwide collaboration. The chemical experiments are mainly divided into ones in liquid phase and ones in gas phase. In the liquid-phase studies, experiments were carried on the first three transactinide elements, element 104 (Rf), 105 (dubnium, Db), and 106 (seaborgium, Sg). In the gas-phase studies, experiments were carried out on element 104 (Rf) to 108 (hassium, Hs), 112 (copernicium, Cn), and 114 (flerovium, Fl). Various experimental techniques and apparatuses have been developed for realization of such chemical studies of the transactinie elements, which is described in the following section.
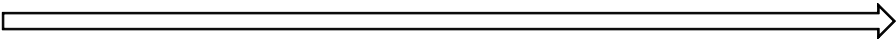
	1	2	3	4	5	6	7	8	9	10	11	12	13	14	15	16	17	18
1	1 H																	2 He
2	3 Li	4 Be											5 B	6 C	7 N	8 O	9 F	10 Ne
3	11 Na	12 Mg											13 Al	14 Si	15 P	16 S	17 Cl	18 Ar
4	19 K	20 Ca	21 Sc	22 Ti	23 V	24 Cr	25 Mn	26 Fe	27 Co	28 Ni	29 Cu	30 Zn	31 Ga	32 Ge	33 As	34 Se	35 Br	36 Kr
5	37 Rb	38 Sr	39 Y	40 Zr	41 Nb	42 Mo	43 Tc	44 Ru	45 Rh	46 Pd	47 Ag	48 Cd	49 In	50 Sn	51 Sb	52 Te	53 I	54 Xe
6	55 Cs	56 Ba	*	72 Hf	73 Ta	74 W	75 Re	76 Os	77 Ir	78 Pt	79 Au	80 Hg	81 Tl	82 Pb	83 Bi	84 Po	85 At	86 Rn

*Lanthanide	57 La	58 Ce	59 Pr	60 Nd	61 Pm	62 Sm	63 Eu	64 Gd	65 Tb	66 Dy	67 Ho	68 Er	69 Tm	70 Yb	71 Lu

**Actinide	89 Ac	90 Th	91 Pa	92 U	93 Np	94 Pu	95 Am	96 Cm	97 Bk	98 Cf	99 Es	100 Fm	101 Md	102 No	103 Lr

7	87 Fr	88 Ra	**	104 Rf	105 Db	106 Sg	107 Bh	108 Hs	109 Mt	110 Ds	111 Rg	112 Cn	113	114 Fl	115	116 Lv	117	118

Transactinide elements

Fig. 1-1. Current periodic table of the elements.

1-2. Experimental Techniques and Instruments

Experimental procedures for chemical studies of the transactinide elements are generally categorized into the following steps:

1) Production of the transactinide elements.

2) Rapid transport of the produced nuclide to the chemistry apparatus.

3) Formation of a chemical species or a compound.

4) Fast chemical separation and characterization.

5) Preparation of a sample for α and SF spectrometry.

6) Detection and identification of the nuclide through its characteristic nuclear decay properties.

In the liquid-phase (aqueous) chemistry, the transactinide elements produced in the nuclear reaction are transported to the chemistry apparatus by a gas-jet technique and are dissolved in an aqueous solution. Generally, the solution contains some ligands to form complexes with the transactinide elements. The complexes are then chemically characterized by partition methods such as ion-exchange chromatography, reversed-phase extraction chromatography, and liquid-liquid extraction. The transactinide elements in a solution sample are identified by detecting α particles and SF fragments originating from its characteristic decay. These procedures must be performed on the single atom basis within the short lifetime of the transactinide elements.

1-2-1. Production and Gas-jet Transport of Transactinide Elements

   The transactinide elements are produced in heavy-ion-induced nuclear reactions using the accelerator. Generally, ^{18}O, ^{19}F, or ^{22}Ne projectiles and ^{248}Cm or ^{249}Bk targets are used to synthesize neutron-rich and relatively long-lived isotopes of the transactinide elements. The gas-jet transport technique has been used to rapidly deliver short-lived transactinide elements from the target chamber to the chemistry apparatus in a remote site [6]. A schematic diagram of the He/KCl gas-jet system is given in Fig. 1-2. As a carrier material of the nuclear reaction products, KCl aerosols are generated by sublimation of KCl powder on a quartz boat in a stainless tube placed in an electric furnace at 620–640 ℃. The KCl aerosols are fed into the target chamber through the Teflon tube with He gas stream. The nuclear reaction products recoiling out of the target are stopped in the He gas, attached to the KCl aerosols, and continuously transported through Teflon tubes to the chemistry apparatus in a few seconds.

1-2-2. Physical Preseparation of Transactinide Elements with Gas-jet Transport
         System Coupled to Gas-filled Separator

   Production rates of the transactinide elements decrease with increasing the atomic numbers Z; atoms per minute for ^{261}Rf (Z = 104) and ^{262}Db (Z = 105), atoms per hour for ^{265}Sg (Z = 106) and ^{267}Bh (Z = 107), and atoms per day for ^{269}Hs (Z = 108) [2]. They are produced together with much larger amounts of "background" radioactivities which hinder the detection of α decay and SF originating from the transactinide elements of interest. To overcome this problem, a technique of physical preseparation of the

14

transactinide elements before chemical separation using the gas-jet transport system coupled to a gas-filled separator has been proposed [2, 7]. The pioneering experiment with the Recoil Transfer Chamber (RTC) coupled to the Berkeley Gas-filled Separator (BGS) was performed by Omtvedt et al. [8]. The very short-lived isotope ^{257}Rf ($T_{1/2} =$ 4.7 s) physically separated from the large amount of radioactive by-products was identified by liquid scintillation after liquid-liquid extraction with SISAK system. A detailed description on the SISAK system is given in chapter 1-2-3. (c).

In the RIKEN linear accelerator (RILAC) facility, the gas-jet transport system for the chemical studies of the transactinide elements was installed at the focal plane of the Gas-filled Recoil Ion Separator (GARIS) [9]. A schematic of the GARIS gas-jet system is given in Fig. 1-3. The isotopes ^{261}Rf [10], ^{265}Sg [11], and ^{262}Db [12] were successfully transported to a chemistry laboratory under low background condition using the GARIS gas-jet system.

1-2-3.   Automated On-line Chemistry Apparatus for Aqueous Chemistry

Almost all aqueous chemical studies of the transactinide elements are performed in discontinuous batch-wise operations with a large numbers of cyclic repetitions. For the precision and reproducibility of the chemical separations, automated chemical separation systems are preferable. Today, most chemical studies of the transactinide elements have been carried out with the automated instruments as below.

(a) Automated Rapid Chemistry Apparatus (ARCA)

Extensive studies on chemical behavior of Rf, Db, and Sg in aqueous solution have been performed with the "Automated Rapid Chemistry Apparatus" (ARCA) which was originally developed by Schädel et al. [13]. ARCA allows fast, repetitive chromatographic separations in two column magazines equipped with 20 miniaturized columns (8 mm long, 1.6 mm inner diameter (i.d.)) for each magazine. Depending on the chemical separations, columns were filled with cation- or anion-exchange resin or an organic extractant on an inert support material. In Japan, a slightly modified ARCA has been developed by the group of JAEA [14] in collaboration with the group of GSI. A schematic of the modified ARCA is given in Fig. 1-4. Typical separation procedures with ARCA are as follows; the nuclear reaction products transported by the He/KCl gas-jet system are collected on the hollow surface of a slider (see "front view" in Fig. 1-4). One of the columns is pre-conditioned with the first eluent. At the end of a suitable collection time, the slider moves to just above the pre-conditioned column. Then, the collected reaction products are dissolved with the first eluent and are subsequently fed into the column. The first effluents are collected on a Ta disk. After the elution, the column magazine moves forward to place the column in the second flow path (see "side view" in Fig. 1-4). Then, the reaction products remaining in the column are eluted with the second eluent. The second effluents are collected on another Ta disc. The effluents collected on the Ta discs are evaporated to dryness by IR light and hot He gas. Then the Ta discs are placed in a Si semiconductor detector chamber for α and SF spectrometry. In the experiments with ARCA, the typical separation time is between 5 s and 10 s and evaporation of the solution sample takes approximately 20 s.

16

(b) Automated Ion-exchange Separation Apparatus Coupled with the Detection System

    for Alpha Spectroscopy (AIDA)

The procedures of the sample preparation for α and SF spectrometry and placing the samples in detector chambers in the experiments with ARCA were automated in the "Automated Ion-exchange separation apparatus coupled with the Detection system for Alpha spectroscopy" (AIDA) which was developed by the JAEA group [15]. A schematic of AIDA is shown in Fig. 1-5. AIDA consists of the modified ARCA and an automated on-line α-particle detection system with eight detector chambers equipped with 600 mm^2 passivated ion-implanted planar silicon (PIPS) detectors. Effluents from the column of ARCA are collected on Ta discs and then the Ta discs are delivered under a halogen heat lump with a carrying table. After evaporation of the effluents to dryness by the halogen heat lump and hot He gas (it takes approximately 20–30 s), the Ta discs are put in the detector chambers with a robotic arm.

(c) Short-lived Isotopes Studied by the AKUFVE-technique (SISAK)

The "Short-lived Isotopes Studied by the AKUFVE-technique" (SISAK) system performs continuous rapid liquid-liquid extractions using small-volume separator centrifuges [16]. The term "AKUFVE" is a Swedish acronym for an arrangement for continuous investigations of distribution ratios in liquid-liquid extraction. A schematic diagram of the SISAK liquid-liquid extraction system is shown in Fig. 1-6. Nuclear reaction products are transported to the apparatus with gas-jet. The gas-jet is mixed with

the aqueous solution to dissolve the reaction products, and the carrier gas is removed in a degasser centrifuge. The aqueous solution is then mixed with an organic solution which contains an extractant and the two liquid phases are separated in a separator centrifuge. A liquid scintillator is then mixed with the organic solution, and this mixed solution passes through liquid scintillation detection system.

In SISAK system, α particles and SF fragments are detected by liquid scintillation detectors whereas Si semiconductor detectors have been generally used in chemical experiments of the transactinide elements. This is mainly because the liquid scintillation detection is the only the suitable method to perform α and SF spectroscopy on the continuously flowing solution at high flow rates (0.5–2.0 mL/s) without time-consuming evaporation of the solution. Liquid scintillation counting has high detection efficiency of α particles and SF fragments (almost 100%), but suffers from relatively poor energy resolution and is also sensitive to β particles and γ rays. In the production of the transactinide elements, α, β, and γ-emitting by-products are produced with orders of magnitude higher yield than the desired transactinide elements. It is impossible to identify the α decay and SF originating from the transactinide elements under such conditions. To overcome this problem, a technique of physical preseparation of the transactinide elements with the Berkeley Gas-filled Separator (BGS) was demonstrated by Omtvedt et al. [8]. With the SISAK system coupled to the BGS, physically preseparated ^{257}Rf ($T_{1/2}$ = 4.7 s) was successfully identified by liquid scintillation. Overview of the BGS-SISAK system is shown in Fig. 1-7. Development and progress of the on-line liquid scintillation detection system in SISAK system have been reported by Wierczinski et al. [17] and by Stavsetra et al. [18, 19, 20].

In SISAK system, only the organic phase was measured to achieve a sufficient energy

resolution in the liquid scintillation detection. The aqueous phase was not be measured due to sever quenching of the liquid scintillation process. Distribution ratios of the transactinide elements between the two phases were indirectly determined by deducing the amount in the aqueous phase from the measured activity that entered the extraction centrifuge and the amount in the organic phase. To determine the distribution ratios in liquid-liquid extraction more precisely, the SISAK system was recently extended to include a second extraction step in which part or all of the activity remaining in the aqueous phase after the first extraction stage is transferred to a second organic phase [21]. Schematics of three types of experimental setups used in studies of the transactinide elements with SISAK system are shown in Fig. 1-8.
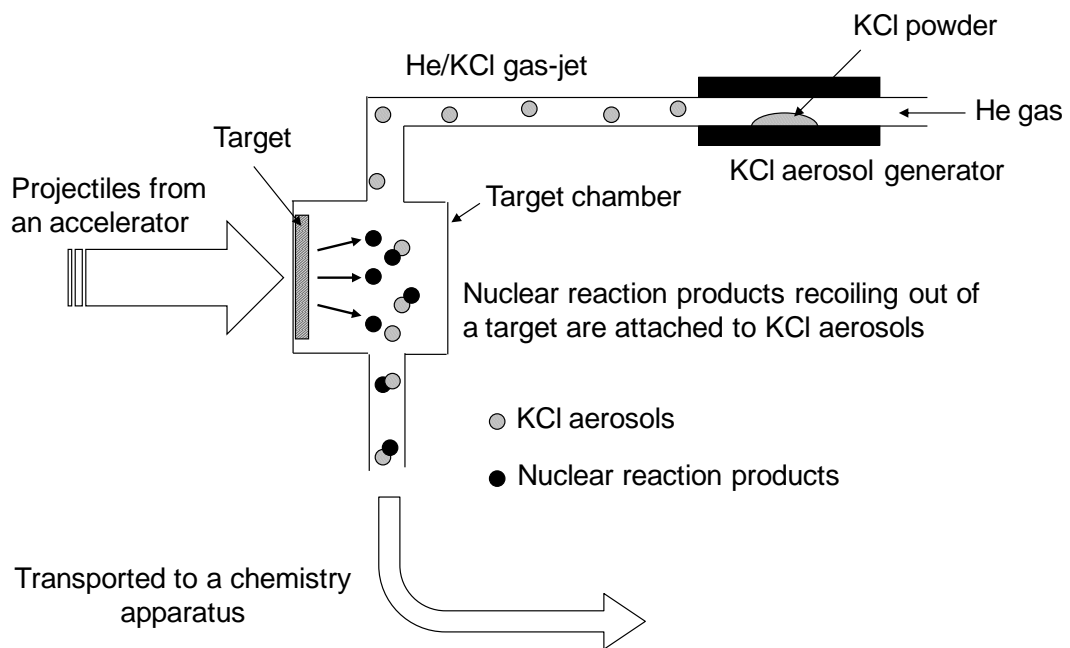
Fig. 1-2. A schematic diagram of the He/KCl gas-jet system.
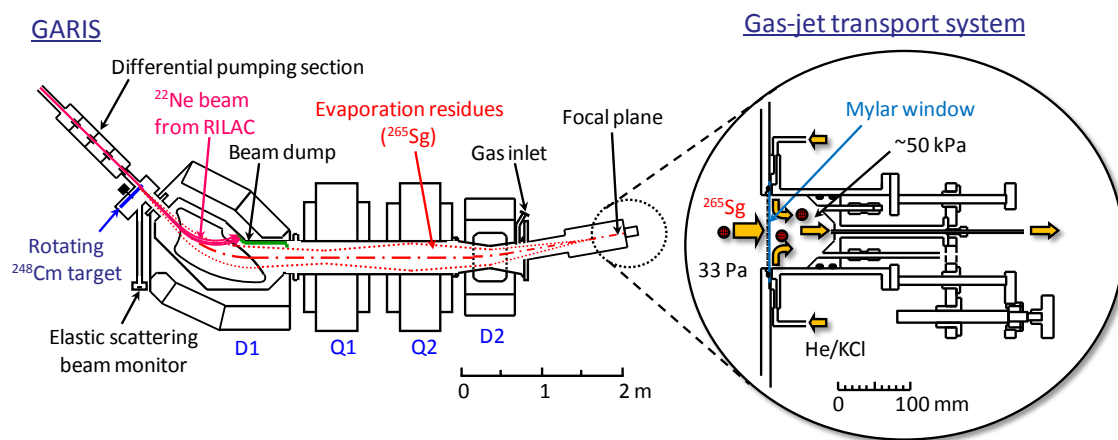
Fig. 1-3. A schematic of the GARIS gas-jet system.
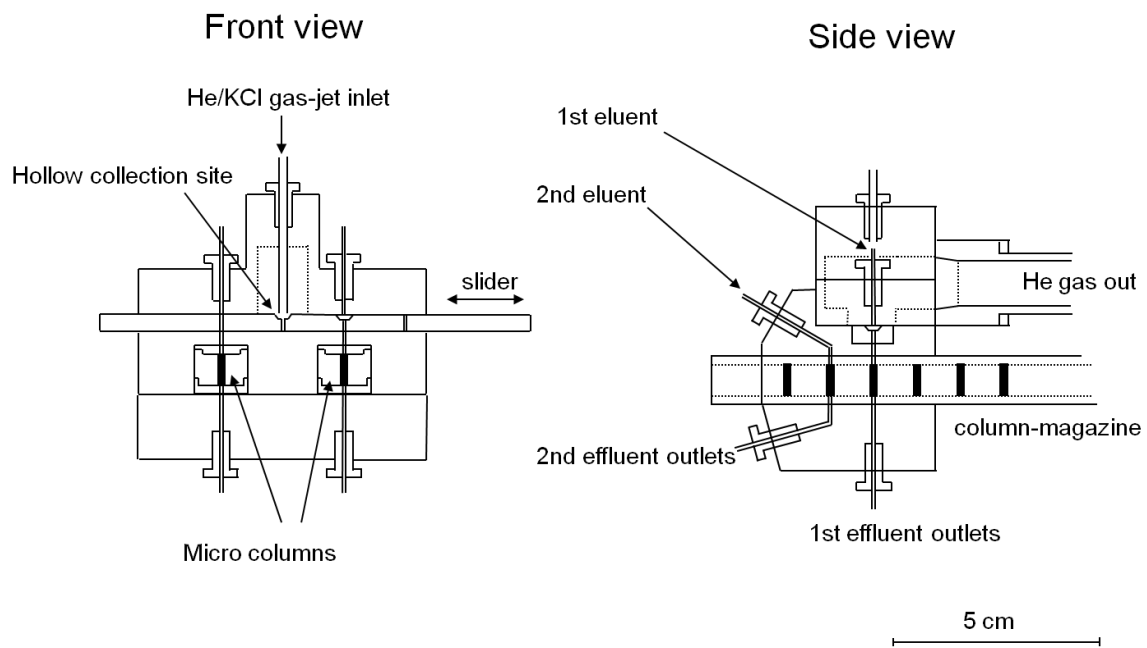
Fig. 1-4. A schematic of the modified ARCA.

Automated **I**on-exchange separation apparatus coupled with the **D**etection system for **A**lpha spectroscopy (AIDA)

Automated on-line α-particle detection system

He/KCl gas-jet inlet

Signal output

ARCA

PIPS detectors

Eluents

Micro-column (ion-exchange resin)

He gas heater

Halogen lamp

Fig. 1-5. Overview of AIDA. AIDA consists of the modified ARCA and an automated on-line α-particle detection system with eight detector chambers equipped with PIPS detectors.
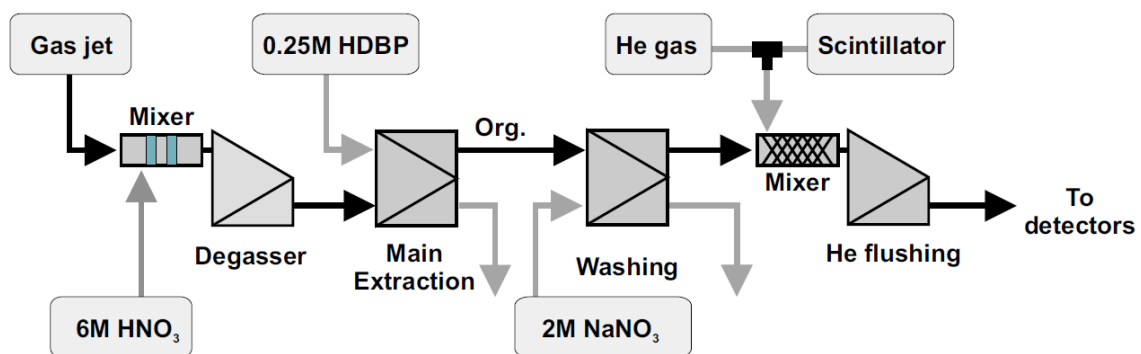
Fig. 1-6. A schematic diagram of the SISAK liquid-liquid extraction system [8].
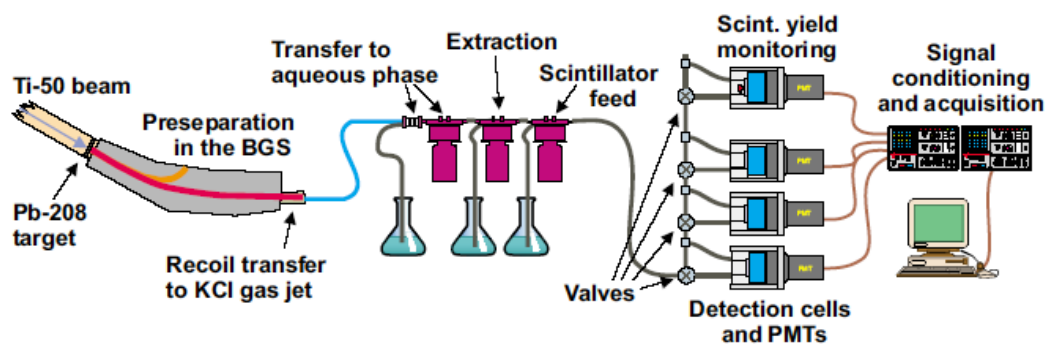
Fig. 1-7. Overview of the SISAK system coupled to the Berkeley Gas-filled Separator [8].
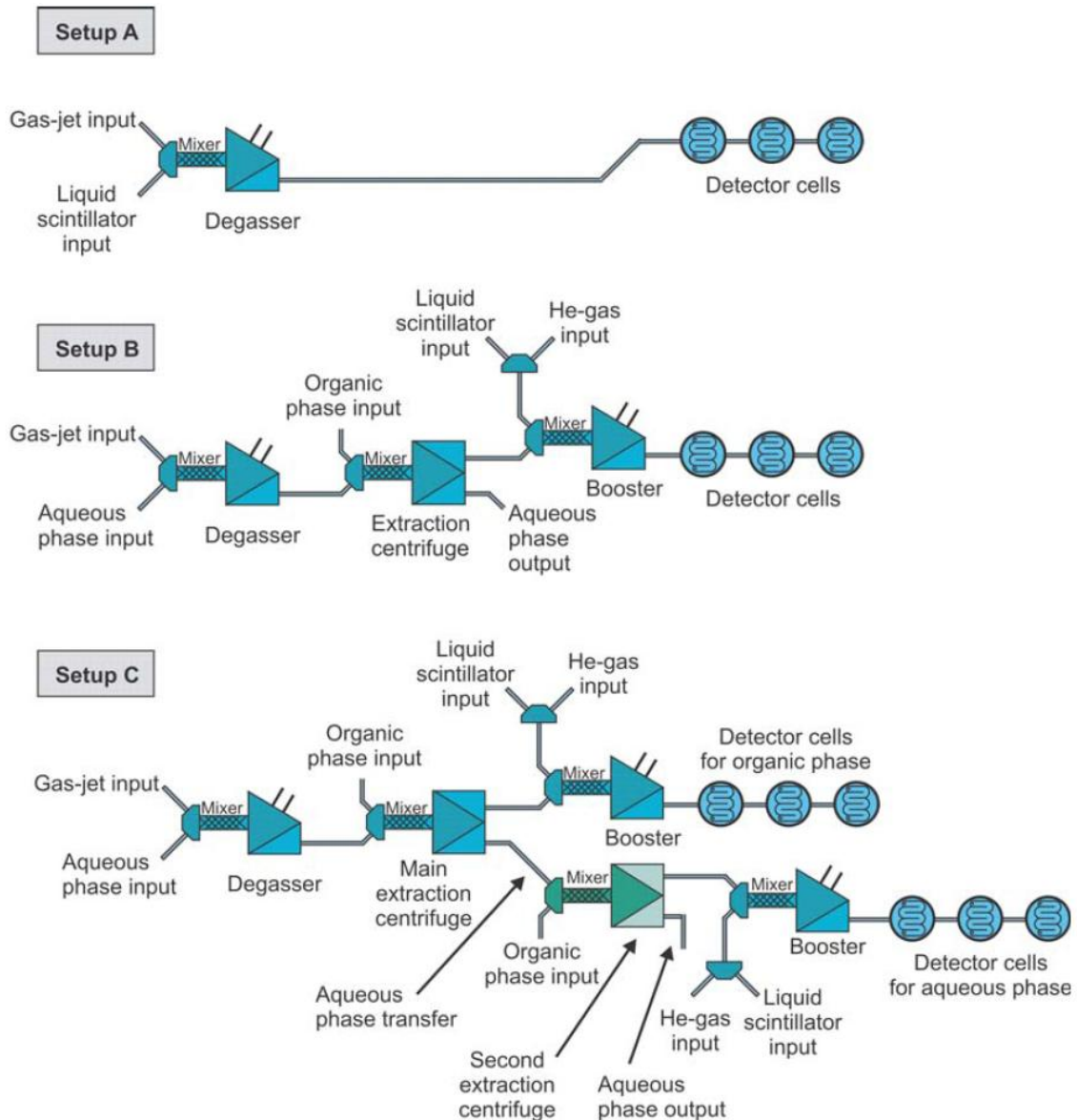
Fig. 1-8. Schematics of SISAK setups used in studies of the transactinide elements [21].
Setup A is used to measure the amount of activity entering the system. The gas-jet
transported activity is directly dissolved in a liquid scintillator and measured. Setup B is
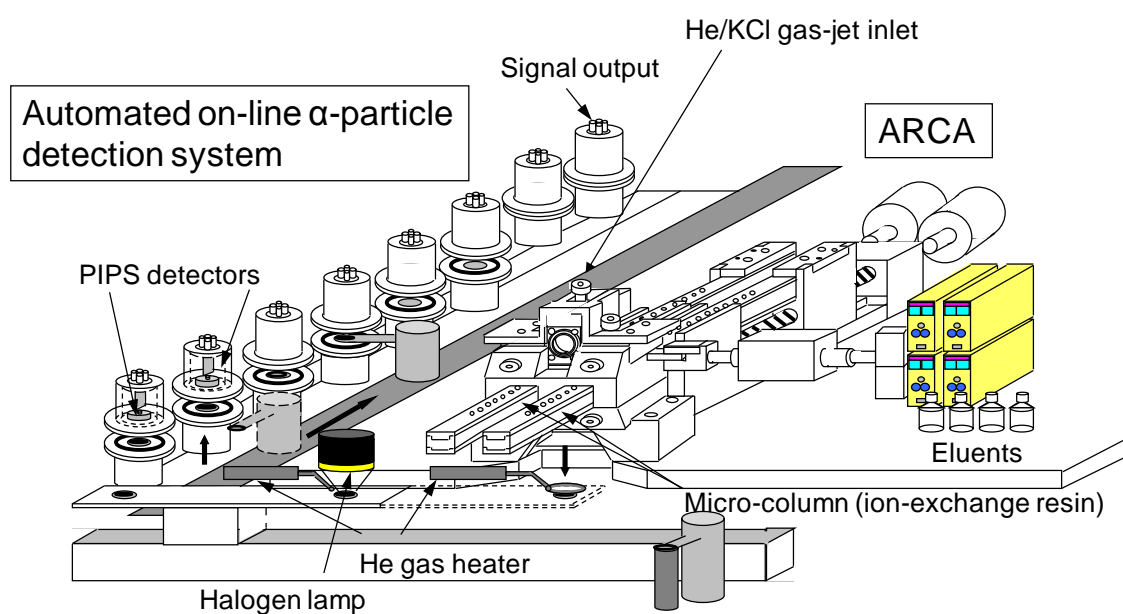used to measure the amount of activity in the organic phase after liquid-liquid extraction.
The amount of activity in the aqueous phase is not measured but is deduced from a
separate experiment with setup A. Setup C enables the measurement of activity in both
phases using a second extraction step and a second array of liquid scintillation detectors.

1-3. Previous Aqueous Chemical Studies of Rf, Db, and Sg

Aqueous chemical studies have been so far carried out on the first three transactinide elements, Rf, Db, and Sg using the automated apparatuses as described in chapter 1-2-3. These studies are mainly focused on complex formation and hydrolysis of these elements [2, 3]. Generally, to perform chemical studies of the transactinide elements becomes more difficult with increasing atomic numbers Z because the production rates and the half-lives become lower and shorter, respectively. Cross sections to produce the isotopes ^{261}Rf [22], ^{262}Db [12], and ^{265}Sg^{a,b} [11] in the nuclear reactions are given in Table 1-1.

As for Rf, the ion-exchange behaviors of ^{261}Rf ($T_{1/2}$ = 68 s) in HF [23], HCl [24], HNO$_3$ [24], and in mixed solutions of HF and HNO$_3$ (HF/HNO$_3$) [25], H$_2$SO$_4$ and HNO$_3$ (H$_2$SO$_4$/HNO$_3$) [26] have been systematically investigated with sufficient statistics by a group of JAEA using AIDA. From these studies, interesting results on complex formation properties of Rf were obtained; for example, fluoride complexation of Rf is remarkably weaker than that of its lighter homologues, zirconium (Zr) and hafnium (Hf) [23, 25] whereas chloride complexation of Rf is stronger than that of Zr and Hf [24]. The group of JAEA has started ion-exchange chromatography experiments on ^{262}Db ($T_{1/2}$ = 34 s) [27, 28]. The production rate of ^{262}Db is approximately one-tenth of that of ^{261}Rf. Therefore, it is more difficult to investigate chemical properties of Db compared with those of Rf due to the shorter half-life and the lower production rate of ^{262}Db.

As for Sg, until now, only two studies on cation-exchange chromatography of ^{265}Sg^{a,b} ($T_{1/2}$ = 8.5 s/14.4 s) in 5×10^{-4} M HF/0.1 M HNO$_3$ [29] and in 0.1 M HNO$_3$ [30]

solutions have been reported by Schädel et al. These experiments were performed with ARCA and the Si semiconductor detector was used for α and SF spectrometry. In the first experiment with 5×10^{-4} M HF/0.1 M HNO_3 solution, it was reported that Sg is eluted from the cation-exchange column like the group-6 lighter homologue, tungsten (W) while group-4 elements, Zr, Hf, and Rf are retained on the column. In the second experiment with 0.1 M HNO_3 solution, it was observed that Sg is not eluted from a cation-exchange column, which is different from the behavior of W. This result was interpreted that Sg has weaker tendency to hydrolyze than W. From these two studies, Scädel et al. concluded that Sg forms neutral or anionic fluoride complexes such as SgO_2F_2 or $SgO_2F_3^-$ in 5×10^{-4} M HF/0.1 M HNO_3 solution. However, in these experiments, α particles originating from Sg were not directly detected; the chemical behavior of Sg was assumed through the detection of time-correlated α-α decay chains from ^{261}Rf and ^{257}No, the daughter nuclides of ^{265}Sg (see the decay pattern for the chain ^{265}Sg$^{a,b} \rightarrow {}^{261}Rf^{a,b} \rightarrow {}^{257}$No $\rightarrow$ shown in Fig. 1-9).

In the previous experiments with ARCA, the Si semiconductor detector has been generally used for α and SF spectrometry. Although the Si semiconductor detector has high-energy resolution, evaporation to dryness of the solution sample is required for α and SF spectrometry because the ranges of α particles and SF fragments in solution are too short to penetrate the thick layer of the solution sample. It takes approximately 20–30 s for the evaporation. The detection efficiency of α particles with the Si semiconductor detector is approximately 35%. The time-consuming evaporation and low detection efficiency are quite disadvantageous for the detection of the short-lived transactinide elements with low production rates such as ^{262}Db ($T_{1/2} = 34$ s) and ^{265}Sg^{a,b} ($T_{1/2} = 8.5$ s/14.4 s).

For further progress in aqueous chemical studies of the heavier transactinide elements such as Db and Sg, development of a new experimental methods and instruments including a new detection system is required in addition to improvements of existing apparatuses. In parallel to the development and improvement of experimental apparatuses, it is also important to determine experimental systems and conditions for the transactinide elements and to obtain the data to be compared with that of the transactinide elements using the lighter homologues.

Table 1-1. Half-lives ($T_{1/2}$) and cross sections (σ) to produce the isotopes ^{261}Rf, ^{262}Db, and ^{265}Sg.

Z	Nuclide	$T_{1/2}$ [s]	Nuclear Reaction	σ [nb]
104	^{261}Rf^a	68	^{248}Cm(^{18}O, 5n)	13
105	^{262}Db	34	^{248}Cm(^{19}F, 5n)	2.1
106	^{265}Sg^a	8.5	^{248}Cm(^{22}Ne, 5n)	0.18
106	^{265}Sg^b	14.4	^{248}Cm(^{22}Ne, 5n)	0.2
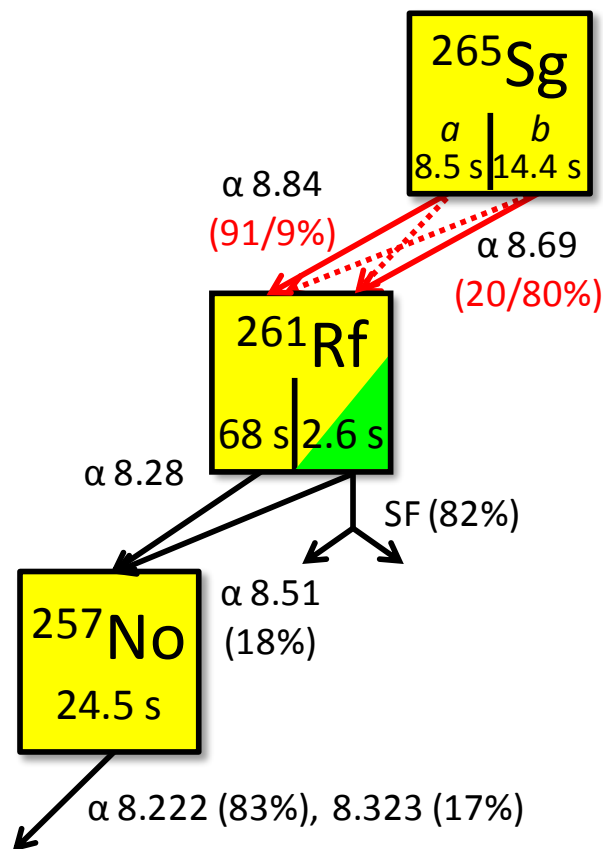
Fig. 1-9. The decay pattern for the chain ^{265}Sg^{a,b} → ^{261}Rf^{a,b} → ^{257}No → reported by Haba et al. [11].

1-4. Purpose of This Study

   For the further progress in the aqueous chemical studies of the transactinide elements, especially for Sg, a more rapid and efficient α-particle and SF detection system is required instead of the Si semiconductor detector. We have adopted the liquid scintillation detector for α and SF spectrometry because it has an advantage of high detection efficiency of α particles and SF fragments (almost 100%). In addition, there is no need for time-consuming evaporation of the solution sample.

   The purpose of this study is to develop an on-line liquid scintillation detection system to detect α particles and SF fragments in solution samples eluted from the chemistry apparatus such as ARCA. To detect the α particles and SF fragments originating from the transactinide elements by liquid scintillation, low background condition is necessary due to some problems such as relatively poor energy resolution and interference from β particles and γ rays as described in chapter 1-2-3. (c). We are planning to remove radioactive by-products using the GARIS gas-jet system to attain the low background condition in the liquid scintillation spectrometry. In this work, a liquid scintillation detection system for on-line measurement was developed. A liquid scintillation detection chamber which consists of a photomultiplier tube, a cell, and a reflector was newly fabricated and the detection performance of α particles and fission fragments was investigated. The developed system was applied to the on-line liquid scintillation measurement of ^{213}Fr ($T_{1/2}$ = 34.6 s) produced in the ^{209}Bi(^{16}O,$4n$)^{221}Pa reaction as a model experiment for the detection of short-lived α-emitting nuclide. Next, on-line liquid scintillation measurement of preseparated ^{262}Db with the GARIS gas-jet system was performed to evaluate the background count rate for the detection of

time-correlated α-α events from ^{262}Db and the daughter nuclide ^{258}Lr ($T_{1/2}$ = 3.8 s).

Another purpose of this study is to investigate experimental conditions applicable for extraction chromatography experiment of Sg using the lighter homologues, Mo and W. We have selected methyl-tricaprylyl ammonium chloride (Aliquat 336) as an extractant for anionic species in aqueous solution. In this study, extraction behaviors of Mo and W onto Aliquat 336-loaded resin from HF and HCl solutions were investigated. It is known that Mo and W form polynuclear species such as $[Mo_7O_{24}]^{6-}$ and $[W_{12}O_{39}]^{6-}$ in solution [31]. On the other hand, Sg cannot form the polynuclear species due to its low production rates and short half-lives. In this study, carrier-free radioisotopes ^{93m}Mo ($T_{1/2}$ = 6.9 h), ^{90}Mo ($T_{1/2}$ = 5.7 h), ^{181}W ($T_{1/2}$ = 121.2 d), and ^{173}W ($T_{1/2}$ = 7.6 m) were used to avoid the polymerization of Mo and W. Distribution coefficients (K_d) of Mo and W were obtained as a function of HF and HCl concentration by a batch method. The on-line extraction chromatography of Mo and W in HCl solution was performed with ARCA.

This thesis is composed of the following chapters. In chapter 2, the development of the on-line liquid scintillation α/SF detection system is presented. In chapter 3, on-line liquid scintillation measurement of preseparated ^{262}Db with the GARIS gas-jet system is described. In chapter 4, extraction behavior of Mo and W onto Aliquat 336-loaded resin from HF and HCl solutions is described. Finally, this work is summarized in chapter 5. The other complementary explanations and experiments related to the development of liquid scintillation detection system are given in appendices.

Chapter 2

Development of On-line Liquid

Scintillation α/SF Detection System

2-1. Introduction

For the further progress in the aqueous chemical studies of the transactinide elements, especially for element 106, Sg, a rapid and efficient α-particle and spontaneous fission (SF) detection system is required instead of the commonly used Si semiconductor detector. We have adopted the liquid scintillation detector for α and SF spectrometry because it has an advantage of high detection efficiency of α particles and SF fragments (almost 100%). In addition, there is no need for time-consuming evaporation of the solution sample.

The purpose of this work is to develop an on-line liquid scintillation detection system to detect α particles and SF fragments in solution samples for aqueous chemical studies of Rf, Db, and Sg. In this chapter, required specifications of the system are described at first. Based on the required specifications and pilot studies, a liquid scintillation detection system for on-line measurement was developed. A liquid scintillation detection chamber which consists of a photomultiplier tube, a cell, and reflector was newly fabricated and the detection performance of α particles and SF fragments was investigated. Finally, the developed system was applied to the on-line liquid scintillation measurement of short-lived α-emitting nuclide, ^{213}Fr ($T_{1/2}$ = 34.6 s) produced in the ^{209}Bi(^{16}O, $4n$)^{221}Pa reaction as a practical application.

2-2.　Required Specifications

The decay pattern for the chain $^{265}\text{Sg}^{a,b} \rightarrow {}^{261}\text{Rf}^{a,b} \rightarrow {}^{257}\text{No} \rightarrow$ reported by Haba et al. [11] is shown in Fig. 2-1. The long-lived $^{265}\text{Sg}^{b}$ decays mainly to $^{261}\text{Rf}^{b}$ ($T_{1/2}$ = 2.6 s) and it subsequently decays mainly by SF. Required specifications of the liquid scintillation detection system for chemical studies of Rf, Db, and Sg are as follows:

・ Detection efficiency of α particles and fission fragments is 100%.

・ Events originating from α particles and SF fragments are distinguishable from those originating from β particles and γ rays by pulse shape discrimination.

・ Sample preparation for liquid scintillation measurement is as fast as to be applicable for $^{265}\text{Sg}^{a,b}$ detection.

・ Procedures of liquid scintillation measurement are automatically repeatable.

The on-line liquid scintillation detection system is composed of the liquid scintillation detection chamber and a flow path of the solution sample eluted from the chemistry apparatus. The detection chamber consists of the photomultiplier tube, the cell, and the reflector. Prior to fabrication of the liquid scintillation detection chamber, the chemistry apparatus to be coupled with the liquid scintillation detection system, a liquid scintillator, and method of sample preparation for liquid scintillation spectrometry were tentatively assumed as follows:

(1) Chemistry Apparatus

A liquid chromatography apparatus, ARCA (Automated Rapid Chemistry Apparatus)

[13], or a liquid-liquid extraction apparatus using a microchannel devices [32] are considered as chemistry apparatuses to be coupled with the liquid scintillation detection system. ARCA has been so far widely used in the chemical experiments of Rf, Db, and Sg [2, 3]. Thus, in this study, ARCA is assumed to be coupled with the liquid scintillation detection system at first. Typical flow rate of aqueous solution in experiments with ARCA is 1 mL/min.

(2) Selection of Liquid Scintillators

A liquid scintillator (sometimes called "scintillation cocktail") is usually composed of an organic solvent such as toluene, xylene, or diisopropylnaphthalene in which a fluor (the light-emitting molecule) is dissolved. Liquid scintillation spectrometry is performed by dissolving radioactive nuclides into the organic liquid scintillator. Generally, there are two ways to perform liquid scintillation spectrometry on radioactive nuclides dissolved in aqueous solution. One is to extract the radioactive nuclides into a liquid scintillator which contains an extractant such as HDEHP (extractive scintillator) from the aqueous solution. The other is to directly mix the aqueous solution which contains the radioactive nuclides with a liquid scintillator which contains an emulsifier (the emulsifier scintillator). In case of using the extractive scintillator, extractability of the radioactive nuclides of interest (which are Rf, Db, and Sg in this work) into the scintillator depends on the affinity of Rf, Db, or Sg with the extractant and on their extraction kinetics, those have not been sufficiently studied yet. In contrast, the emulsifier scintillator has an advantage that Rf, Db, or Sg in aqueous solution can be directly detected independently of their chemical properties. We have adopted the

36

emulsifier scintillator for the detection of Rf, Db, and Sg dissolved in aqueous solution. We have selected a commercially-available emulsifier scintillator, Ultima Gold AB® (PerkinElmer, Inc) which was developed for α/β discrimination measurement.

(3) Sample Preparation for Liquid Scintillation Spectrometry

The aqueous solution sample must be homogeneously mixed with the Ultima Gold AB® for the better energy resolution and α/β discrimination. However, such homogeneous state was not attained by simply injecting the aqueous solution together with the Ultima Gold AB® through a Teflon tube because of high viscosity of the Ultima Gold AB®. Thus, an electromagnetic stirrer is used to mix the solution sample with the Ultima Gold AB®.
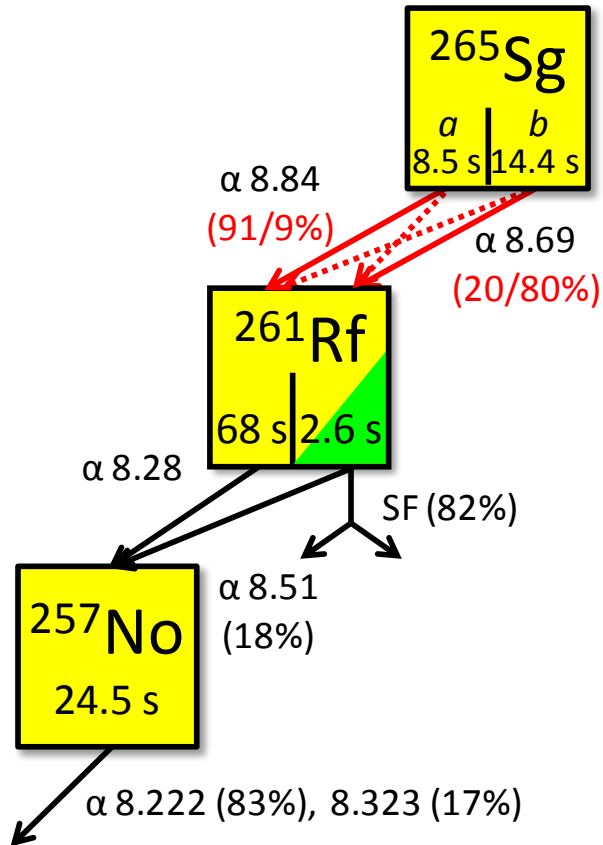
Fig. 2-1. The decay pattern for the chain $^{265}\text{Sg}^{a,b} \rightarrow {}^{261}\text{Rf}^{a,b} \rightarrow {}^{257}\text{No} \rightarrow$ reported by Haba et al. [11].

2-3.   System Composition

2-3-1.   System Composition

   The system composition for on-line liquid scintillation measurement is shown in Fig. 2-2. The detection chambers which consist of a photomultiplier tube and a glass cell are placed on the electromagnetic stirrers (ISIS Co., Ltd., HP30110) to mix the solution sample with the liquid scintillator in the cell. The aqueous solution and the liquid scintillator are delivered to each detection chamber via an auto selector valve (GL Science, Inc., SV-5008AM) through Teflon tubes. Procedures in on-line measurements are as follows; the liquid scintillator (we used the Ultima Gold AB$^®$ in this study) is first injected into the cell and then electromagnetic stirring is started. Next, the solution sample from the chemistry apparatus is injected to the cell. During the injection, the solution sample and the liquid scintillator have been mixing with the electromagnetic stirrer. Measurement is started with the electromagnetic stirring stopped after the mixture became homogeneous in the cell. Because the output signal of the photomultiplier tube is affected by a magnetic field, measurement cannot be started during the electromagnetic stirring. After the measurement, the solution in the cell is drained by a peristaltic pump and the liquid scintillator is newly introduced into the cell for the next measurement. The above procedures are controlled by PC through LabVIEW compact DAQ systems and software (National Instruments Corp).

2-3-2.   Detection Chamber

Schematics and photographs of the detection chamber are shown in Figs. 2-3 and 2-4, respectively. Design drawings of the detection chamber are given in appendix 4. The photomultiplier tube (Hamamatsu Photonics K.K., R331-05) and the glass cell set in an aluminum reflector which is coated with a reflective paint of $BaSO_4$. A silicone oil (Shin-Etsu Chemical Co., Ltd., KF-96-50CS) is filled between the cell and the photomultiplier tube as an optical coupling. The cell has a cylindrical shape of 28 mm in diameter and 19 mm in height. Bottom of the cell is funnel-shaped in order to make it easy to drain the highly viscous liquid scintillator. Four tubes of solution-sample inlet, scintillator inlet, outlet, and leak are attached to the wall of the cell. The leak and the outlet tubes are connected with small electromagnetic valves (Takasago Electric, Inc., MTV-2-N1/4U). A φ1.5 and 15 mm-long magnetic stirring bar (Flonchemial Co. Ltd, M-15) is put in the cell. The solution sample is dripped in the cell from a PTFE tube inserted into the tube of solution-sample inlet, being stirred with the liquid scintillator.

2-3-3.   Electronics for Pulse Shape Discrimination

A diagram of electronics for pulse shape discrimination is given in Fig. 2-5. Scintillation lights originating from α particles decay more slowly than those from β particles due to different linear energy transfer (LET) values [33]. Thus, events originating from α and β particles are distinguishable each other based on the difference in scintillation decay time. The scintillation lights are converted to electric signals by the photomultiplier tube. The anode signal of the photomultiplier tube is amplified and shaped with scintillation preamplifier (ORTEC model 113) and delay line amplifier

(ORTEC model 460). One output of the delay line amplifier is delivered to the signal input of a 16-channel VME-ADC module, A3100 (NIki Glass Co., Ltd) and pulse height, which reflects energy of radiation, is recorded. Another output of the delay line amplifier is delivered to pulse-shape and timing single-channel analyzer (ORTEC model 552). It determines the time difference between two pre-selected fixed points on the decaying part of the unipolar pulse using constant fraction discrimination. The time difference between two points of pulse is measured with time-to-amplitude converter/single-channel analyzer (ORTEC module 567). The TAC output is delivered to the signal input of A3100 and the time difference is recorded. The SCA output is used as a gate signal and delivered to the gate/trigger input of A3100. Events from α and β particles are distinguishable each other by plotting the time difference (time) against the pulse height (energy) of each event. The pulse height and the time difference of each event are registered in list mode to obtain the time information when the event occurs.
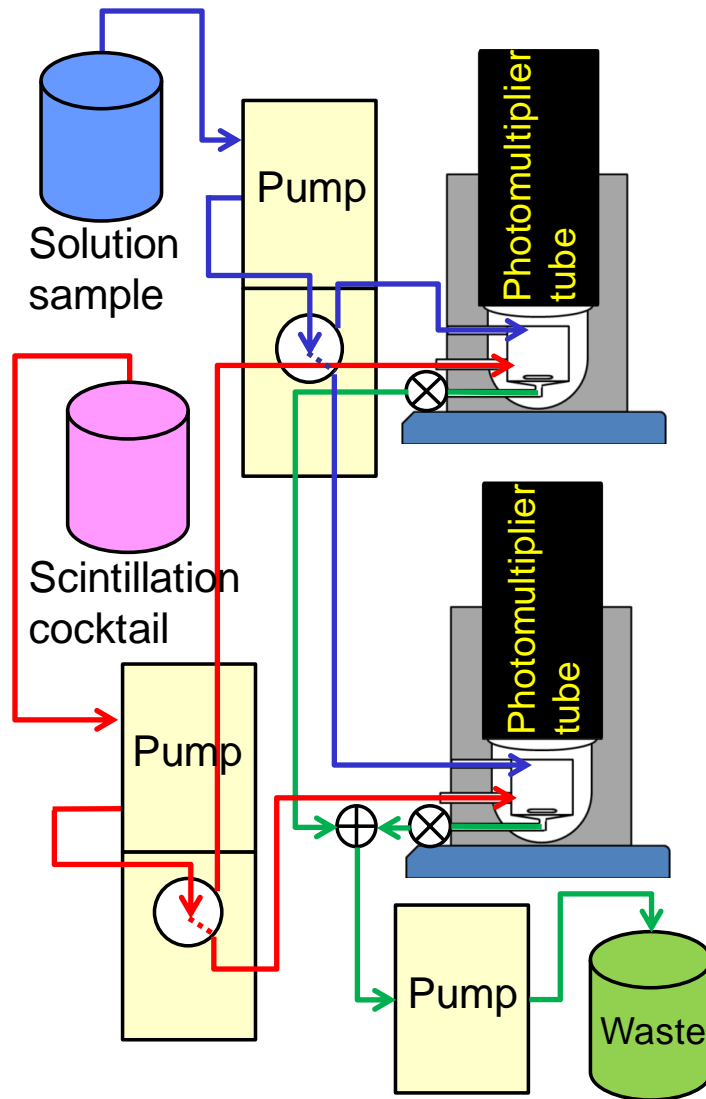
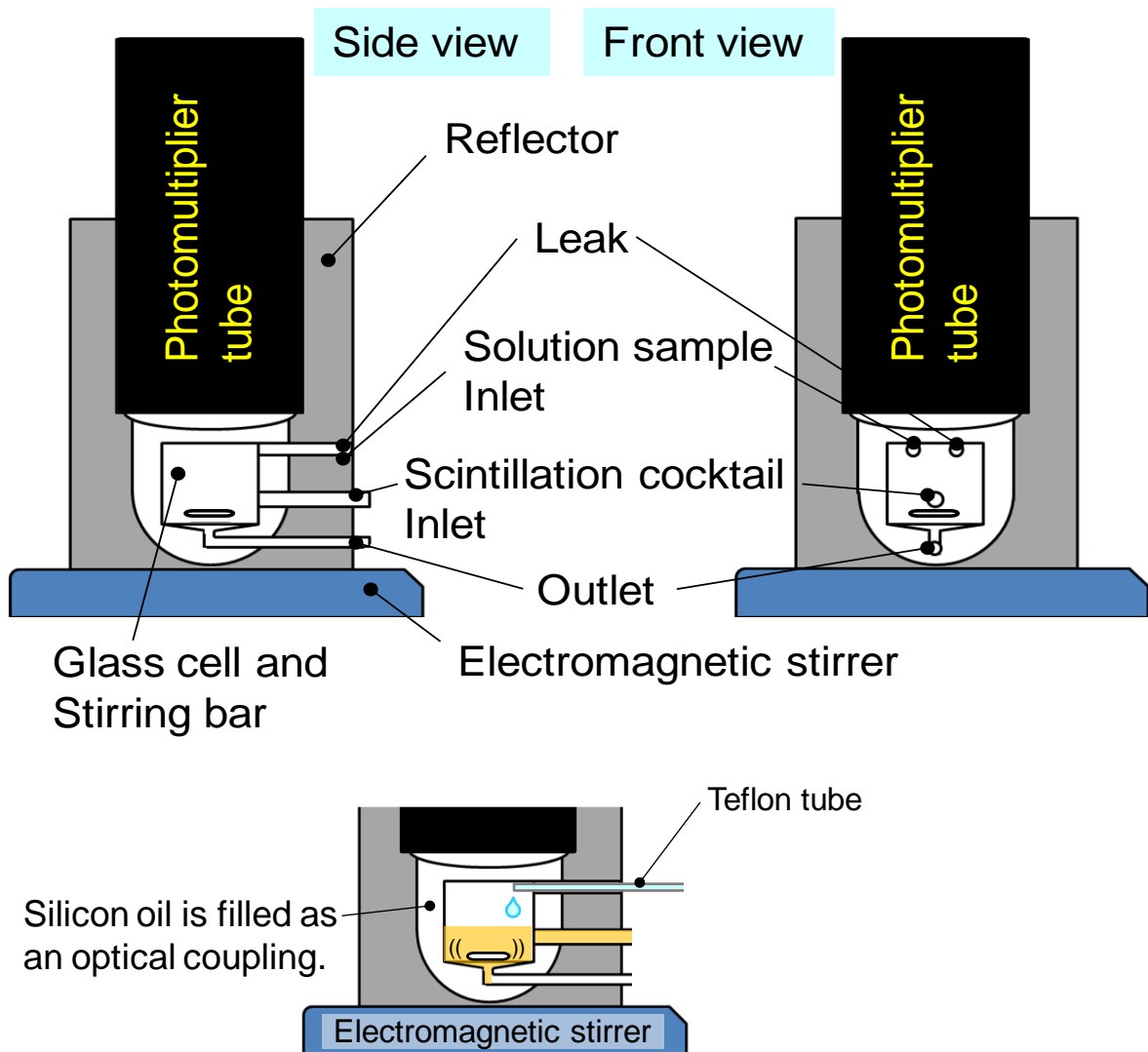Fig. 2-2. A schematic of system composition for on-line liquid scintillation measurement.

Side view Front view

Photomultiplier tube

Reflector

Leak

Solution sample Inlet

Scintillation cocktail Inlet

Outlet

Glass cell and Stirring bar

Electromagnetic stirrer

Photomultiplier tube

Teflon tube

Silicon oil is filled as an optical coupling.

Electromagnetic stirrer

Fig. 2-3.   Schematics of the liquid scintillation detection chamber.
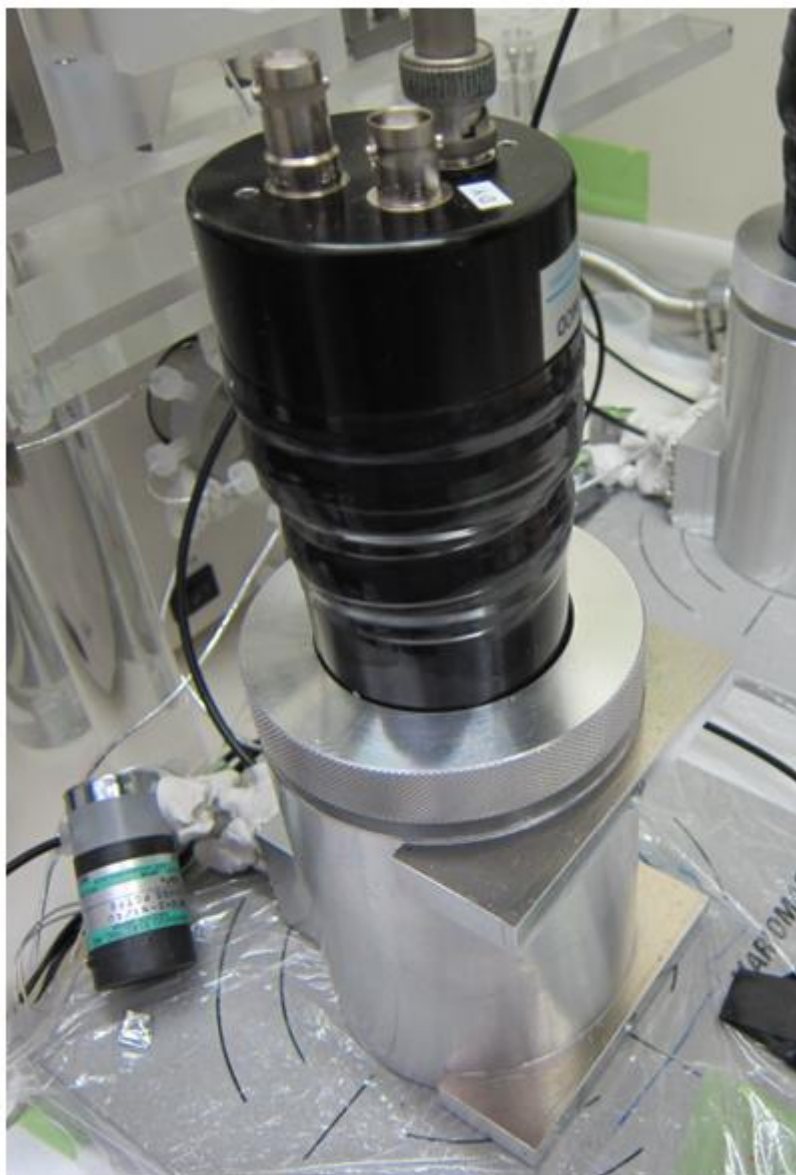
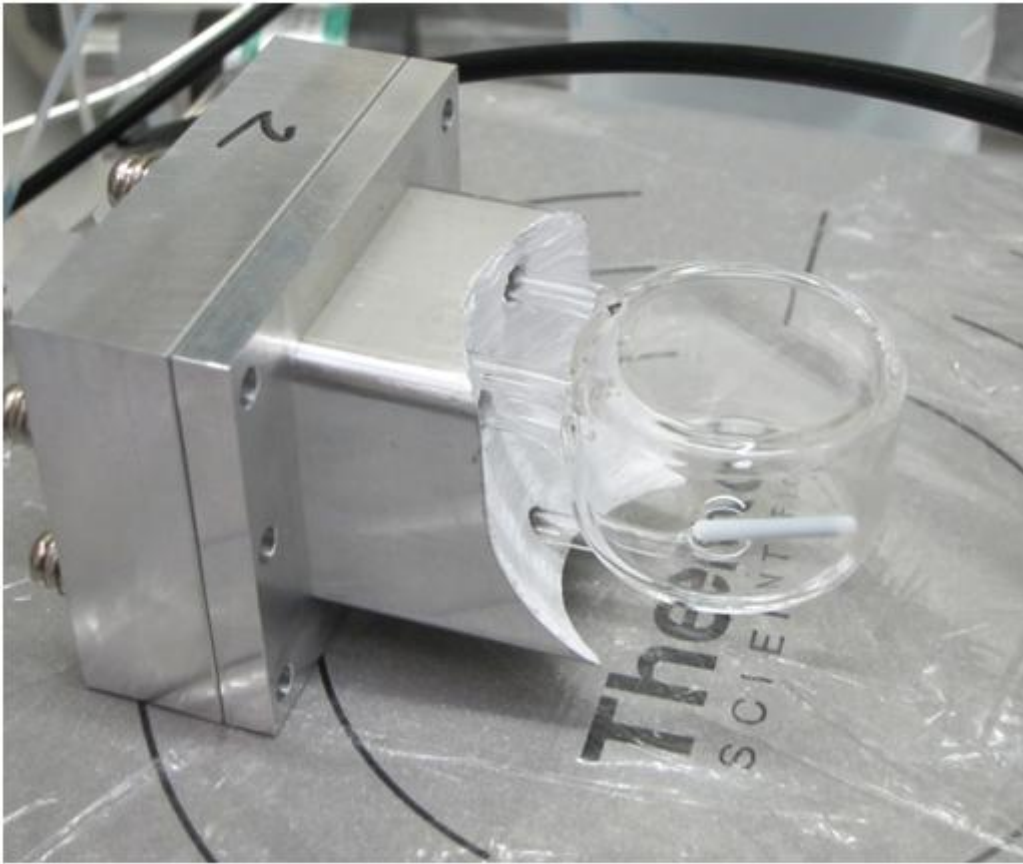Fig. 2-4. A photograph of the liquid scintillation detection chamber.

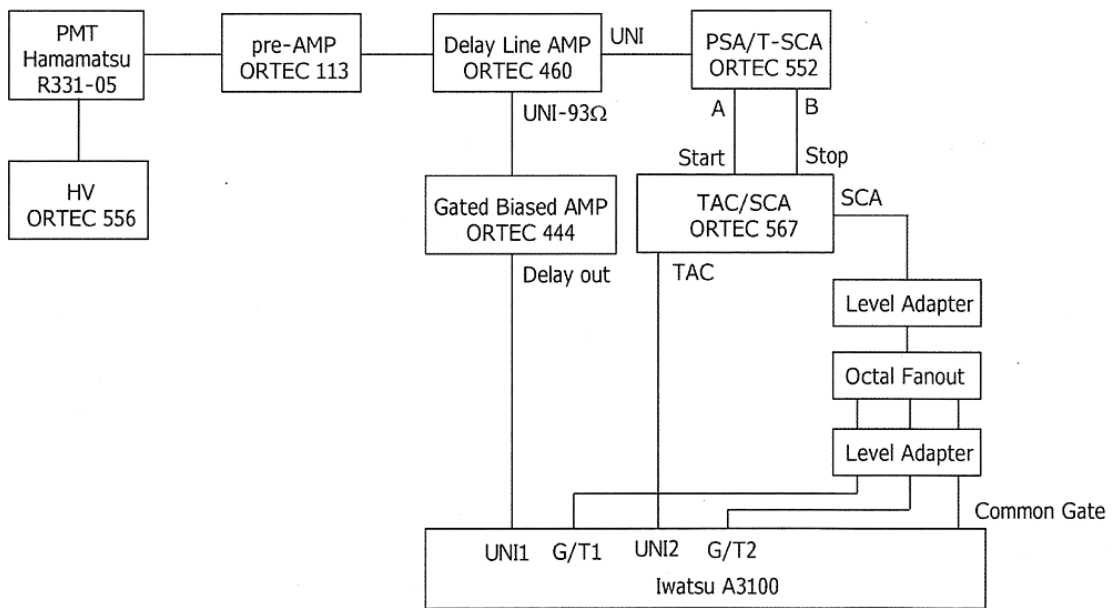Fig. 2-5. A photograph of the glass cell.

Fig. 2-5.   A diagram of electronics for pulse shape discrimination.

2-4. Performance Evaluation

2-4-1.   Energy Resolution and Detection Efficiency of α Particles

Energy resolution and detection efficiency of α particles were investigated with the developed detection chamber using radioisotopes ^{226}Ra and ^{241}Am, respectively. A stock solution of ^{226}Ra dissolved in 0.1 M HNO$_3$/5 × 10^{-3} M HF solution was used to investigate the energy resolution in α-particle detection. A standard solution of ^{241}Am dissolved in 0.5 M HCl solution was used to investigate the detection efficiency of α particles. Sample solutions for liquid scintillation counting were prepared by mixing 200 μL of the each stock solution of ^{226}Ra and ^{241}Am with 4 mL of the Ultima Gold AB$^{®}$. These sample solutions were transferred to the glass cell and measured in a static condition, with the four tubes of solution-sample inlet, scintillator inlet, outlet, and leak were plugged with silicone-rubber plugs. The pulse height and pulse shape parameter of each event was registered in list mode.

A two-dimensional plot of time versus energy for ^{226}Ra and its decay products is shown in Fig. 2-6. It is found that α events of ^{226}Ra, ^{222}Rn, ^{218}Po and ^{214}Po are discriminated from continuous β components. A pulse height (energy) spectrum of α particles from ^{226}Ra and its decay products is shown in Fig. 2-7, being separated from β events. The energy resolution for ^{226}Ra ($E_α$ = 4.784 MeV) and ^{214}Po ($E_α$ = 7.687 MeV) were approximately 300-keV and 500-keV full width at half maximum (FWHM), respectively. The detection efficiency for α particles of ^{241}Am was 99 ± 1 %, found to be almost 100%.

2-4-2.　Response to Spontaneous Fission

Response to SF was investigated using the isotope ^{252}Cf as a SF source. A stock solution of ^{252}Cf dissolved in 0.1 M HNO$_3$/5 × 10^{-3} M HF solution was used to investigate response to SF events. The stock solution of ^{252}Cf contains isotopes 0.24% ^{249}Cf, 10.74% ^{250}Cf, and 0.07% ^{251}Cf in activity. A sample solution for liquid scintillation counting was prepared by mixing 200 μL of the stock solution of ^{252}Cf with 4 mL of the Ultima Gold AB$^{®}$. This sample solution was transferred to the glass cell and measured in a static condition, with the four tubes of solution-sample inlet, scintillator inlet, outlet, and leak were plugged with silicone-rubber plugs. The pulse height and pulse shape parameter of each event was registered in list mode.

Two-dimensional plots of time versus energy for ^{252}Cf are shown in Figs. 2-8 (a) and (b). Figs. 2-8 (a) and (b) were individually obtained by varying the gain of the delay line amplifier and constant-fraction parameter of the pulse-shape analyzer shown in Fig. 2-5. Events from 6.1-MeV α particles of ^{252}Cf and from other isotopes $^{249–251}$Cf are shown in Fig. 2-8 (a). Events from 180-MeV SF are shown in Fig. 2-8 (b). The SF events are observed in the wide energy region which corresponds to approximately 15–30 MeV α energy, being discriminated from β events. It is consistent with the previously reported results that SF events were observed in the α-energy range of 10–25 MeV using an extractive scintillator [17]. The count-rate ratio of α to SF was 34.9 ± 0.7, which is in agreement with the value of 35.3 derived from the isotopic ratio of $^{249–252}$Cf and the SF-branching ratio. This indicates that the detection efficiency of SF is 101 ± 2%.

2-4-3. Sample Preparation Time for Liquid Scintillation Spectrometry

In the on-line liquid scintillation measurement, the solution sample eluted from the chemistry apparatus has been mixed with the Ultima Gold AB® by the electromagnetic stirring during the injection of the sample into the cell as shown in Fig. 2-9. The stirring continues until the he mixture becomes homogeneous in the cell. A time interval ΔT until the mixture becomes homogeneous after the stop of the sample injection has been investigated using the nuclide ^{224}Ra ($T_{1/2}$ = 3.66 d) and its decay products. Stock solution of ^{224}Ra was prepared by milking with 8 M HNO_3 from ^{228}Th adsorbed on an anion-exchange column. The effluent of ^{224}Ra was evaporated to dryness and dissolved in 0.1 M HNO_3. Prior to measurement, 4 mL of the Ultima Gold AB® was introduced into the cell and then electromagnetic stirring was started. The stock solution of ^{224}Ra was injected into the cell at a flow rate of 1 mL/min for 12 s. The solution and the Ultima Gold AB® had been mixing in the cell during the injection and additional ΔT. After ΔT, electromagnetic stirring was stopped and then measurement was started. Energy resolution and the degree of α/β discrimination were investigated by varying ΔT as 1, 2, 3, 60 s.

A two-dimensional plot of time versus energy for ^{224}Ra and its decay products obtained without mixing of the aqueous solution sample with the Ultima Gold AB® is shown in Fig. 2-10. Energy resolution and α/β discrimination is not enough in such the inhomogeneous solution. Two-dimensional plots of time versus energy for ^{224}Ra and its decay products obtained with mixing for 12 s (sample injection) + 1 s (ΔT) and for 12 s (sample injection) + 60 s (ΔT) is shown in Figs. 2-11 (a) and (b), respectively. It was found that clear α/β discrimination is attained in 1 s of ΔT. Energy spectra of ^{226}Ra and

its decay products in $\varDelta T = 1, 2, 3, 60$ s are shown in Fig. 2-12, being separated from β components. The FWHM of the energy peak of ^{224}Ra and ^{220}Rn in $\varDelta T = 1, 2, 3, 60$ s is summarized in Table 2-1. It seems that energy resolution in $\varDelta T = 1$ s is almost comparable to that in $\varDelta T = 60$ s. The total volume of the flow path of the presented system is estimated to be around 20–30 μL. It takes approximately 1–2 s to pass through the volume at a flow rate of 1 mL/min. From these results, it is considered that the aqueous solution sample can be subjected to α/SF spectrometry in a few seconds after the end of the chemical separation.
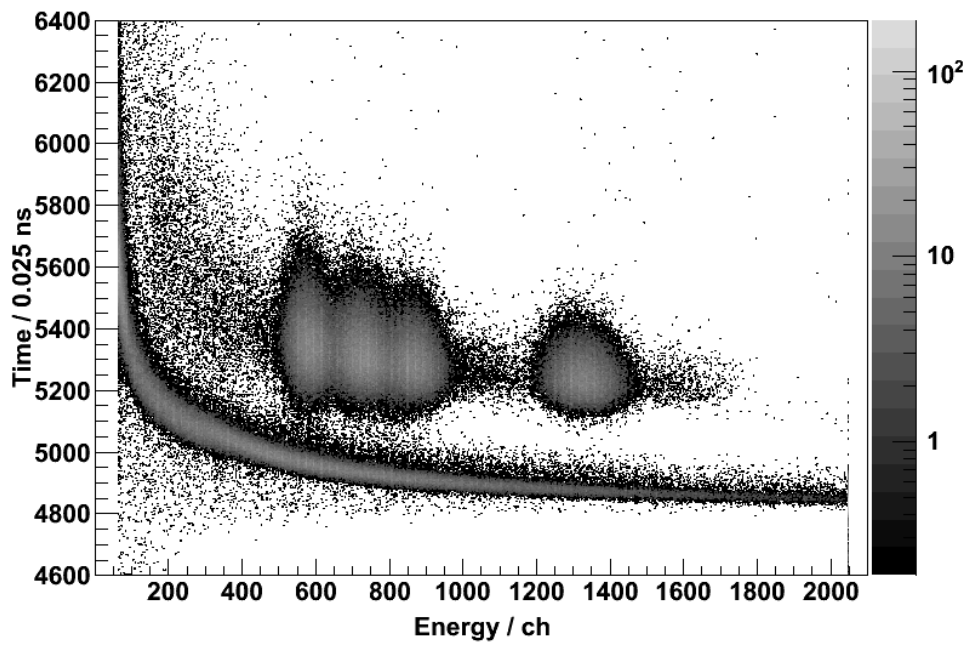
Fig. 2-6. A two-dimensional plot of time versus energy for ^{226}Ra and its decay products.
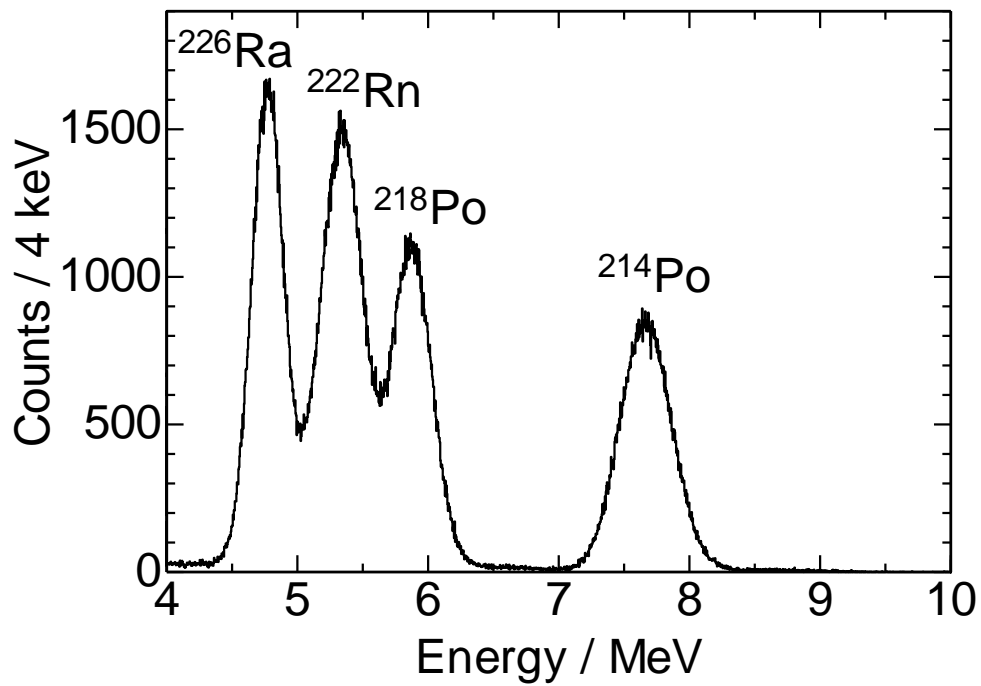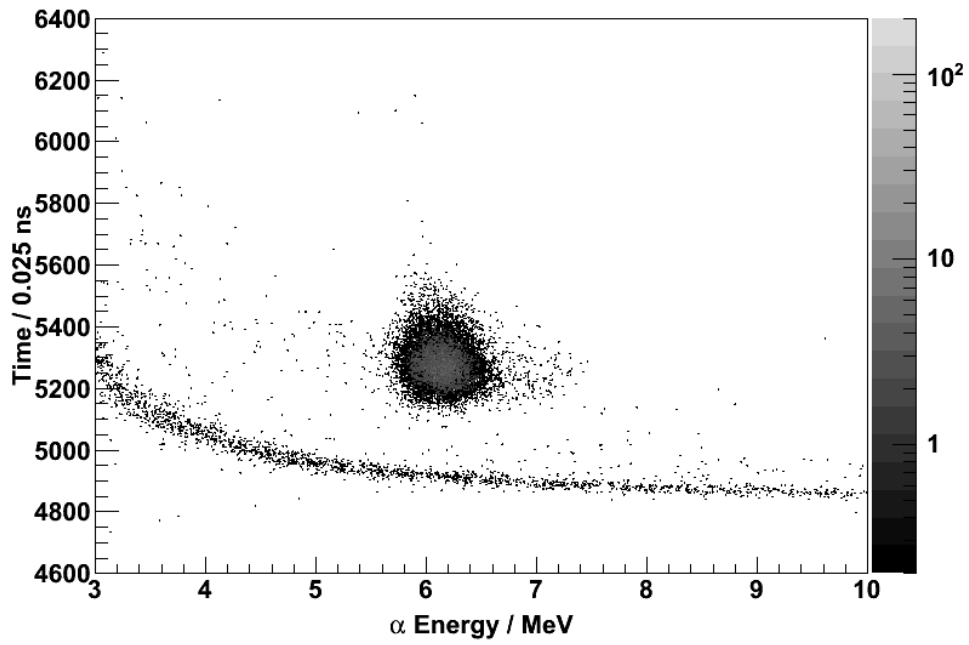

Fig. 2-7. An energy spectrum of ^{226}Ra and its decay products. The β components are removed by pulse shape discrimination.
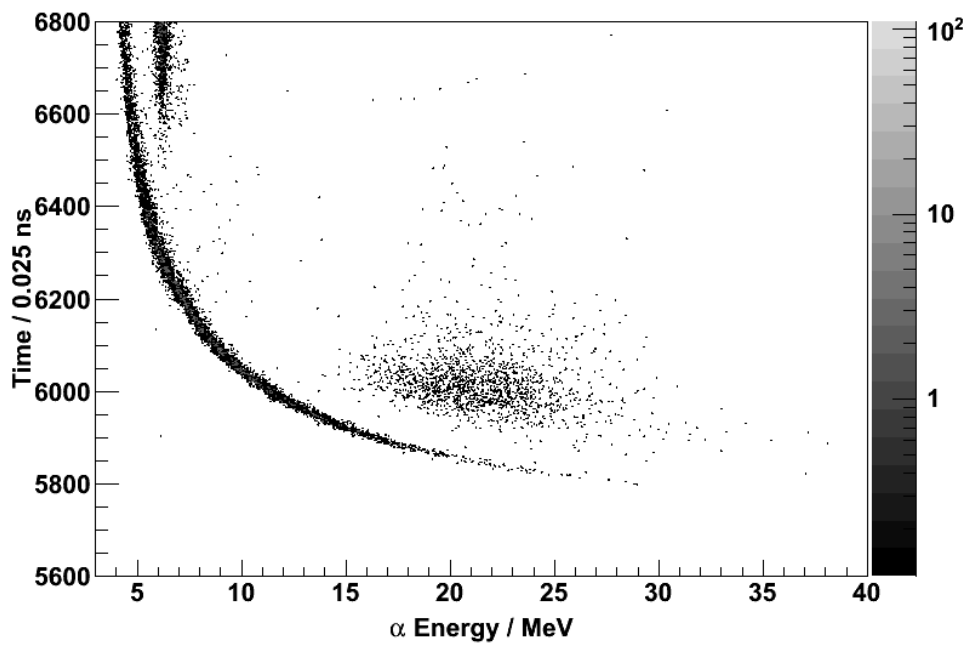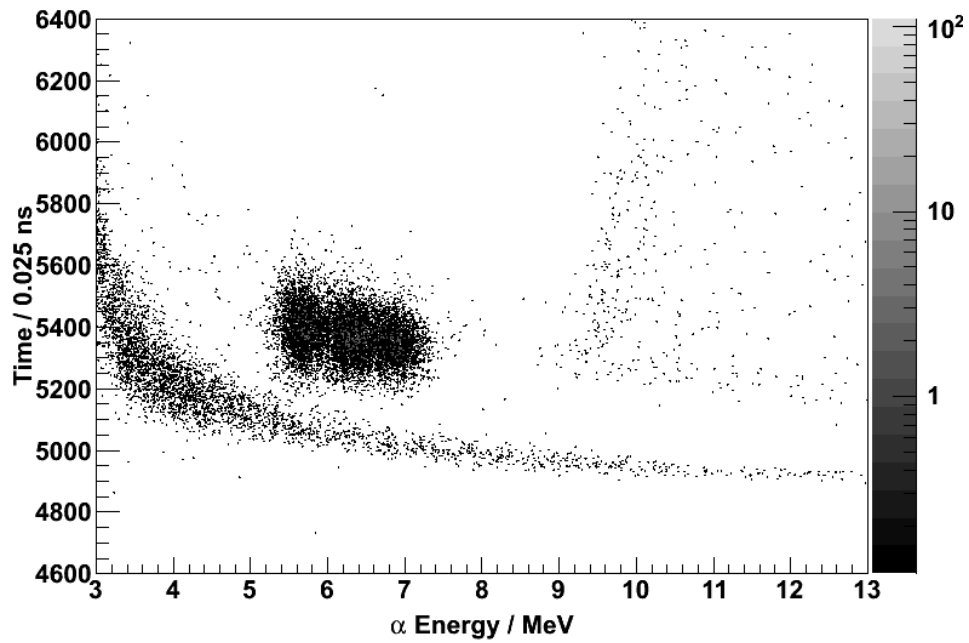
(a)

(b)

Fig. 2-8.   Two-dimensional plots of time versus energy for ^{252}Cf.

Fig. 2-9. Time relations of sample preparation for on-line liquid scintillation measurement after the end of collection of the nuclear reaction products on the chemistry apparatus.

Fig. 2-10. A two-dimensional plot of time versus energy for [224]Ra and its decay products obtained without mixing of the aqueous solution sample with the Ultima Gold AB[®].
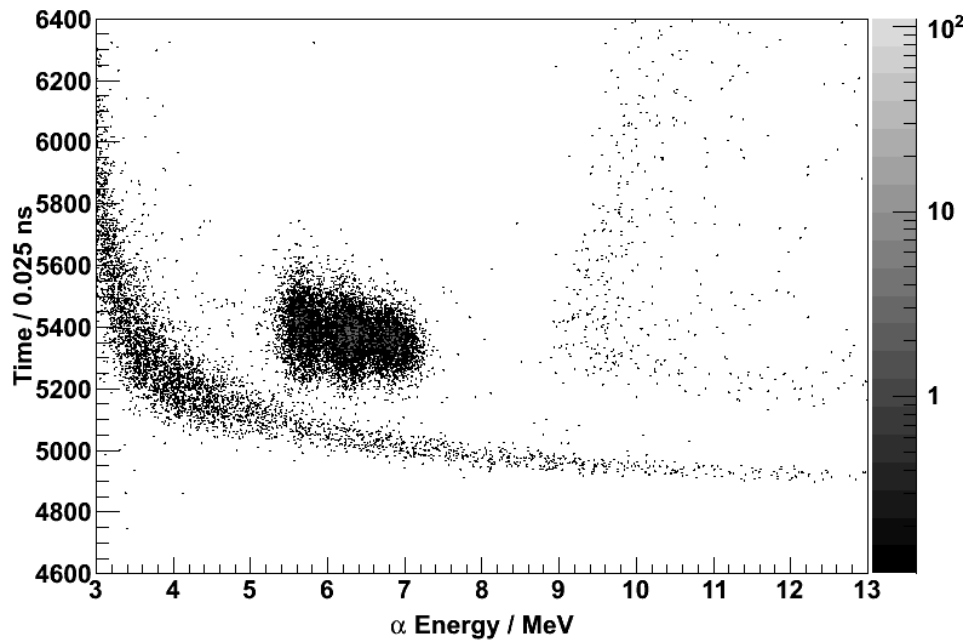
(a)

(b)

Fig. 2-11. Two-dimensional plots of time versus energy for ^{224}Ra and its decay products obtained with (a) mixing for 12 s (sample injection) + 1 s ($\varDelta$T) and (b) for 12 s (sample injection) + 60 s ($\varDelta$T).
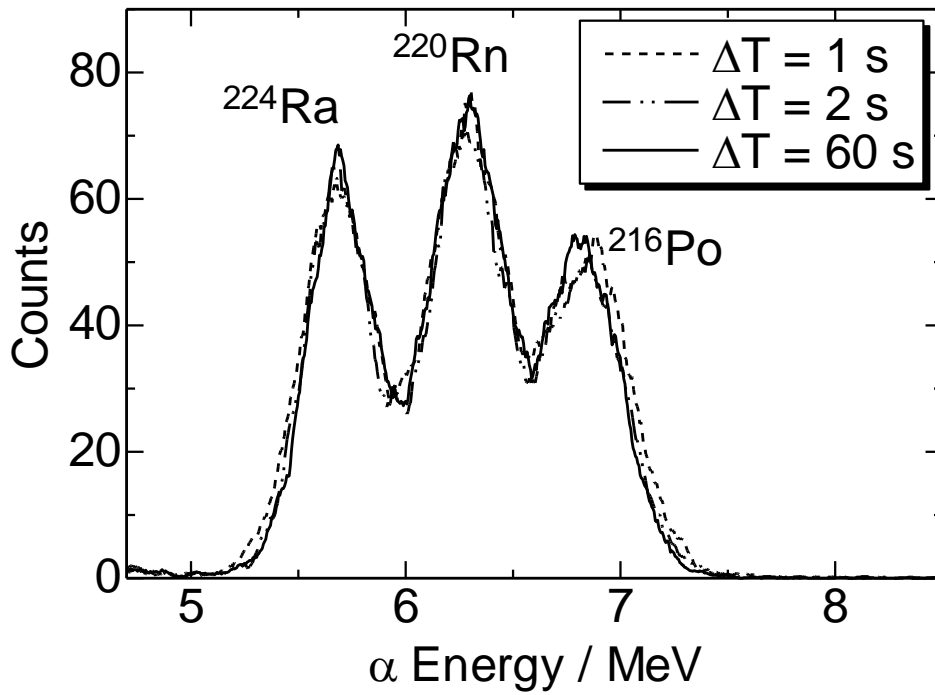
54

Fig. 2-12. Energy spectra of ^{226}Ra and its decay products in $\mathit{\Delta}$T = 1, 2, 3, 60 s. The β components are removed by pulse shape discrimination.

Table 2-1   The FWHM of the energy peak of ^{224}Ra and ^{220}Rn in $\mathit{\Delta}$T = 1, 2, 3, 60 s.

$\mathit{\Delta}$T [s]	^{224}Ra (5.69 MeV) FWHM [keV]	^{220}Rn (6.29 MeV) FWHM [keV]
1	310	290
2	270	260
3	340	320
60	260	290

2-5. Quenching in Liquid Scintillation α Spectrometry

One of the most serious problems in liquid scintillation α spectrometry is quenching. Generally, quenching causes a shift of the α energy peak to lower-energy region in the energy (pulse height) spectrum, loss of the energy resolution, and loss of the ability to discriminate α events from β events by pulse shape discrimination. Detailed mechanisms and kinds of quenching are described in Ref. [33]. In the chemical quenching process, the organic solvent (main component of the liquid scintillator) excited by radiation transfers its energy to a non-light-producing molecule instead of the fluor. Such molecules dissipate their energy in molecular vibrational and rotational modes and thus produce heat rather than light when they return to their ground state. Examples of chemical quenchers are water, oxygen, ketones, alcolols, and especially nitrates (which is also a color quencher that absorbs lights emitted by fluors).

Liquid scintillation α spectrometry using the emulsifier scintillator suffers the quenching effects by water and chemical reagents in the aqueous solution sample more directly than that using the extractive scintillator. The degree of the quenching depends on the kinds and concentration of the reagents. Therefore, it is necessary to preliminarily investigate the degree of quenching by the reagents which are to be used in the chemical experiments. In this study, the quenching effects of several kinds of acid (HF, HCl, and HNO_3) solutions and a KSCN solution on the energy resolution and on the ability of α/β discrimination were investigated.

The stock solution of ^{226}Ra was evaporated to dryness and then dissolved in various concentrations of HF, HCl, HNO_3, or KSCN solutions. Samples for liquid scintillation spectrometry were prepared by mixing 50 μL of each aqueous solutions of ^{226}Ra with 1

mL of the Ultima Gold AB® in φ10 mm and 75-mm long disposable test tubes. These samples were subjected to liquid scintillation spectrometry with a liquid scintillation detector for off-line measurement as shown in Fig. 2-13.

Examples of two-dimensional plots of time versus energy for measurements of HF, HCl, and KSCN solution samples are presented in Figs. 2-14, 2-15, and 2-16, respectively. It was found that the time difference between α and β events decreases with increasing concentrations of acids or salts in the aqueous solutions. An example of time spectrum which is clipped out in the area of 7.687 MeV α peak of [214]Po is given in Fig. 2-17. It is observable that α peak and β peak overlap each other. These two components were fitted with asymmetric Gaussian function to derive fractions of β component which is spilled over into α-event region. FWHM for 7.687 MeV α peak of [214]Po, the time difference between α and β events, and fractions of β component spilled over α-event region are summarized in Table 2-2. Among the investigated acid solutions, quenching effect to reduce the time difference between α and β events seems to increase in the order of HF < HCl < HNO_3.

Next, neutralization of the acid solution samples was attempted to reduce the quenching effects. 200 μL of 1 M, 50 μL of 10 M, and 125 μL of 10 M NaOH solutions were added into the mixtures of 50 μL of 4 M, 10 M HCl and 26 M HF solutions of [226]Ra with 1 mL of the Ultima Gold AB®, respectively. The resulting two-dimensional plots of time versus energy for these samples are shown in Figs. 2-18, 2-19, and 2-20, respectively, together with those before neutralization. It was found that the time difference between α and β events in the area of α energy peak of [214]Po increased from 4–5 ns to around 8 ns in every sample after neutralization. It indicates that oxonium ions contribute to the reduction in the time difference between α and β events in samples

contain HF and HCl solutions. Significant degradation of the energy resolution is observed in neutralized samples of 10 M HCl and 26 M HF solutions. This is probably due to increasing concentration of salts such as NaCl and NaF in these samples and these salts would interfere with the energy transfer of radiation. As for the samples of HNO_3 solutions, the time difference between α and β events didn't increase by neutralization.
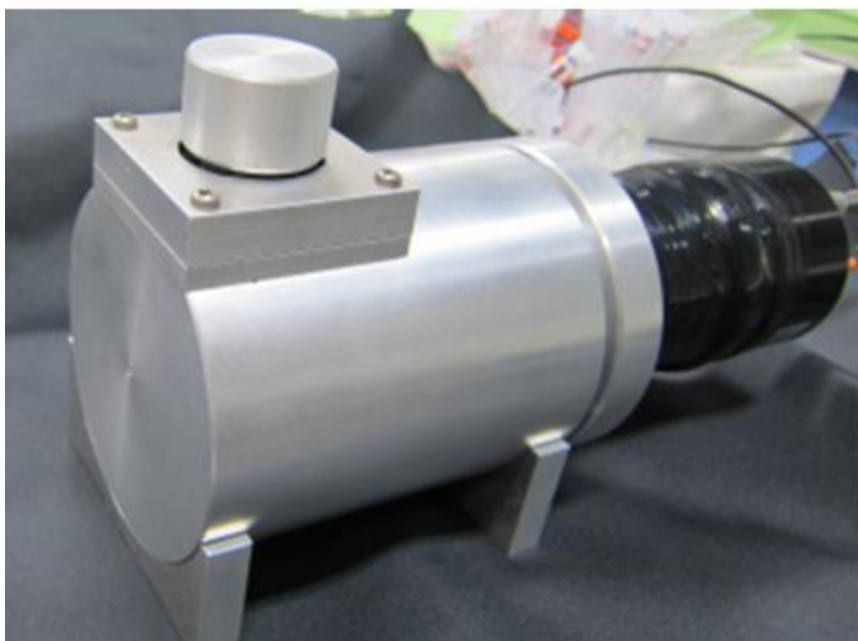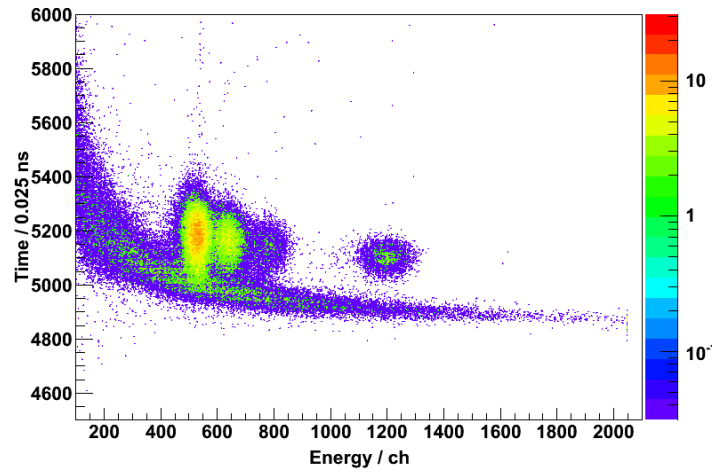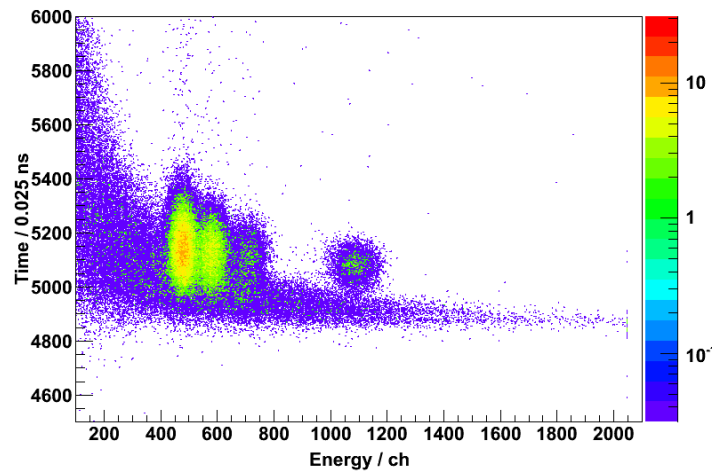
Fig. 2-13. A photograph of a liquid detection chamber for off-line measurement used in the investigation of quenching by various aqueous solutions.
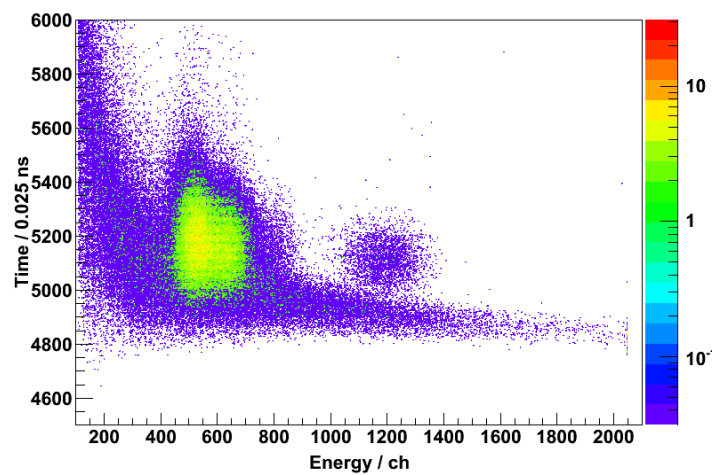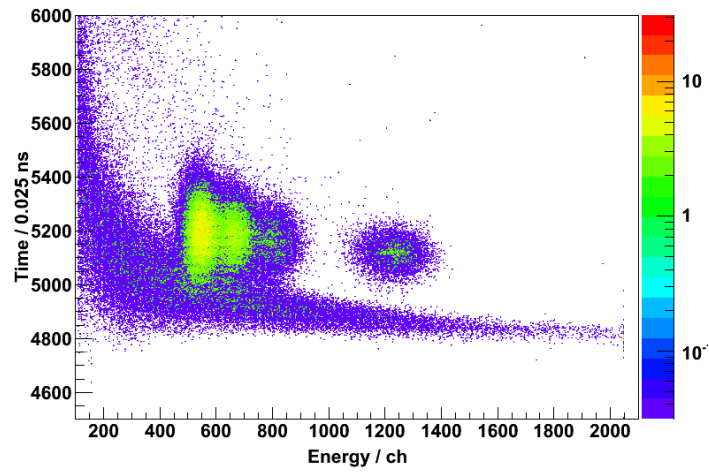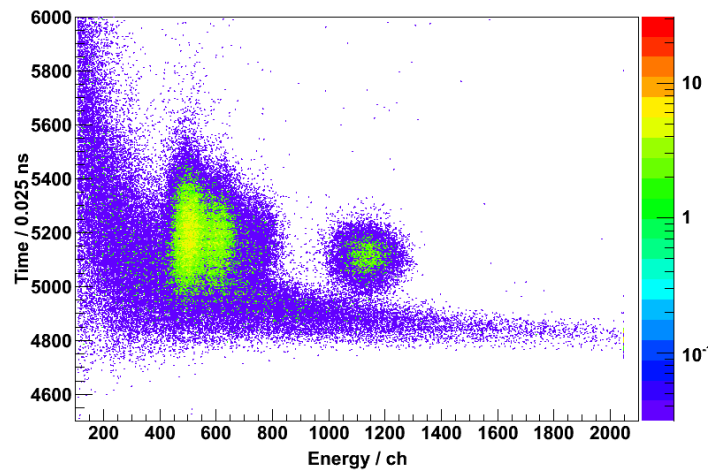
(a)

(b)

(c)

Fig. 2-14. Two-dimensional plots of time versus energy for ^{226}Ra and its decay products in (a) 1 M, (b) 4 M, and (c) 10 M HCl solution samples.
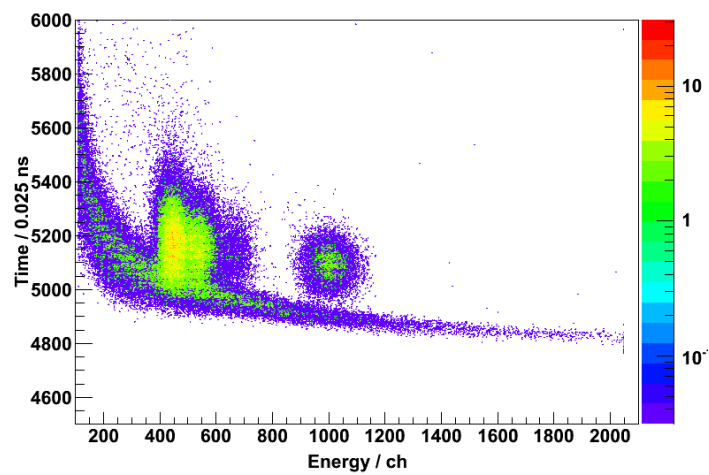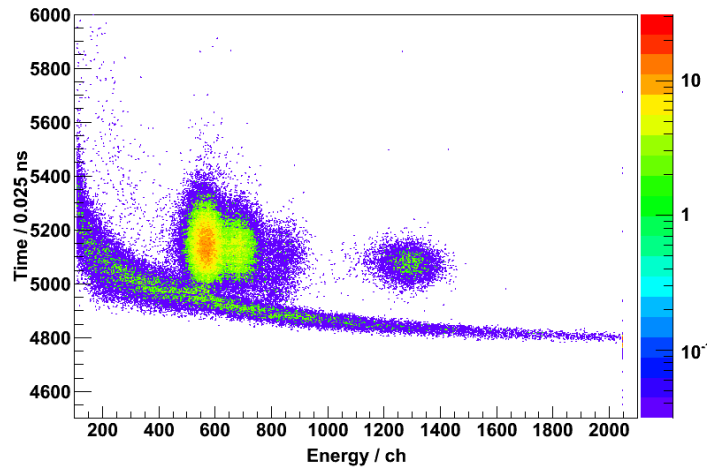
(a)

(b)

(c)

Fig. 2-15. Two-dimensional plots of time versus energy for ^{226}Ra and its decay products in (a) 6 M, (b) 13 M, and (c) 26 M HF solution samples.

(a)

(b)

(c)

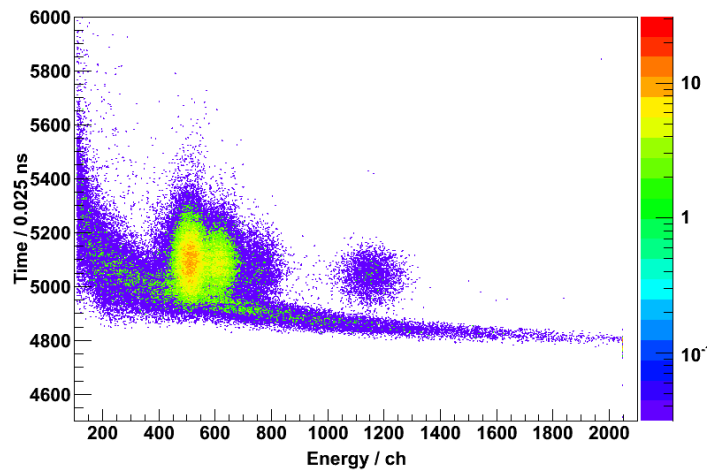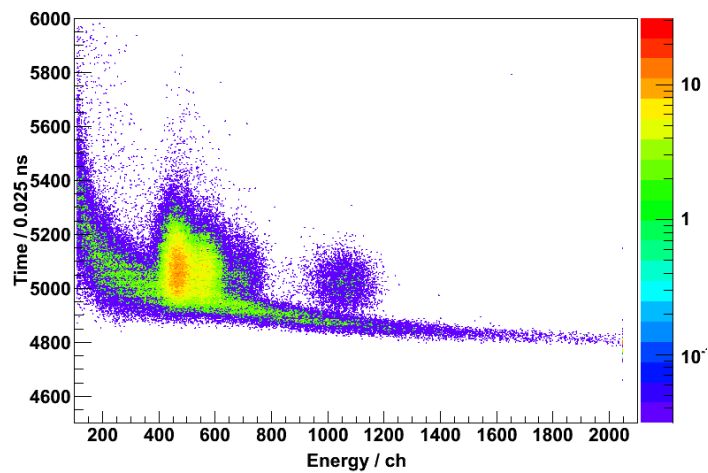Fig. 2-16. Two-dimensional plots of time versus energy for ^{226}Ra and its decay products in (a) 1 M, (b) 4 M, and (c) 8 M KSCN solution samples.
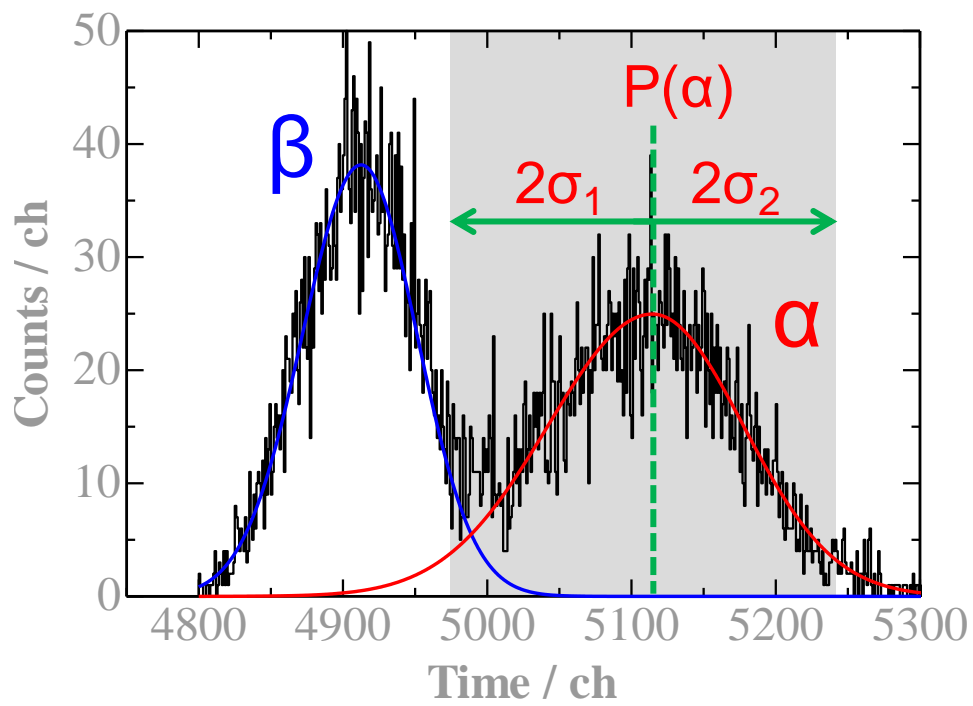
Fig. 2-17. An example of time spectrum which is clipped out in the area of 7.687 MeV α peak of ^{214}Po. The α and β peaks were fitted with asymmetric Gaussian function. The gray band indicates ROI of α-event region.

Table 2-2. Summary of FWHM for 7.687 MeV α peak of ^{214}Po, the difference in fluorescence lifetime between α and β events, and fractions of β component spilled over FWHM for 7.687 MeV α peak of ^{214}Po, the difference in fluorescence lifetime between α and β events, and fractions of β component spilled over into α-event region.

Acid or salt	Concentration [M]	^{214}Po FWHM [keV]	β spillover [%]
HCl	1	431	0.0
HCl	4	444	2.5
HCl	6	461	0.1
HCl	10	736	6.7
HF	3	569	0.007
HF	6	597	0.000
HF	13	618	0.7
HF	26	575	0.010
KSCN	1	515	0.00
KSCN	4	552	0.00070
KSCN	8	609	2.0
HNO_3	1	454	0.0069
HNO_3	2	467	8.3
HNO_3	4	—	74

(a)
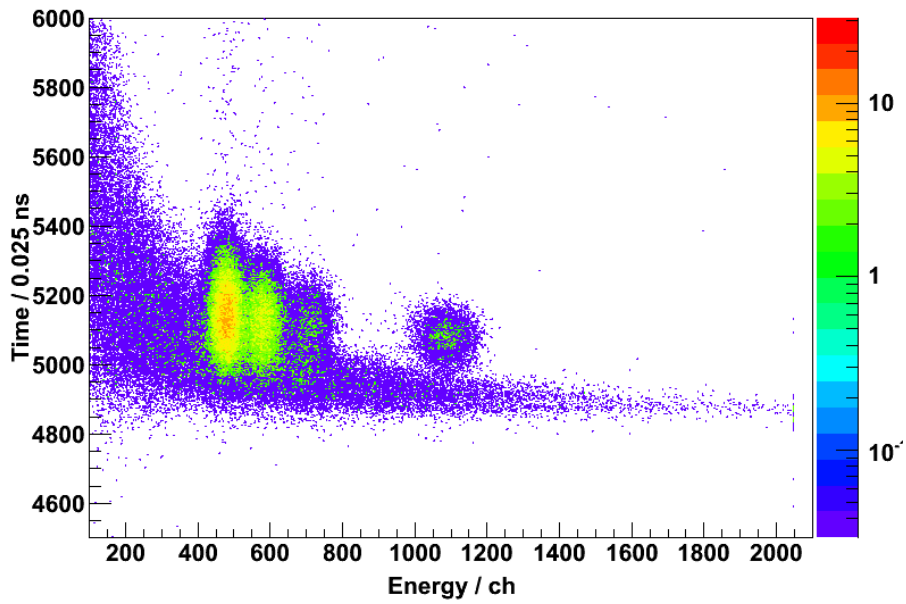
(b)
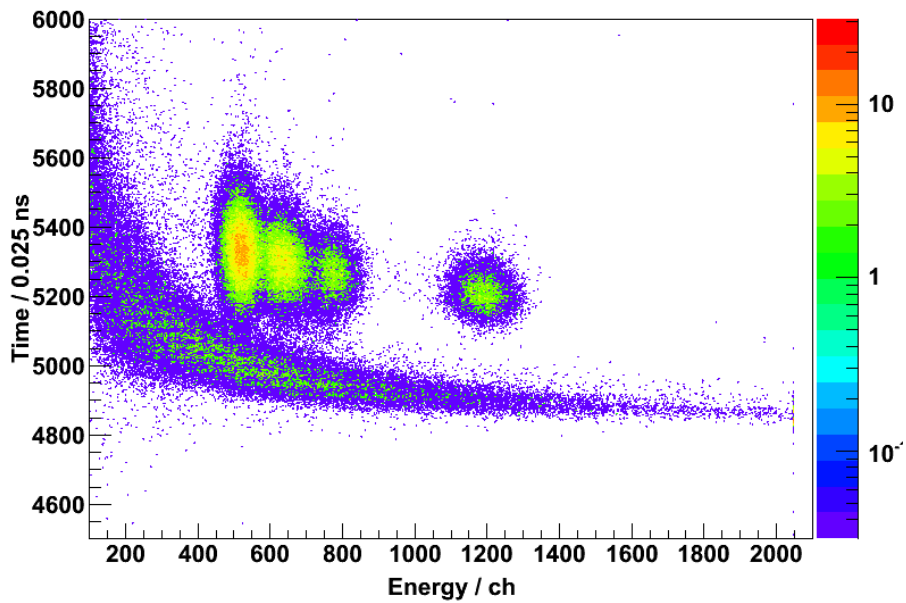
Figs. 2-18. (a) A two-dimensional plot of time versus energy for the sample which contains 50 μL of 4 M HCl solution of ^{226}Ra in 1 mL of the Ultima Gold AB® and (b) that after neutralization by adding 200 μL of 1 M NaOH solution.

(a)

(b)

Fig. 2-19. (a) A two-dimensional plot of time versus energy for the sample which contains 50 μL of 10 M HCl solution of ^{226}Ra in 1 mL of the Ultima Gold AB$^®$ and (b) that after neutralization by adding 50 μL of 10 M NaOH solution.
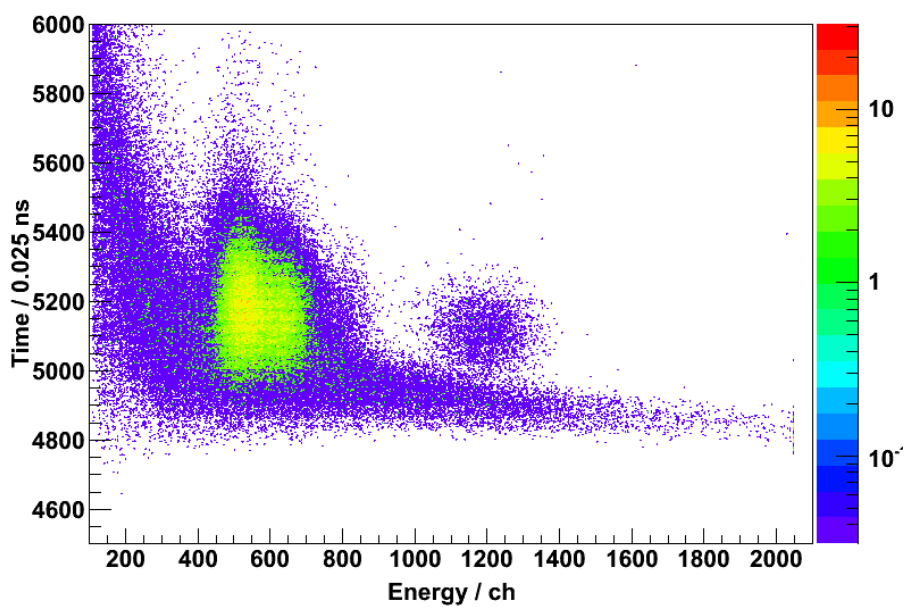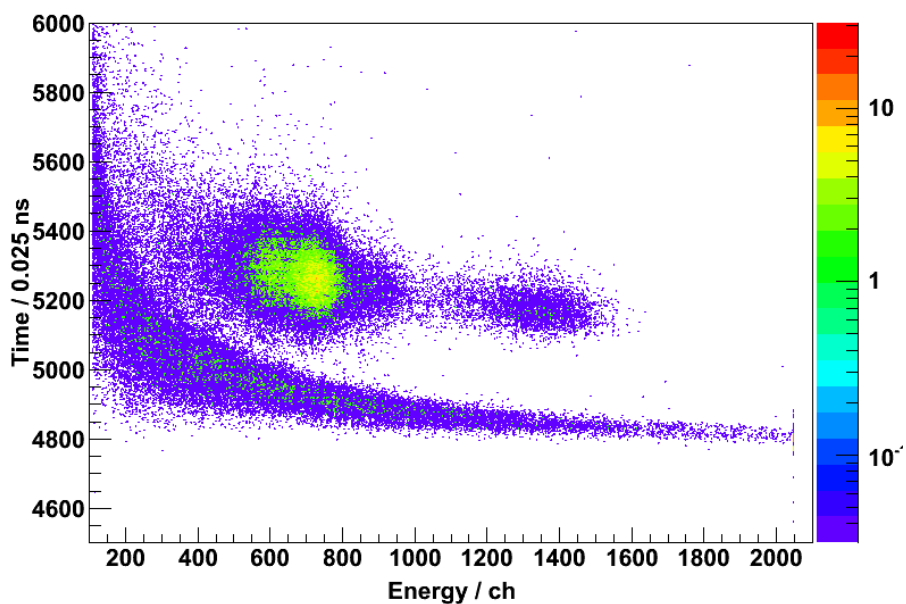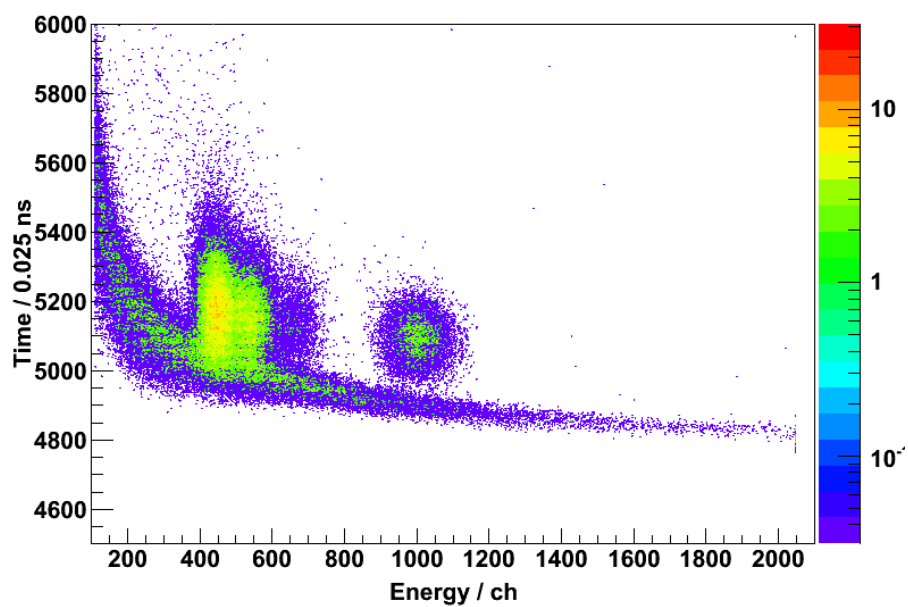
(a)
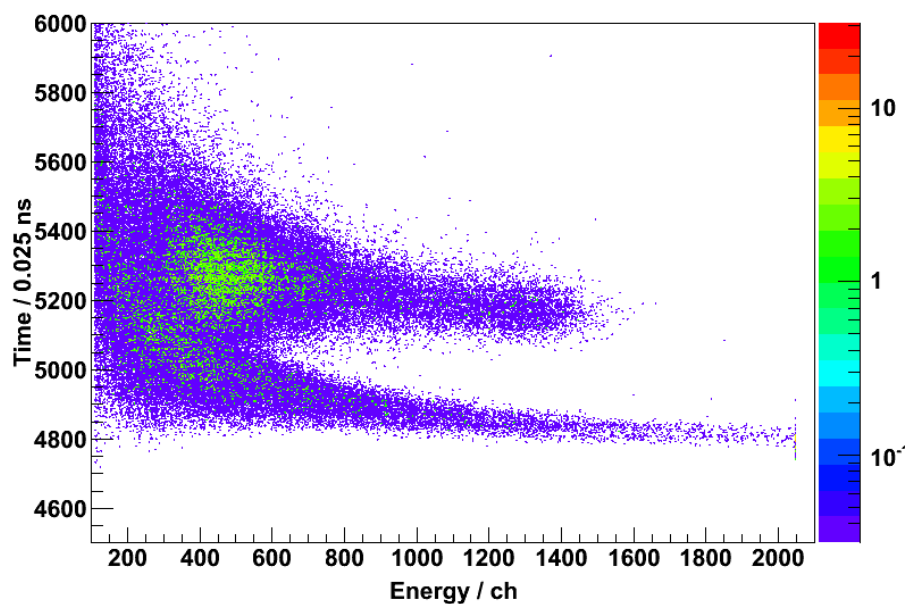

(b)

Fig. 2-20. (a) A two-dimensional plot of time versus energy for the sample which contains 50 μL of 26 M HCl solution of ^{226}Ra in 1 mL of the Ultima Gold AB® and (b) that after neutralization by adding 125 μL of 10 M NaOH solution.

2-6. Practical Application: On-line Measurement of Short-lived α-emitting Nuclide, ^{213}Fr

On-line liquid scintillation measurement of the isotope ^{213}Fr ($T_{1/2}$ = 34.6 s, $E_α$ = 6.78 MeV) was performed with the developed system and ARCA. In this experiment, ARCA was used to dissolve the nuclear reaction products into an aqueous solution and no resins were filled into columns of ARCA. The isotope ^{213}Fr was produced in the ^{209}Bi(^{16}O, $4n$)^{221}Pa reaction using the AVF cyclotron at Research Center for Nuclear Physics (RCNP), Osaka University. The ^{209}Bi target of 0.31 mg/cm^2 thickness was prepared by vacuum deposition of natural Bi onto a 2.2 mg/cm^2-thick titanium backing foil. The 130-MeV ^{16}O beam passed through a titanium vacuum window, helium cooling gas, the titanium target backing, and finally entered the ^{209}Bi target at 120 MeV. The typical beam intensity was 100 pnA. The recoiling products were stopped in helium gas, attached to KCl aerosols generated by sublimation of KCl powder at 620 ∘C, and were continuously transported through a Teflon capillary to a chemistry laboratory by He gas flow at a flow rate of 2.5 L/min.

The nuclear reaction products transported to the chemistry laboratory were identified by α and γ spectrometry with Si semiconductor detectors and Ge detectors, respectively. The transported reaction products attached to KCl aerosols were collected for 1 min on a PET film or a glass filter set in an aerosol-collection apparatus. After the collection, the PET film and the glass filter were subjected to α and γ spectrometry, respectively. An α-particle spectrum for the reaction products with the Si semiconductor detectors is given in Fig. 2-22. In addition to ^{213}Fr, which is the main products, other α-emitting nuclides as ^{211}Fr ($T_{1/2}$ = 3.1 m), ^{212}Fr ($T_{1/2}$ = 20 min), ^{211m}Po ($T_{1/2}$ = 25.2 s) were also

produced. The α disintegration rates of these nuclides after the collection for 1 min were approximately 710 s^{-1} for ^{213}Fr, 10 s^{-1} for ^{211}Fr and ^{212}Fr, 110 s^{-1} for ^{211m}Po. A γ-ray spectrum for the reaction products measured with the Ge detectors is given in Fig. 2-23. In γ-ray spectrum, ^{53m}Fe ($T_{1/2}$ = 2.58 m), ^{53}Fe ($T_{1/2}$ = 8.51 m), ^{52m}Mn ($T_{1/2}$ = 21.1 m), ^{28}Al ($T_{1/2}$ = 2.24 m) were observed.

The experimental setup for on-line liquid scintillation measurement of ^{213}Fr is shown in Fig. 2-21. The transported reaction products were deposited in a collection site of ARCA at first. The collected reaction products were then dissolved in aqueous solution and the solution was delivered to the glass cell set in the detection chamber via the auto selector valve though the Teflon tubes (0.17 mm i.d. × 55 cm length). The Teflon tubes were wrapped in a black vinyl tape and connections between the tubes and valves and between the tubes and the detection chambers were covered with putty for protection of the photomultiplier tubes from light.

Prior to the liquid scintillation measurement, a dissolution efficiency and a dissolution curve of the reaction products were investigated. The dissolution efficiency and the dissolution curve were obtained by monitoring the dissolution behavior of ^{53m}Fe with 701 keV γ rays. The transported reaction products were deposited on the collection site of the ARCA for 1 min. In measurement of the dissolution efficiency, the collected products were dissolved in 0.1 M HNO$_3$/5 × 10^{-3} M HF solution and eluted at a flow rate of 1 mL/min for 12 s. The solution eluted from the outlet of the Teflon tube inserted into the glass cell was collected in a PP tube. The PP tube sample was subjected to γ spectrometry with Ge detectors. The radioactivities in the solution sample were compared to those in the glass filter samples on which the reaction products were collected. The average dissolution efficiency of the reaction products deposited on the

left and right side of the collection site of ARCA was 49 ± 9% and 69 ± 11%, respectively. Therefore, the following experiments were performed using only the right side of the collection site of ARCA. The error values of the dissolution efficiency are standard deviations in four-times trials.

In measurement of the dissolution curve, the collected products were dissolved in 0.1 M HNO_3/5×10^{-3} M HF solution and eluted at a flow rate of 1 mL/min for 30 s. The solution eluted from at the outlet of the Teflon tube inserted into the glass cell was collected for every 3 s (which corresponds to approximately 50 μL) in 10 PP tubes. Each tube sample was subjected to γ spectrometry with Ge detectors. The dissolution curves of the reaction products are given in Figs. 2-24 (a) and (b). It was found that the almost all reaction products enter into the glass cell in 10 s with the elution volume of 150–160 μL from the start of the dissolution.

In on-line liquid scintillation measurement of ^{213}Fr, the reaction products were deposited on the collection site of the ARCA for 1 min. During the collection of the reaction products, 4 mL of the Ultima Gold AB® was injected into the cell via the auto selector valve through a black Teflon tube (2-mm i.d.) for 8.3 s. The collected products on ARCA were then dissolved in 0.1 M HNO_3/5×10^{-3} M HF solution and delivered to the glass cell via another auto selector valve through a Teflon tube at a flow rate of 1 mL/min for 12 s, being mixed with the Ultima Gold AB® in the cell. Liquid scintillation measurement was performed for 122 s after the mixing. Start of the measurement was approximately 15 s after the end of collection. After the measurement, the solution in the cell was drained for 30 s and the 4 mL of the Ultima Gold AB® was newly injected into the cell for the next measurement. Each measurement was performed alternately with the two detection chambers. These procedures were automatically repeated for

approximately 2 hours.

Two-dimensional plots of time versus energy for the reaction products obtained with the detection chamber 1 and 2 are given in Fig. 2-25 (a) and (b), respectively. It is observed that α events are discriminated from β events. Variation of the center position of the α peak in the pulse height spectra during the repeated measurement is shown in Fig. 2-26. The peak position is almost constant. It indicates that the aqueous solution sample and the Ultima Gold AB® were stably supplied to the cell with constant volumes in every cycle of the measurement. Due to the constant volume ratio of the aqueous solution sample to the Ultima Gold AB®, the degree of quenching was kept constant during the repeated measurement. In 9th, 10th, 11th, and 49th cycle, the volume of the aqueous solution sample may have been smaller than usual. In another possibility, the volume of the Ultima Gold AB® may have been larger than usual. Consequently, the peak position (which corresponds to the amount of photons emitted from the scintillator) may shifts to higher energy region due to the decrease of quenching. Variation of the α counts of ^{213}Fr during the repeated measurement is given in Fig. 2-27. The α counts vary in each cycle of the measurement, which seems to be mainly attributed to the variation of the dissolution efficiency of the reaction products.
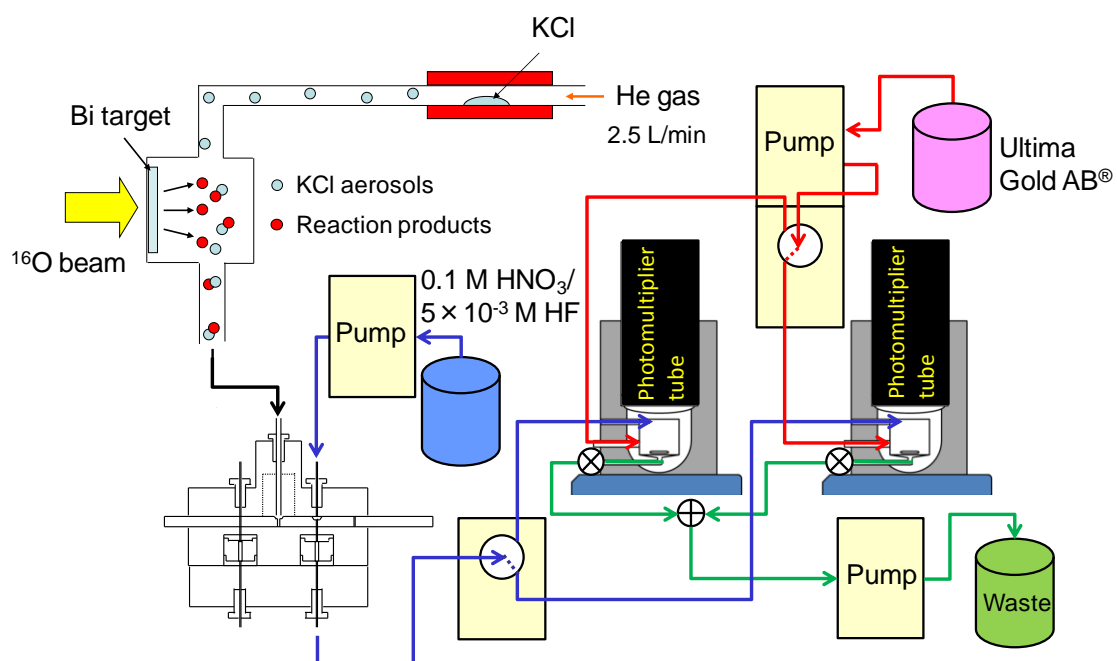
Fig. 2-21. The experimental setup for on-line liquid scintillation measurement of ^{213}Fr.
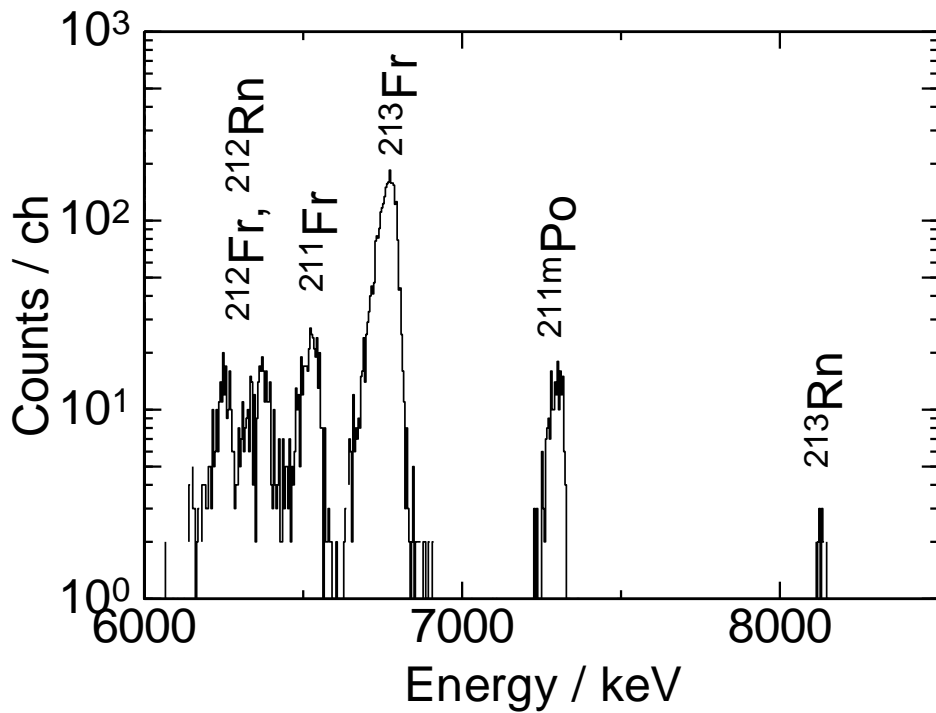
Fig. 2-22. An α-particle spectrum for the reaction products with the Si semiconductor detectors. Collection time: 60 s. Cooling time: 66 s. Measurement time: 181 s.
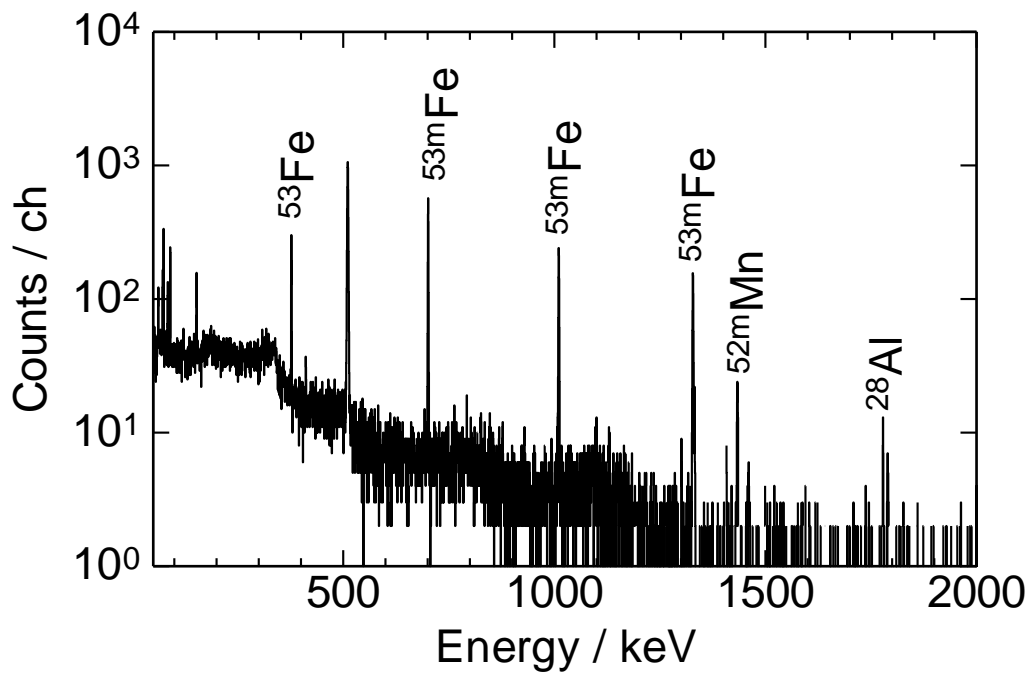
Fig. 2-23. A γ-ray spectrum for the reaction products measured with the Ge detectors. Collection time: 60 s. Cooling time: 59 s. Measurement time: 300 s.

(a)
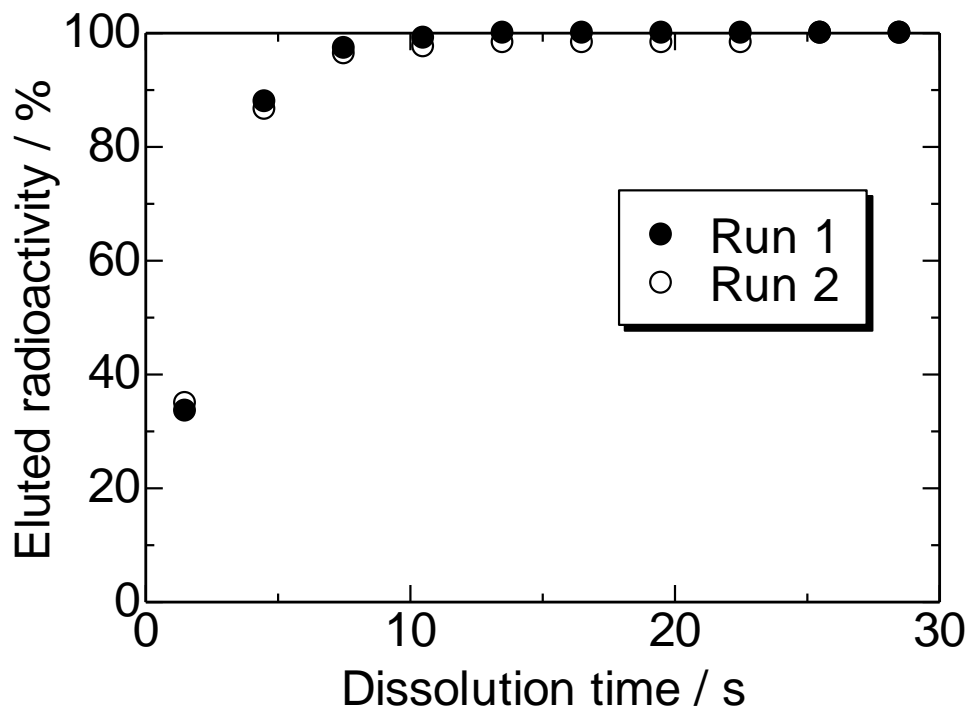
(b)
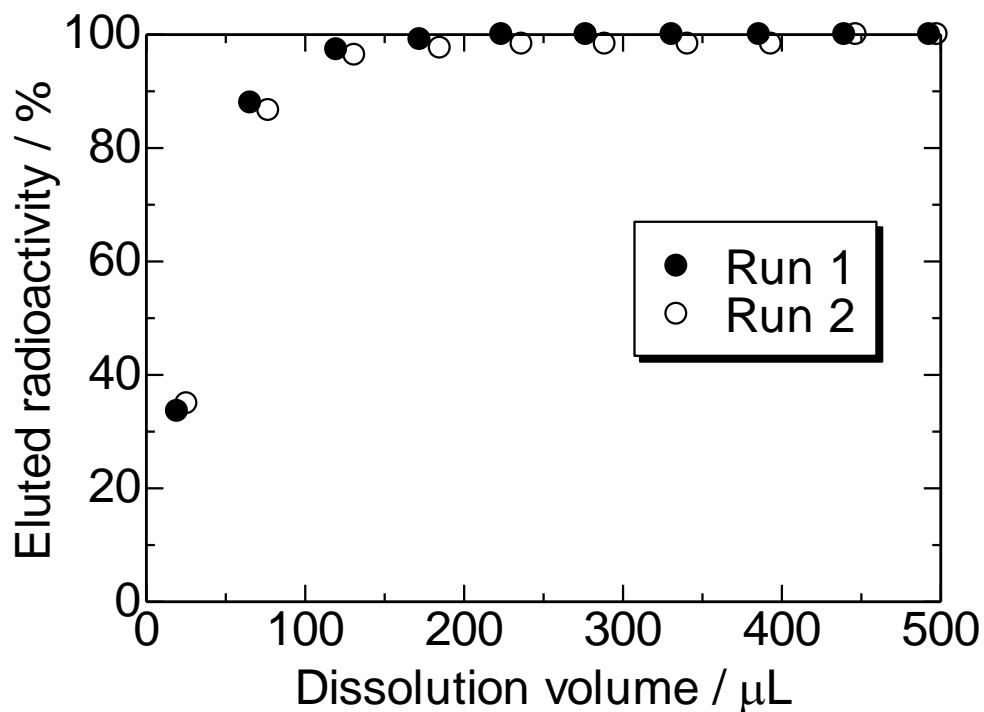
Figs. 2-24. Cumulative dissolution curves of the nuclear reaction products obtained at the outlet of the Teflon tube inserted into the glass cell at a flow rate of 1 mL/min. The eluted radioactivity is plotted against (a) dissolution time or (b) dissolution volume.

(a)
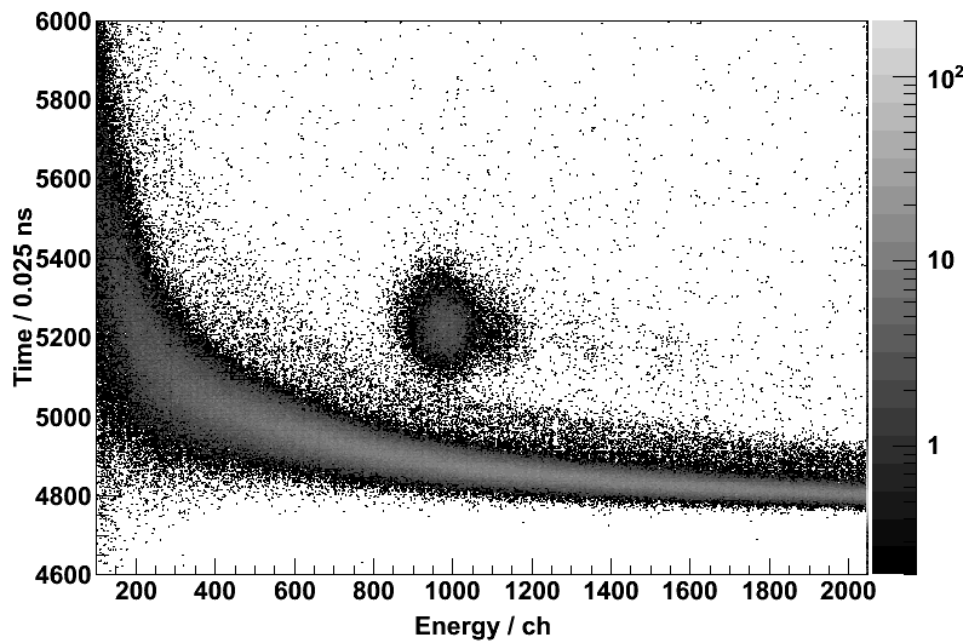
(b)
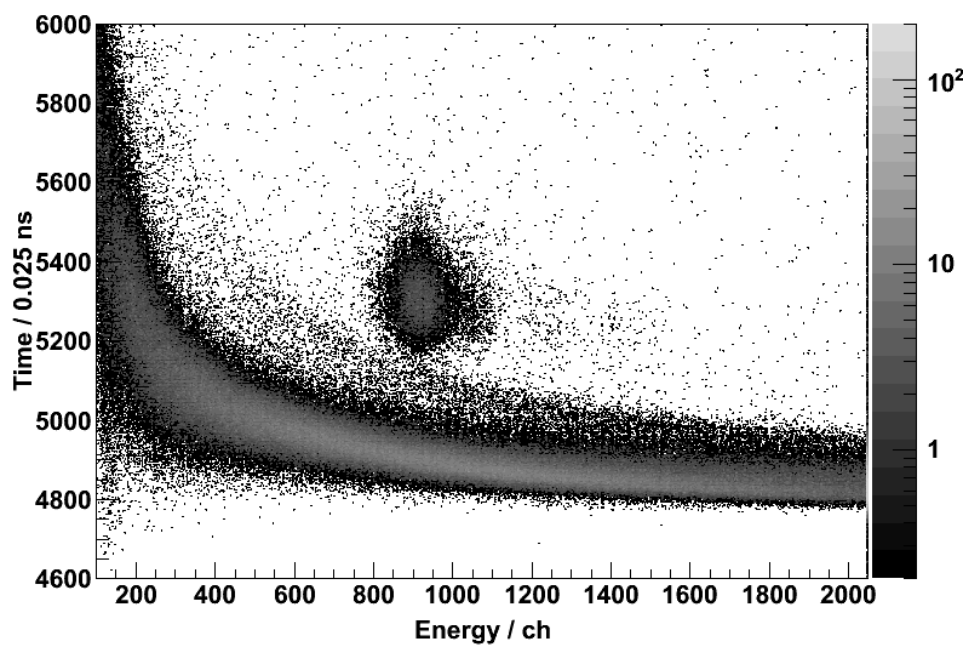
Fig. 2-25.   Two-dimensional plots of time versus pulse height for the nuclear reaction products obtained with (a) the detection chamber 1 and (b) the detection chamber 2. Start of measurement of the products was approximately 15 s after the end of collection. Measurement time was 122 s.
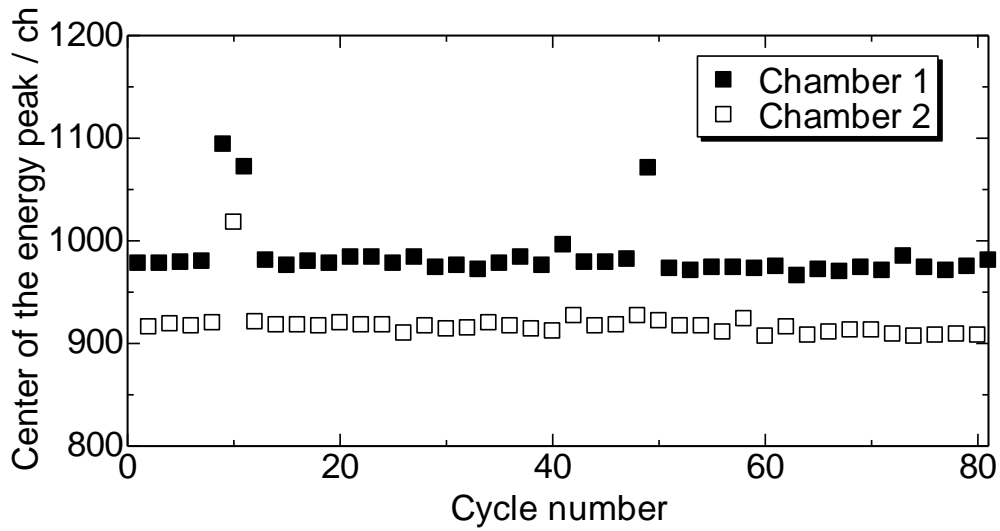
Fig. 2-26. Variation of the center position of the α peak in the pulse height spectra during the repeated measurement.
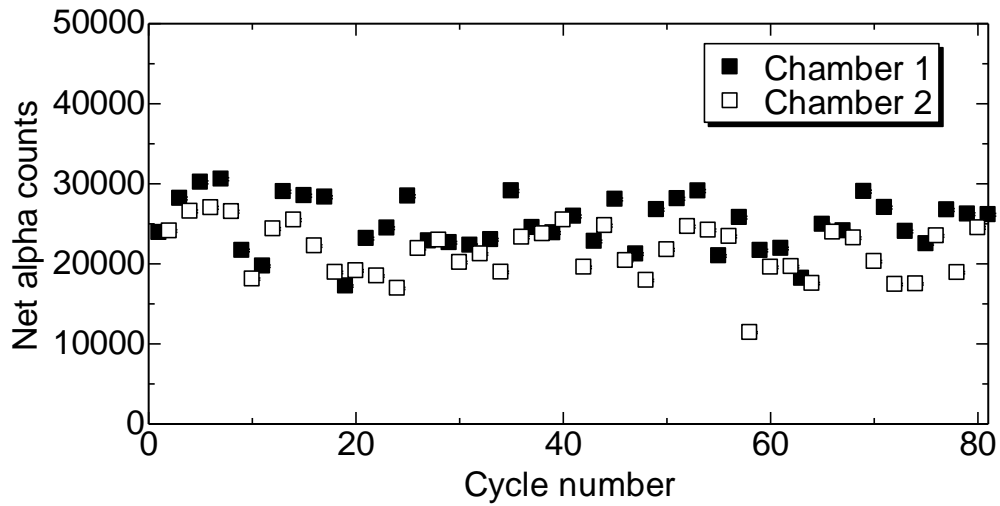
Fig. 2-27. Variation of the α counts of ^{213}Fr during the repeated measurement.

2-7. Discussion

The liquid scintillation detection system presented in this work has advantages over the Si semiconductor detector as follows; high detection efficiency, fast sample preparation, and acceptance of solution samples which contains relatively high concentration of salts or extractants. The detection efficiency of α particles and SF fragments of the developed liquid scintillation detection system is almost 100% while that of the Si semiconductor detector is approximately 35%. The high detection efficiency of the liquid scintillation detection system is especially favorable in the detection of successive α-α-α or α-SF decay chains (sometimes called "time-correlated events") originating from $^{265}Sg^a$ and $^{265}Sg^b$, respectively (see Fig. 2-1). To detect such decay chains provides strong reliability in the identification of the transactinide elements. Next, the developed detection system has achieved fast sample preparation which takes as short as 1 s after the end of chemical separation whereas the Si semiconductor detector takes approximately 20–30 s for evaporation of the solution sample. In addition, the liquid scintillation detection system presented in this work is applicable to the solution sample which contains relatively high concentration of salts or extractants as far as the degree of quenching is acceptable. Such solution sample cannot be applied in α and SF spectrometry with the Si semiconductor detector because evaporation residues cause self-absorption of α particles and SF fragments.

In order to use the liquid scintillation detection system in the chemical experiments of Rf, Db, and Sg, low background conditions are necessary because of its relatively poor energy resolution and high sensitivity to β particles and γ rays as well as α particles. We are planning to remove radioactive by-products using the GARIS gas-jet system as a

preseparator in the chemical experiments. Recently, the isotopes [261]Rf, [262]Db, and [265]Sg[a,b] were successfully transported to a chemistry laboratory under low background condition using the GARIS gas-jet system [9–12].

Expected detection rates in the chemical experiments of [261]Rf, [262]Db, and [265]Sg[a,b] with the present detection system and the GARIS gas-jet system are given in Table 2-3. The experimental conditions are assumed as follows; the target thickness: 200 μg/cm^2, beam intensity: 4 pμA, transport efficiency of GARIS: 8, 9.2, and 15% for [261]Rf, [262]Db, and [265]Sg[a,b], respectively, transparency of support mesh for a 0.54-μm thin Mylar window in GARIS: 84%, gas-jet efficiency: 50%, transport time of the reaction products to the chemistry laboratory: 2.7 s, collection time of the reaction products: 30 s, dissolution and chemical separation time: 12 s, sample preparation time after the end of the chemical separation: 1 s, chemical yield: 50%, and detection efficiency: 100%. It shows a sufficient detection rates for [261]Rf. As for [262]Db, the detection rate is considered to be acceptable to perform chemical experiments for several days. As for [265]Sg[a,b], the detection rates are quite as small as total 2.5 events/d. However, when a Si semiconductor detector was used, the detection rates of [265]Sg[a] and [265]Sg[b] are assumed to be 0.046 and 0.23 events/d, respectively, with the detection efficiency for α particles and SF fragments: 35% and the sample preparation time: 20 s. In the previous aqueous chemical studies of Sg with ARCA and the Si semiconductor detector [29, 30], α particles originating from Sg were not directly detected and the detection were hindered with large amounts of radioactivity from by-products. By using the liquid scintillation detection system and GARIS gas-jet system, the decay sequence of Sg would be effectively detected under low background condition.

The liquid scintillation detection system used in SISAK system, which were

developed to perform α and SF spectroscopy on the continuously flowing solution at high flow rates (0.5–2.0 mL/s) after liquid-liquid extraction, activity remaining in the aqueous phase was not measured or measured by transferring into organic phase after the second extraction step [21]. In contrast, the liquid scintillation detection system presented in this work allows to direct detection of α particles and SF fragments in aqueous solution samples (as far as the degree of quenching is acceptable) by using the emulsifier scintillator. Therefore, this system would be applicable to column chromatography and liquid-liquid experiments by connecting with column chromatography apparatus such as ARCA and liquid-liquid extraction apparatus based on microchip, respectively.

Table 2-3. Estimation of the detection rates of ^{261}Rf, ^{262}Db, and ^{265}Sg[a,b] with the present detection system using GARIS gas-jet system as a preseparator.

Nuclide	$T_{1/2}$ [s]	σ [nb]	Beam [pμA]	Coll. time [s]	GARIS eff. [%]	Chem. time [s]	Prep. time [s]	Det. eff. [%]	Det. rates [events/d]
^{261}Rf[a]	68	13	4	30	8	10	1	100	171
^{262}Db	34	2.1	4	30	9.2	10	1	100	24
^{265}Sg[a]	8.5	0.18	4	30	15	10	1	100	0.73
^{265}Sg[b]	14.4	0.2	4	30	15	10	1	100	1.8

2-8. Conclusion

An on-line liquid scintillation detection system with α/β discrimination capability has been developed for aqueous chemical studies of the transactinide elements. The presented system allows to detect α particles and SF fragments in aqueous solution sample with almost 100% detection efficiency. The aqueous solution sample can be subjected to α/SF spectrometry in a few seconds after the end of the chemical separation. In the on-line measurement of the isotope ^{213}Fr ($T_{1/2} = 34.6$ s) with the detection system coupled to ARCA, procedures of the collection of the reaction products, dissolution into the aqueous solution, mixing with the liquid scintillator and liquid scintillation detection were automatically repeated with good stability. Start of the measurement of the reaction products was approximately 15 s after the end of collection. The developed system would be used in column chromatography or liquid-liquid extraction experiments of Rf, Db, and Sg by using the GARIS gas-jet system as a preseparator.

Chapter 3

On-line Liquid Scintillation Measurement of ^{262}Db Preseparated with GARIS Gas-jet System

3-1. Introduction

We have developed an on-line liquid scintillation detection system to detect α particles and spontaneous fission (SF) fragments in solution samples for aqueous chemical studies of Rf, Db, and Sg. Liquid scintillation counting has advantages of high detection efficiency of α particles and fission fragments and rapid sample preparation. On the other hand, liquid scintillation counting has problems such as relatively poor energy resolution compared to a Si semiconductor detector and interference from β particles, γ rays, and neutrons. Therefore, detection of time-correlated events of α particles and fission fragments emitted by sequential decay of the transactinide elements under low background condition is required for reliable identification of the nuclide.

Recently, a technique of physical preseparation of the transactinide elements from large amounts of radioactive by-products has been developed for chemical studies of the transacninides. In the RIKEN linear accelerator (RILAC) facility, a gas-jet transport system has been installed behind the gas-filled recoil ion separator (GARIS) and the isotopes ^{261}Rf ($T_{1/2}$ = 68 s) [10], ^{265}Sg^{a,b} ($T_{1/2}$ = 8.5 s/14.4 s) [11], and ^{262}Db ($T_{1/2}$ = 34 s) [12] were successfully extracted to a chemistry laboratory. We are planning to use the GARIS gas-jet system as a preseparator in chemical experiments of the transactinides to attain low background condition in liquid scintillation measurement.

In this work, we performed on-line liquid scintillation measurement of ^{262}Db produced in the ^{248}Cm(^{19}F, $5n$)^{262}Db reaction and preseparated with the GARIS gas-jet system to evaluate the background count rate for the detection of time-correlated α-α events from ^{262}Db and the daughter nuclide ^{258}Lr ($T_{1/2}$ = 3.8 s). Decay patterns of ^{262}Db [12] are shown in Fig. 3-1.
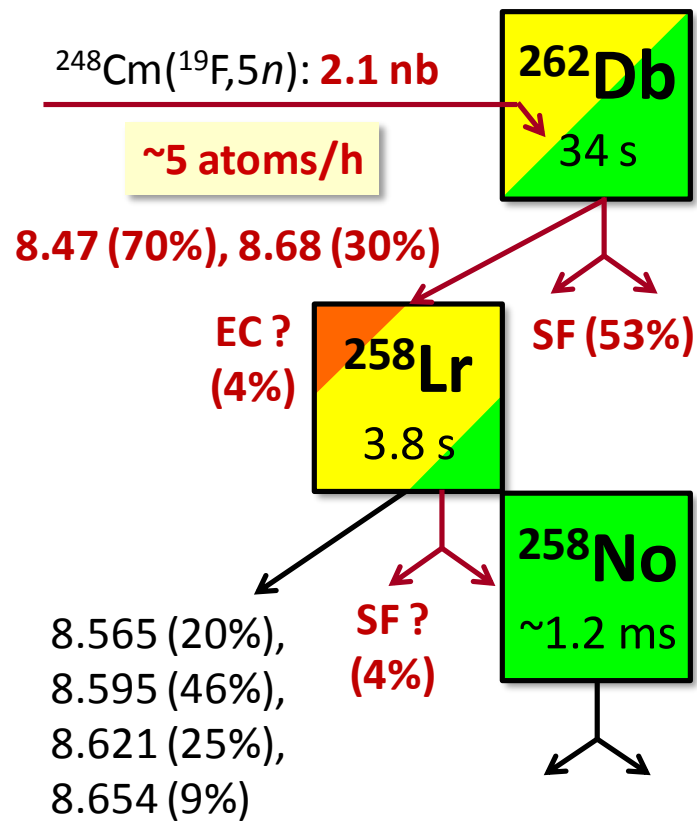
Fig. 3-1. Decay patterns of ^{262}Db [12].

3-2. Experimental

3-2-1. Setup for Production and Transport of ^{262}Db by GARIS Gas-jet system

Experiments were performed in the RIKEN linear accelerator (RILAC) facility. A schematic of the beam line in the RILAC is shown in Fig. 3-2. A schematic of the GARIS gas-jet system and a rotating wheel system for measurement of α and spontaneous fission decays (MANON) is shown in Fig. 3-3.

3-2-2. Setup for On-line Liquid Scintillation Measurement

On-line liquid scintillation measurement of the isotope ^{262}Db was performed with the developed system coupled to a liquid chromatography apparatus, ARCA [13]. In this experiment, ARCA was used to dissolve the nuclear reaction products into an aqueous solution and no resins were filled into columns of ARCA. The experimental setup for the on-line liquid scintillation measurement is given in Fig. 3-4. The transported reaction products were deposited in a collection site of ARCA at first. The collected reaction products were then dissolved in aqueous solution and the solution was delivered to the glass cell set in the detection chamber via the auto selector valve though the Teflon tubes (0.17 mm i.d. × 55 cm length). The Teflon tubes were wrapped in an alminum tape and connections between the tubes and valves and between the tubes and the detection chambers were covered with putty for protection of the photomultiplier tubes from light. Large amounts of fast neutrons and γ rays are generated and are spread over the chemistry laboratory under beam irradiation because the chemistry laboratory

is next to the irradiation room as shown in Fig. 3-2. Fast neutrons and γ rays generate recoil protons and electrons by interacting with the liquid scintillator, respectively. Recoil protons are observed in α-event region in the two-dimensional plot of fluorescence lifetime versus energy for pulse shape α/β discrimination, which interfere the detection of α particles. Thus, the detection chambers were shielded with polyethylene blocks against fast neutrons as shown in Fig. 3-4 (b).
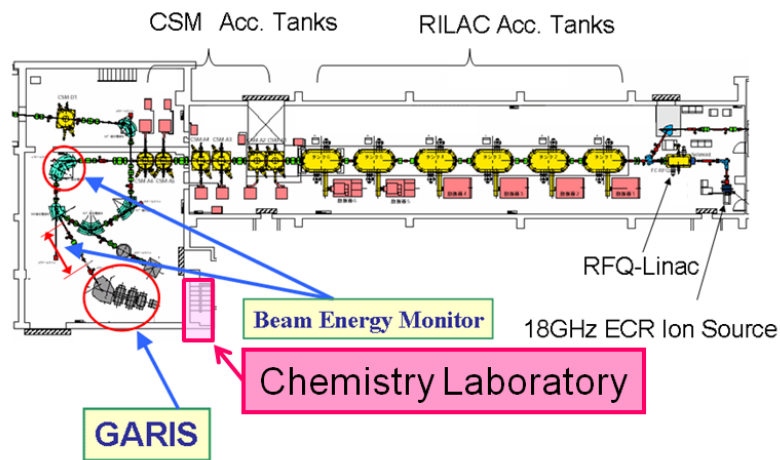
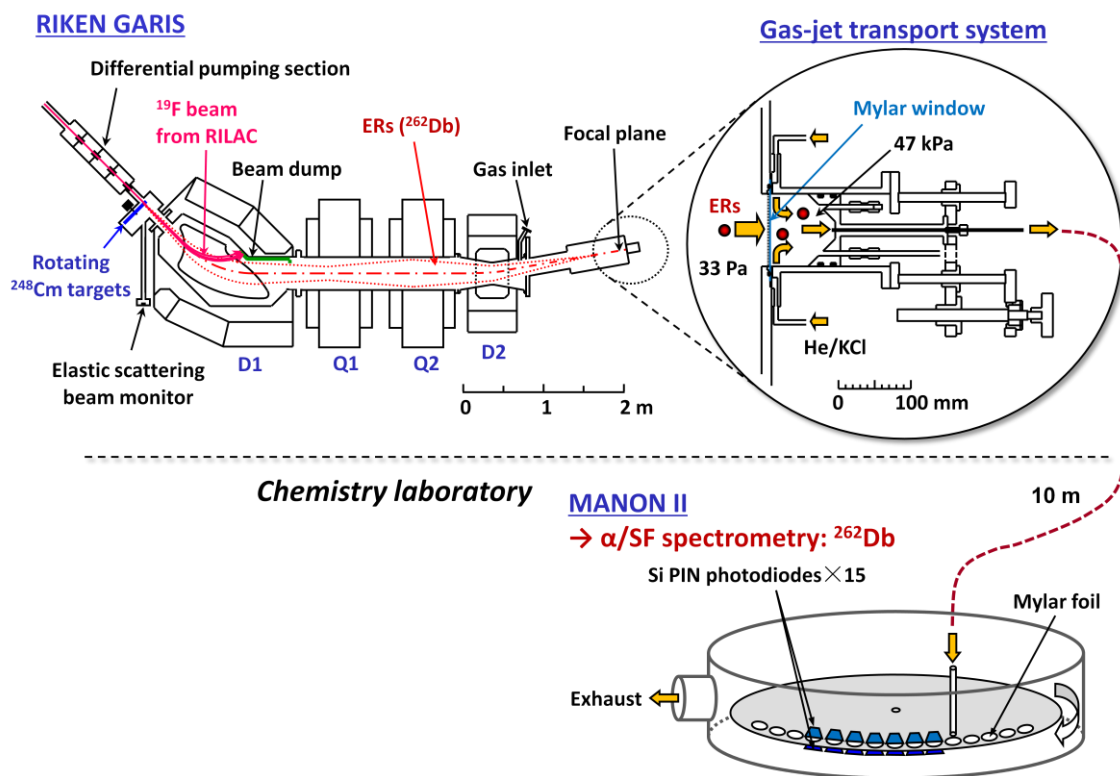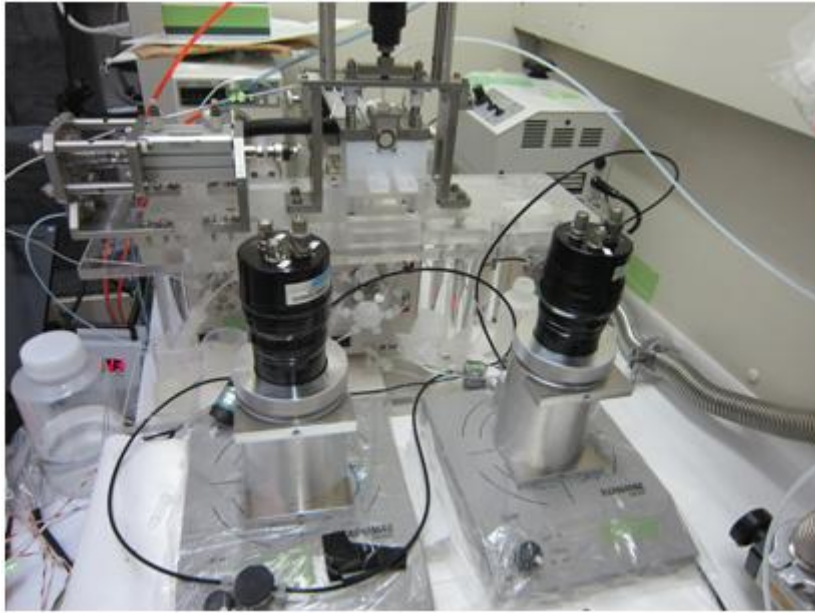Fig. 3-2. A schematic of the beam line in the RILAC.

Fig. 3-3. A schematic of the GARIS gas-jet system and the rotating wheel system MANON for α and SF spectrometry.
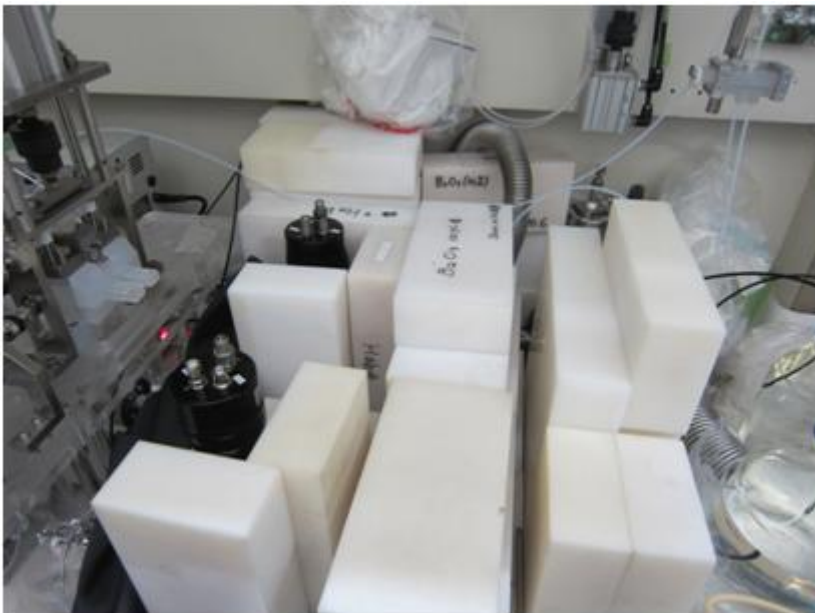
(a)

(b)

Fig. 3-4. Experimental setup for the on-line liquid scintillation measurement.

3-2-3. Data Acquisition System for Liquid Scintillation Measurement

In this experiment, a four-channel pulse shape discrimination module, MPD-4 [34], was used to discriminate α/β events and SF/β events. A detailed description about MPD-4 is given in appendix 3. The anode signal of the photomultiplier tube was divided into two identical signals using a signal divider. These signals were deliverd to the input of the MPD-4 and were set different gains for measurement of α-energy and SF-energy region, respectively. Both the amplitude (energy) and the time-to-amplitude converter (TAC) outputs of MPD-4 were recorded with A3100 for two-dimensional analysis of TAC versus energy. Each event was registered by list mode to obtain the time information when the event occurs. 5 V TTL signals which indicate the start and stop of the liquid scintillation measurement were input to A3100. The block diagram of data acquisition system for liquid scintillation measurement is shown in Fig. 3-5.

3-2-4. Energy Calibration of Liquid Scintillation Detectors

Energy calibration of the detectors was performed to determine region of interest (ROI) for α, β, and SF events using ^{226}Ra and ^{252}Cf as α and SF sources, respectively. These samples were prepared by 200 μL of stock solutions of ^{226}Ra or ^{252}Cf dissolved in 0.1 M HNO$_3$/5 × 10^{-3} M HF solution with 4 mL of the Ultima Gold AB. Examples of two-dimensional plot for ^{226}Ra and ^{252}Cf are given in Fig. 3-6 and 3-7, respectively. Energy axis is converted from channel to α energy. The energy resolution of the detection chamber 1 was approximately 560 keV FWHM for 7.687 MeV α peak of ^{214}Po. That of the detection chamber 2 was approximately 584 keV FWHM.
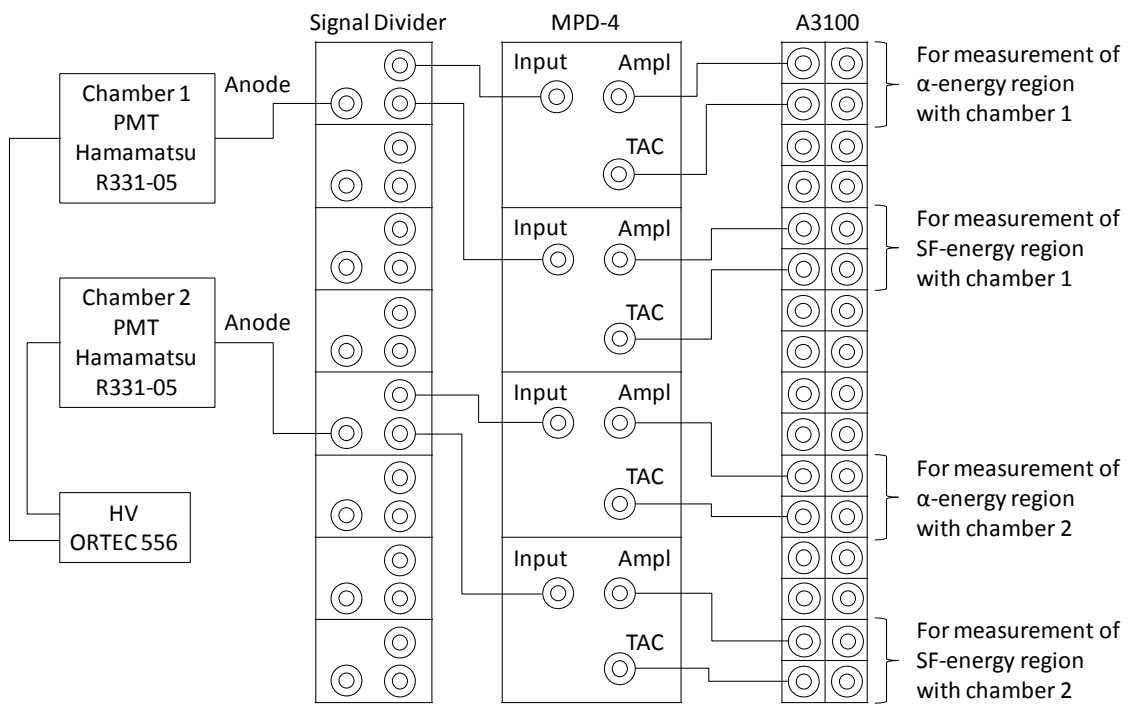
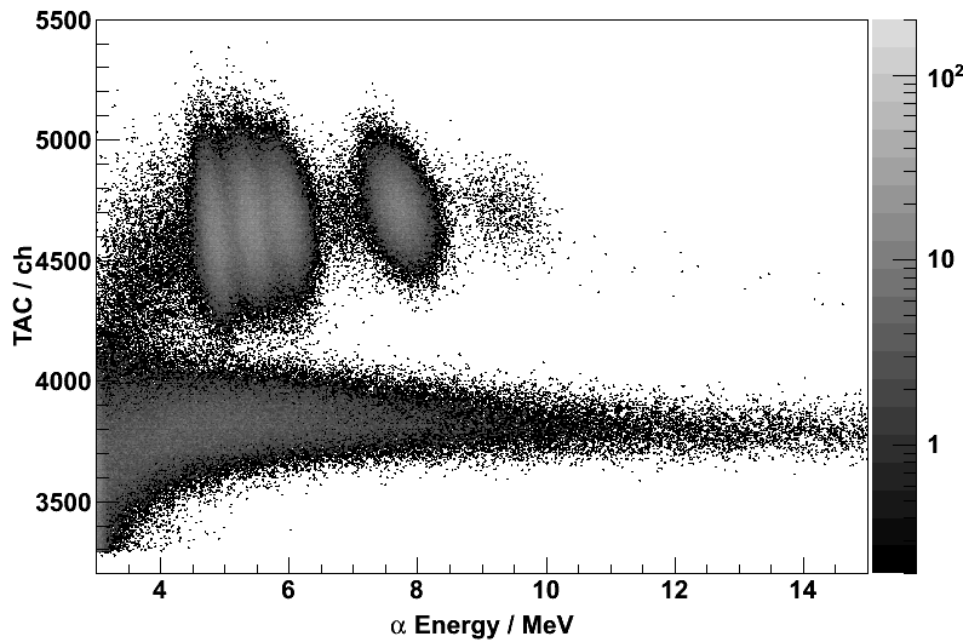Fig. 3-5. The block diagram of data acquisition system for liquid scintillation measurement.

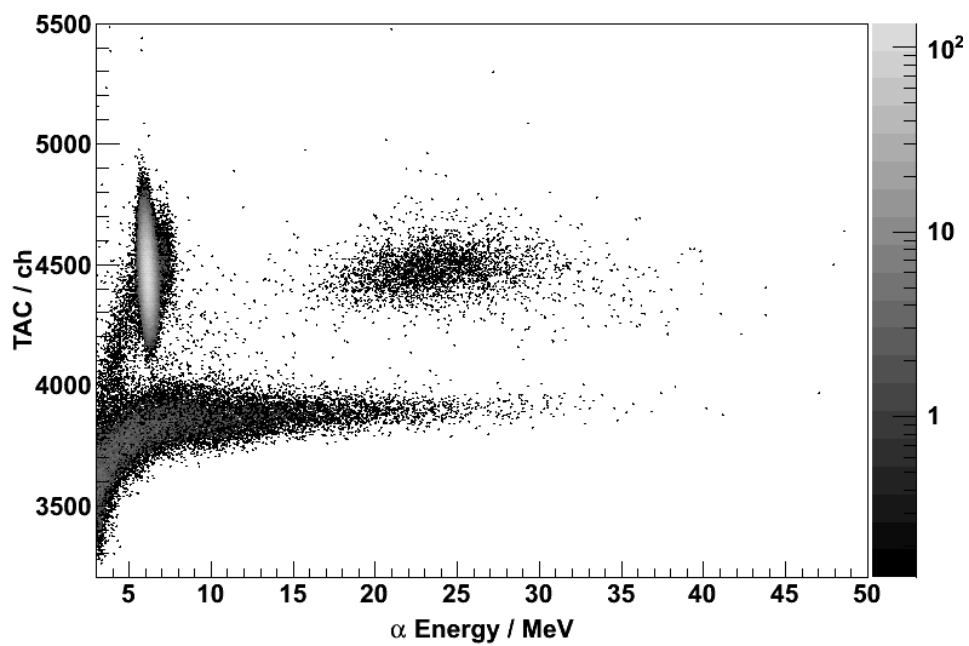Fig. 3-6. A two-dimensional plot of TAC versus energy for ^{226}Ra and its decay products.

Fig. 3-6. A two-dimensional plot of TAC versus energy for ^{252}Cf.

3-2-5.   Production and Transport of ^{262}Db by GARIS Gas-jet System

The isotope of element 105, dubnium (^{262}Db, $T_{1/2}$ = 34 s) was produced in the ^{248}Cm(^{19}F, 5n)^{262}Db reaction. The ^{19}F^{9+} ion beam was extracted from the RILAC. A ^{248}Cm$_2$O$_3$ target of 290 μg/cm^2 thickness was prepared by electrodeposition onto a 0.90 mg/cm^2 Ti backing foil. The eight arc-shaped targets were mounted on a rotating wheel of 100 mm in diameter. The wheel was rotated during the irradiation at 1000 rpm. The beam energy was 103.1 MeV at the middle of the target, and the average beam intensity was 3 particle μA. GARIS was filled with helium at a pressure of 33 Pa. The magnetic rigidity of GARIS was set at 1.92 Tm. The evaporation residues of interest were separated in-flight from the beam and the majority of the nuclear transfer products by GARIS and then guided into the gas-jet chamber of 100-mm i.d. × 20-mm depth through a Mylar window of 0.54-μm thickness which was supported by a honeycomb-hole grid with 84% transparency. The ^{262}Db atoms were stopped in helium gas, attached to KCl aerosol particles, and were continuously transported through a Teflon capillary (2.0-mm i.d. × 10-m length) to the rotating wheel apparatus MANON for α spectrometry. The flow rate of the helium gas was 2 L/min, and the inner pressure of the gas-jet chamber was 47 kPa. In MANON, the aerosol particles were deposited on 200-position Mylar foils of 0.5-μm thickness placed at the periphery of a 420-mm diameter stainless steel wheel. The wheel was stepped at 15.5-s intervals to position the foils between 15 pairs of Si PIN photodiodes (Hamamatsu S3204-09). Each detector had an active area of 18 × 18 mm^2 and a 38% counting efficiency for α particles. The energy resolution was approximately 50 keV FWHM for the detectors which look at the sample from the collection side. All events were registered in an event-by-event mode.

3-2-6.   On-line Liquid Scintillation Measurement

(a) Blank Samples

To evaluate background count rate derived from fast neutrons and γ rays generated by beam irradiation, blank samples were measured under the beam on and beam off condition. The blank sample was prepared by mixing 200 μL of 0.1M $HNO_3/5 \times 10^{-3}$ M HF solution with 4 mL of the Ultima Gold AB®. Beam intensity and magnetic rigidity of GARIS during the measurement of the blank samples are listed in Table 3-1.

(b) Reaction Products

The isotope ^{262}Db was produced and transported to the chemistry laboratory by the GARIS gas-jet system as described in section 3-2-5. The magnetic rigidity of GARIS was set at 1.92 Tm where provides maximum yield of ^{262}Db. The reaction products preseparated and transported by the GARIS gas-jet system were deposited for 70 s on the collection site of ARCA. The collected products were then dissolved in 0.1 M $HNO_3/5 \times 10^{-3}$ M HF solution and the solution was transferred to the glass cell set in the detection chamber at a flow rate of 1 mL/min for 12 s. The solution was mixed with 4 mL of the Ultima Gold AB®, and then measured for 108 s. The measurement of the reaction products was started approximately 15 s after the end of collection. After the measurement, the solution in the cell was drained and the 4 mL of the Ultima Gold AB® was newly injected into the cell for the next measurement. Each measurement was performed alternately with two detection chambers. These procedures were

automatically repeated. The time sequence of experimental procedures of the on-line liquid scintillation measurement is given in Fig. 3-7. Beam intensity and repeated cycle number during the on-line liquid scintillation measurement of the reaction products are listed in Table 3-2.

Table 3-1. Beam intensity and magnetic rigidity of GARIS during the measurement of the blank samples.

Run	Beam on/off	Magnetic rigidity [Tm]	Beam intensity [pμA]	Measurement time [s]	Dose [10^{17}]
Blank_1	on	1.92	2.79	19104.4	3.32
Blank_2	on	1.92	2.65	18917.4	3.13
Blank_3	on	1.92	2.62	27003.1	4.41
Blank_4	on	1.80	2.60	1744.3	0.28
Blank_5	on	1.80	2.51	24074.4	3.78
Blank_6	on	2.05	2.33	28916.9	4.20
Blank_7	on	2.05	3.01	27318.0	5.13
Blank_8	off	—	—	2778.0	—
Blank_9	off	—	—	29524.4	—
Blank_10	off	—	—	109950.9	—

Table 3-2. Beam intensity and repeated cycle number during the on-line liquid scintillation measurement of the reaction products.

Run	Beam intensity [pμA]	Experiment time [s]	Repeated cycle number
Db_1	2.72	2119.8	12
Db_2	2.64	6760.0	40
Db_3	2.61	797.3	3.5
Db_4	2.56	7242.9	42.5
Db_5	2.42	7369.6	43.5
Db_6	2.67	1845.9	9.5
Db_7	2.67	4707.5	27.5
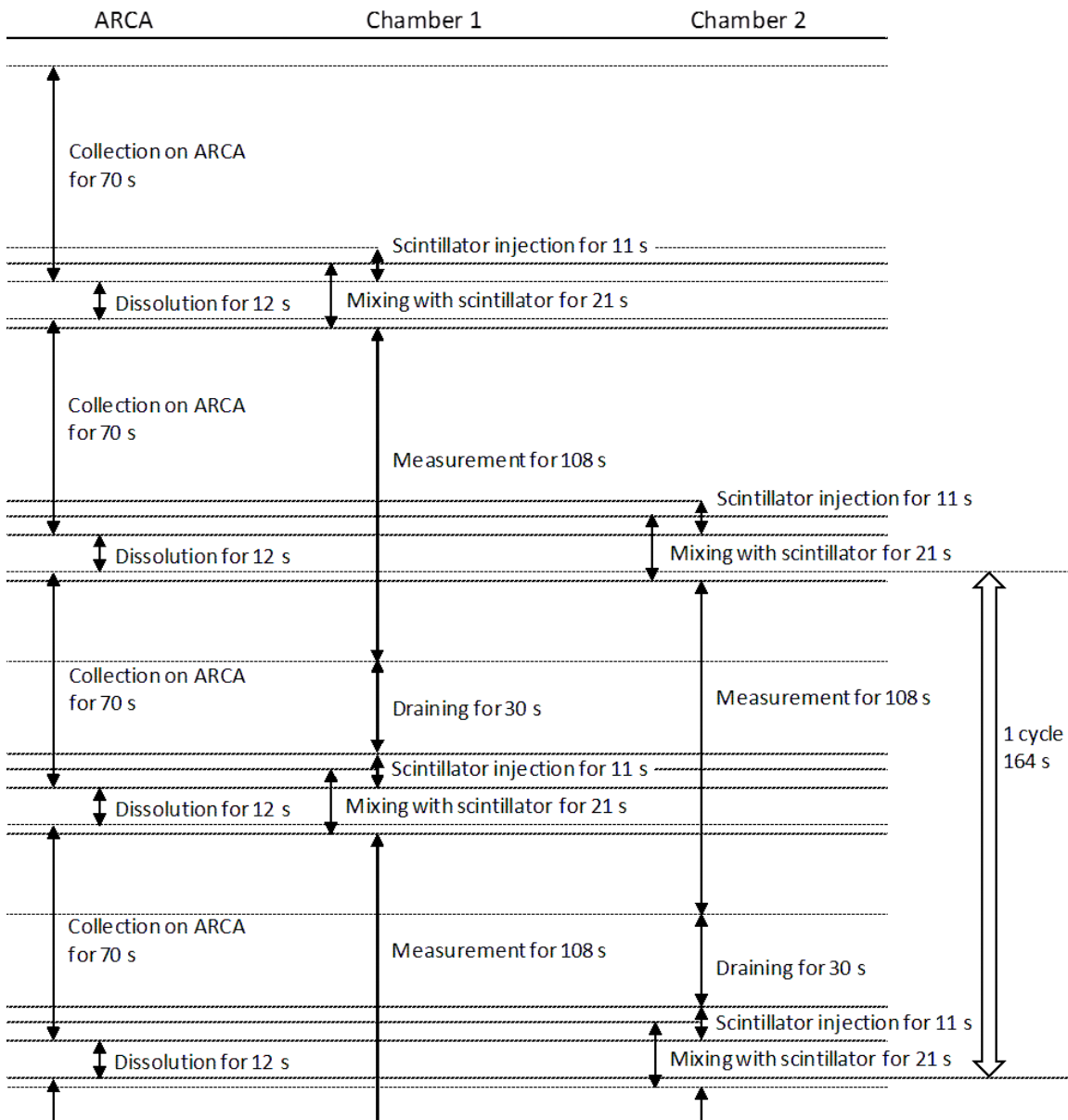
Fig. 3-7. The time sequence of experimental procedures of the on-line liquid scintillation measurement.

3-3. Results and Discussion

3-3-1. Production and transport of ^{262}Db by the GARIS

Fig. 3-8 shows sum of α-particle spectra in the 15 top detectors of MANON. It is observed that α-emitting by-products which hinder the detection of ^{262}Db are greatly removed by the GARIS gas-jet system.

Fig. 3-8. Sum of α-particle spectra in the 15 top detectors of MANON for the reaction products preseparated and transported by the GARIS gas-jet system.

3-3-2. On-line Liquid Scintillation Measurement

(a) Blank Samples

Examples of two-dimensional plot of TAC versus energy for the blank samples obtained with the detection chamber 1 and 2 are given in Fig. 3-9 and 3-10, respectively. It is observed that continuous components are sparsely spread above a thick band of β components. These continuous components observed in α-event region are considered to be recoil protons originating from fast neutrons. Count rates of α and β events in the α-energy range of 7.5–9.7 MeV (α-energy region) and those of SF events and β events in the α-energy range of MeV (SF-energy region) are shown in Table 3-3. The count rates under the beam on condition are larger than those under the beam off condition due to the fast neutrons and γ rays generated by beam irradiation.

(b) Reaction Products

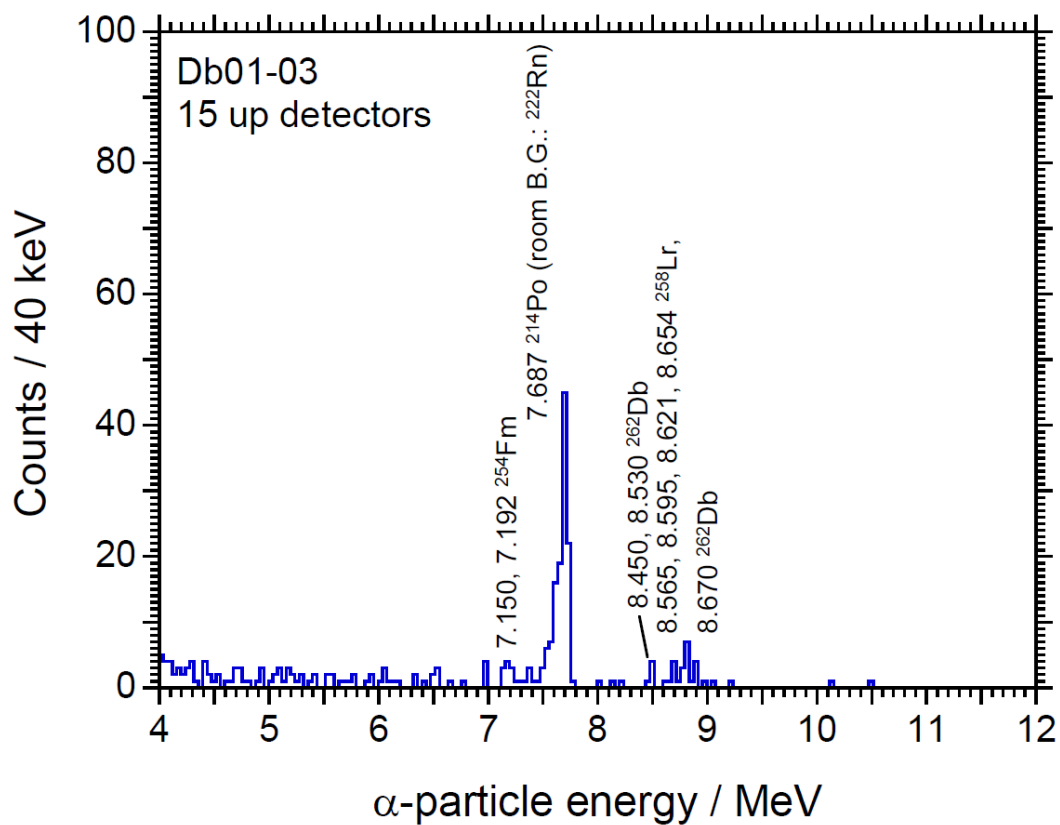Examples of two-dimensional plot of TAC versus energy for the reaction products obtained with the detection chamber 1 and 2 are given in Fig. 3-11 and 3-12, respectively. Count rates of α and β events in the α-energy range of 7.5–9.7 MeV (α-energy region) and those of SF events and β events in the α-energy range of MeV (SF-energy region) are shown in Table 3-4.

Total α and SF events obtained in the measurement of the reaction products are listed in Table 3-5. Time-correlated α-α and α-SF events originating from the decay of ^{262}Db → ^{258}Lr → were searched from these events. Successively observed events within a

time interval of 19 s, which corresponds to five times the half-life of ^{258}Lr, were assumed to be candidates for the time-correlated events. In this experiment, the time-correlated events, which were expected to be 1.4 α-α and 0.12 α-SF correlations, were not observed. This is acceptable considering statistical fluctuations.
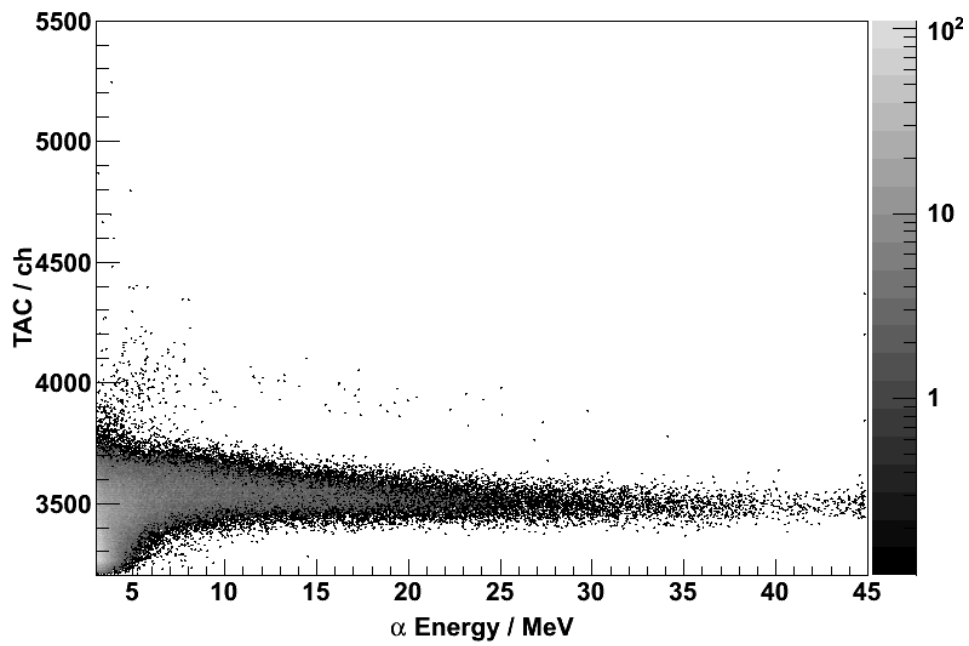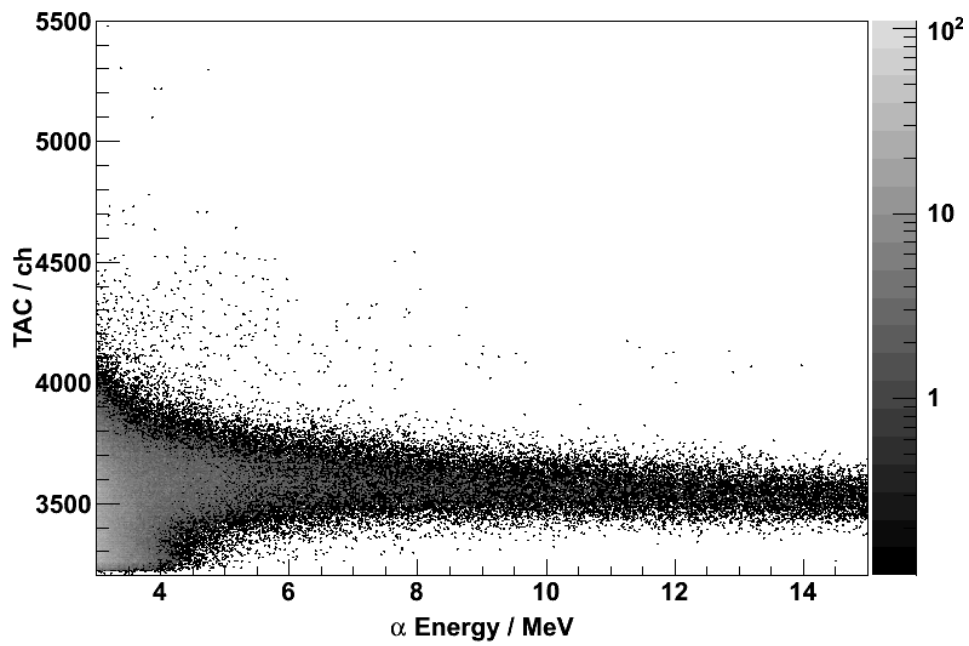
Fig. 3-9. Two-dimensional plot of TAC versus energy for the blank samples obtained with the detection chamber 1.
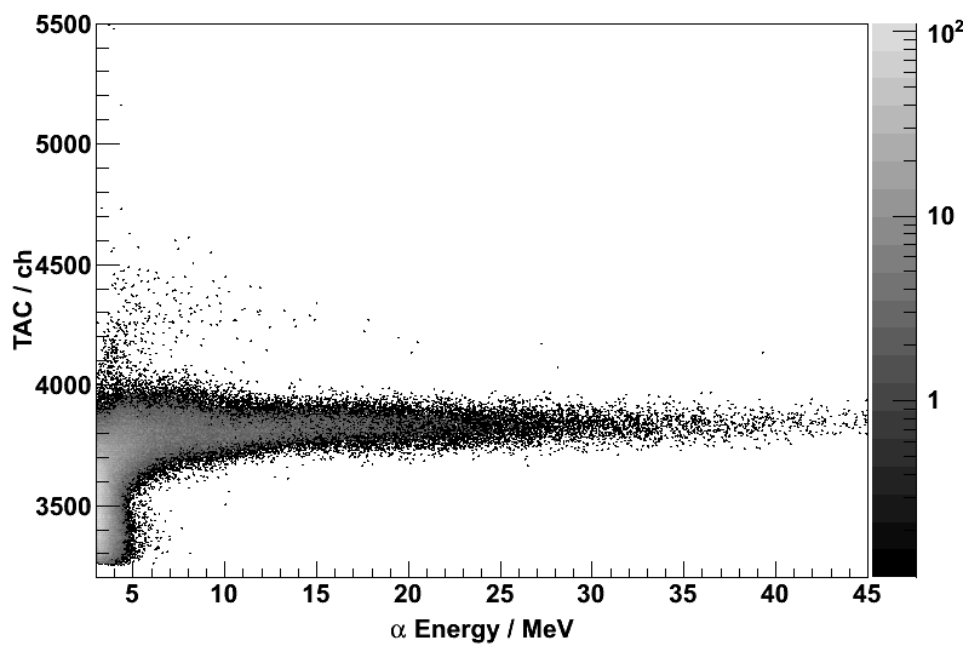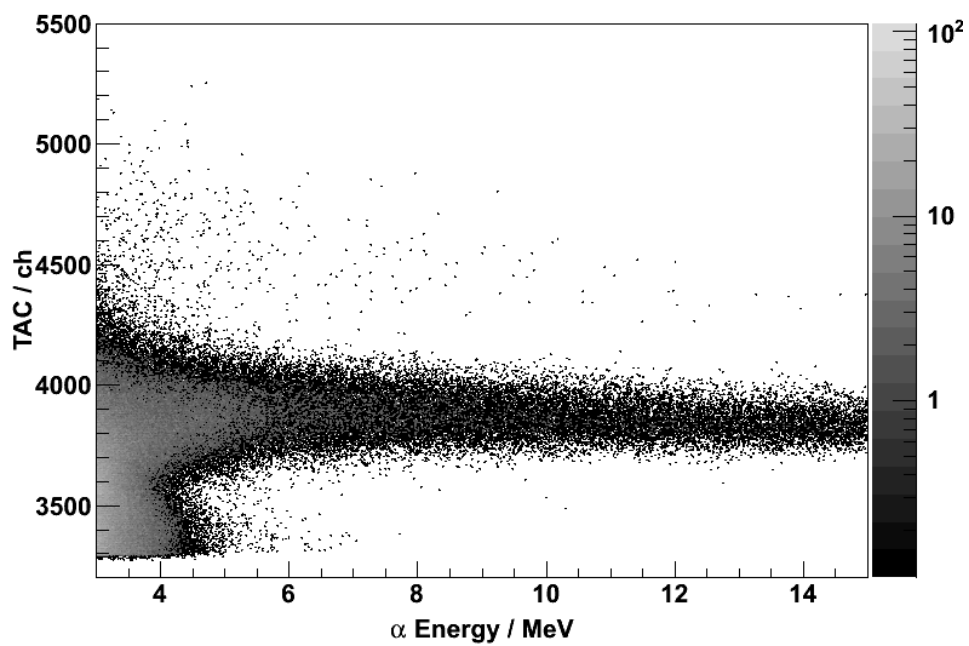
Fig. 3-10. Two-dimensional plot of TAC versus energy for the blank samples obtained with the detection chamber 2.

Table 3-3. Count rates of α and β events in the α-energy range of 7.5–9.7 MeV (α-energy region) and those of SF events and β events in the α-energy range of MeV (SF-energy region) obtained in measurement of the blank samples.

Run	Beam on/off	Chamber	α energy region		SF enegy region	
			α events [10^{-3} cps]	β events [cps]	SF events [10^{-3} cps]	β events [cps]
Blank_1	on	1	1.2 ± 0.3	0.44 ± 0.01	1.3 ± 0.3	0.59 ± 0.01
		2	1.8 ± 0.3	0.42 ± 0.01	0.10 ± 0.07	0.49 ± 0.01
Blank_2	on	1	1.5 ± 0.3	0.41 ± 0.01	0.63 ± 0.18	0.55 ± 0.01
		2	1.5 ± 0.3	0.37 ± 0.01	0.11 ± 0.07	0.43 ± 0.01
Blank_3	on	1	1.3 ± 0.2	0.41 ± 0.01	0.41 ± 0.12	0.56 ± 0.01
		2	1.0 ± 0.2	0.39 ± 0.01	0.26 ± 0.10	0.43 ± 0.01
Blank_4	on	1	1.1 ± 0.8	0.37 ± 0.01	0.57 ± 0.57	0.52 ± 0.02
		2	0.6 ± 0.6	0.32 ± 0.01	0 ± 0	0.37 ± 0.01
Blank_5	on	1	1.0 ± 0.2	0.34 ± 0.01	0.62 ± 0.16	0.47 ± 0.01
		2	1.2 ± 0.2	0.31 ± 0.01	0.17 ± 0.08	0.34 ± 0.01
Blank_6	on	1	0.8 ± 0.2	0.39 ± 0.01	0.45 ± 0.12	0.53 ± 0.01
		2	0.9 ± 0.2	0.36 ± 0.01	0.035 ± 0.035	0.37 ± 0.01
Blank_7	on	1	1.0 ± 0.2	0.52 ± 0.01	0.48 ± 0.13	0.71 ± 0.01
		2	1.3 ± 0.2	0.47 ± 0.01	0.40 ± 0.12	0.48 ± 0.01
Blank_8	off	1	0.36 ± 0.36	0.049 ± 0.004	0.36 ± 0.36	0.059 ± 0.005
		2	0 ± 0	0.059 ± 0.005	0.36 ± 0.36	0.053 ± 0.004
Blank_9	off	1	0.17 ± 0.08	0.028 ± 0.001	0 ± 0	0.062 ± 0.001
		2	0.068 ± 0.048	0.049 ± 0.001	0.034 ± 0.034	0.050 ± 0.001
Blank_10	off	1	0.19 ± 0.04	0.056 ± 0.001	0 ± 0	0.076 ± 0.001
		2	0.064 ± 0.024	0.062 ± 0.001	0.0091 ± 0.0091	0.065 ± 0.001

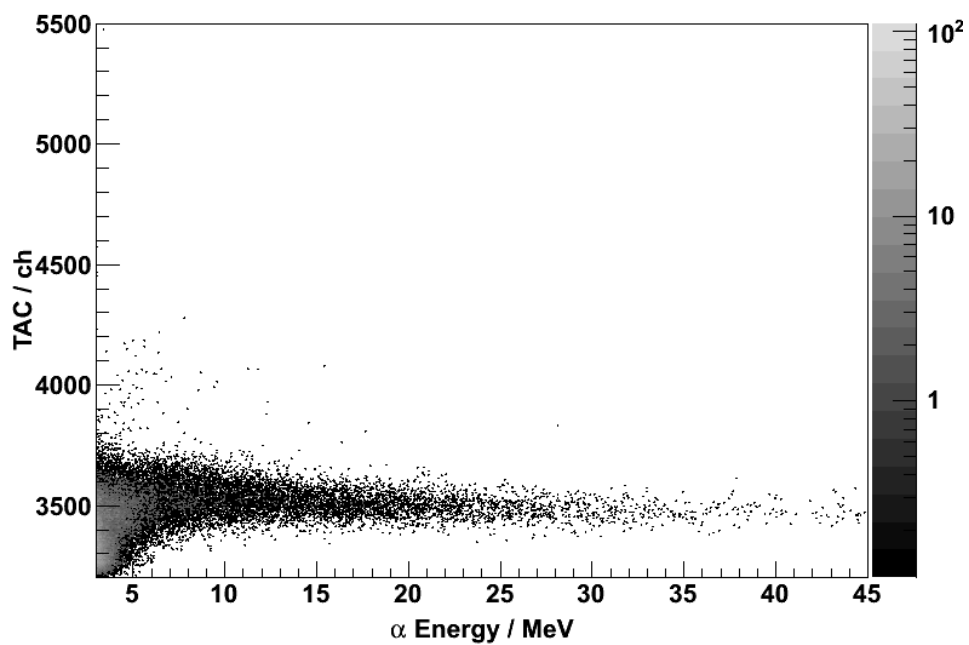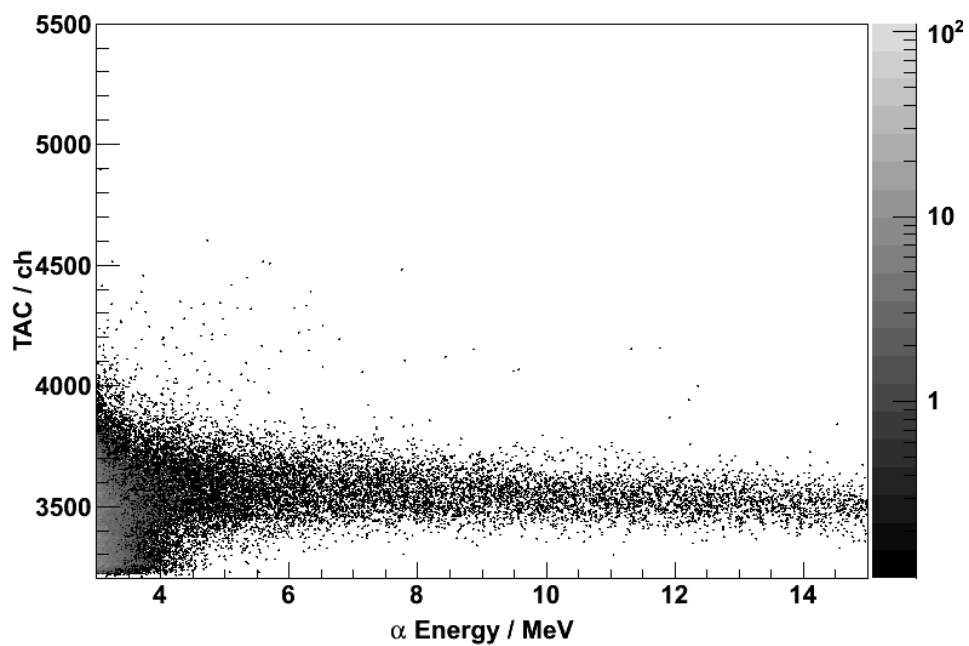| Run	Beam on/off	Chamber	α energy region		SF enegy region	
			α events [10^{-3} cps]	β events [cps]	SF events [10^{-3} cps]	β events [cps]
Sum Blank_1-7	on	1	1.1 ± 0.1	0.42 ± 0.01	0.61 ± 0.06	0.57 ± 0.01
		2	1.2 ± 0.1	0.39 ± 0.01	0.18 ± 0.04	0.42 ± 0.01
	on	Ave.	1.2 ± 0.1	0.40 ± 0.01	0.40 ± 0.04	0.49 ± 0.01
Sum Blank_8-10	off	1	0.19 ± 0.04	0.050 ± 0.001	0.0070 ± 0.0070	0.073 ± 0.001
		2	0.063 ± 0.021	0.060 ± 0.001	0.021 ± 0.012	0.061 ± 0.001
	off	Ave.	0.13 ± 0.02	0.055 ± 0.001	0.014 ± 0.007	0.067 ± 0.001

Fig. 3-11. Two-dimensional plot of TAC versus energy for the reaction products obtained with the detection chamber 1.
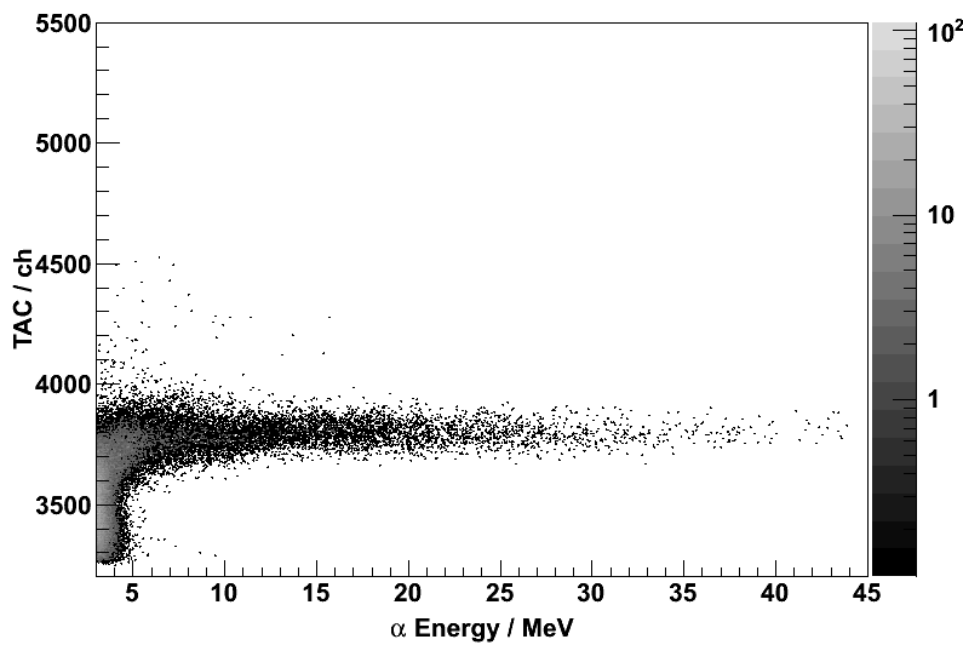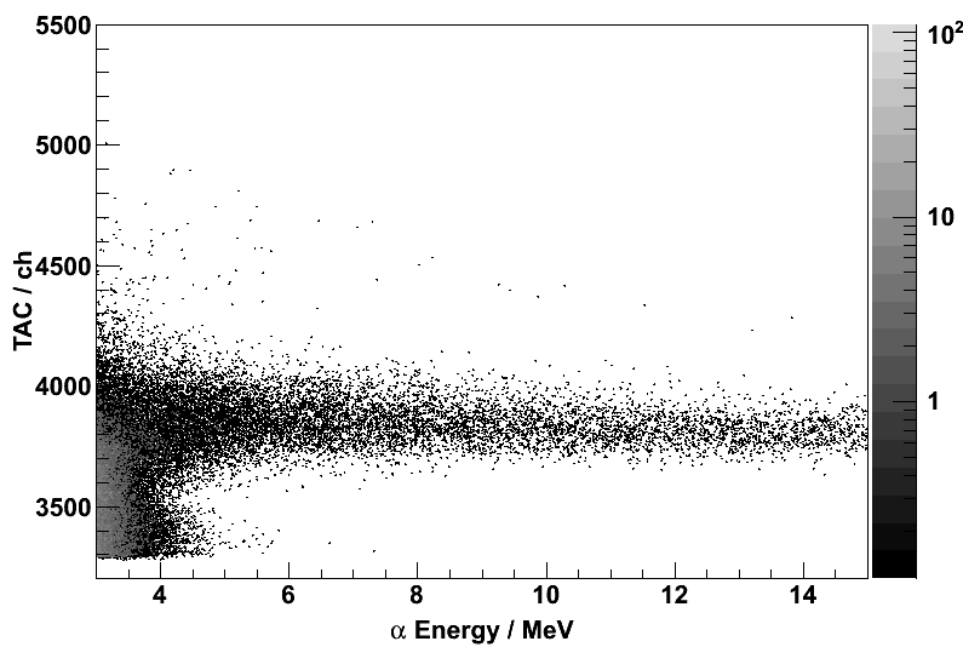
Fig. 3-12. Two-dimensional plot of TAC versus energy for the reaction products obtained with the detection chamber 2.

Table 3-4. Count rates of α and β events in the α-energy range of 7.5–9.7 MeV (α-energy region) and those of SF events and β events in the α-energy range of MeV (SF-energy region) obtained in measurement of the reaction products.

Run	Chamber	Accumulated meas. time [s]	α energy region						SF energy region					
			α events [10^{-3} cps]			β events [cps]			SF events [10^{-3} cps]			β events [cps]		
Db_1	1	1286.2	0	±	0	0.44	±	0.02	0.78	±	0.78	0.58	±	0.02
	2	1320.6	0.76	±	0.76	0.40	±	0.02	0	±	0	0.45	±	0.02
Db_2	1	4433.6	1.4	±	0.6	0.41	±	0.01	0.45	±	0.32	0.54	±	0.01
	2	4366.1	1.4	±	0.6	0.38	±	0.01	0	±	0	0.43	±	0.01
Db_3	1	538.2	1.9	±	1.9	0.45	±	0.03	0	±	0	0.55	±	0.03
	2	329.2	3.0	±	3.0	0.47	±	0.04	0	±	0	0.45	±	0.04
Db_4	1	4739.2	1.3	±	0.5	0.36	±	0.01	0.84	±	0.42	0.48	±	0.01
	2	4586.3	2.0	±	0.7	0.35	±	0.01	0.22	±	0.22	0.36	±	0.01
Db_5	1	4809.5	1.2	±	0.5	0.35	±	0.01	0.83	±	0.42	0.45	±	0.01
	2	4693.9	0.43	±	0.30	0.33	±	0.01	0	±	0	0.32	±	0.01
Db_6	1	1241.5	0	±	0	0.36	±	0.02	0	±	0	0.50	±	0.02
	2	988.2	2.0	±	1.4	0.39	±	0.02	0	±	0	0.40	±	0.02
Db_7	1	3067.3	2.0	±	0.8	0.45	±	0.01	2.0	±	0.8	0.58	±	0.01
	2	2939.8	0.68	±	0.48	0.40	±	0.01	0	±	0	0.37	±	0.01
Sum Db_1-7	1	20115.5	1.2	±	0.2	0.39	±	0.01	0.85	±	0.20	0.51	±	0.01
	2	19224.1	1.2	±	0.2	0.37	±	0.01	0.052	±	0.052	0.38	±	0.01
	Ave.		1.2	±	0.2	0.38	±	0.01	0.46	±	0.11	0.45	±	0.01

Table 3-5. Total α and SF events obtained in the measurement of the reaction products.

Run	Chamber	α events	SF events
Db_1	1	0	1
	2	1	0
Db_2	1	6	2
	2	6	0
Db_3	1	1	0
	2	1	0
Db_4	1	6	4
	2	9	1
Db_5	1	6	4
	2	2	0
Db_6	1	0	0
	2	2	0
Db_7	1	6	6
	2	2	0

3-3-3. Discussion

   Average count rates of α, β, and SF events in measurement of the blank samples and the reaction products are summarized in Table 3-6. The increase of the count rates of α and SF events in measurement of the blank samples under the beam on condition compared to those under the beam off condition is attributed to the fast neutrons. The increase of the count rates of β events is attributed to the γ rays. The count rates in measurement of reaction products are comparable to those of blank samples under the beam on condition, indicating that α, β, and γ-emitting by-products were removed by the GARIS gas-jet system.

   Signal-to-noise ratio (S/N) in the detection of time-correlated α-α and α-SF events from ^{262}Db and ^{258}Lr was evaluated. Expected detection rates of α-α and α-SF correlations from ^{262}Db and ^{258}Lr in this experiment is given in Table 3-7 as signal (S) in S/N. As for the single SF events from ^{262}Db, the expected detection rate is also given in Table 3-7. In the search for the correlated events, successively observed events in a time interval of 19 s, which corresponds to five times the half-life of ^{258}Lr, were assumed to be candidates for the time-correlated events. Probability that one or more events randomly occur in the time interval of 19 s in α-event region, $P_{1,\alpha}$ ($X \geq 1$), are derived from the Poisson distribution as follows:

$$P_k (X = k) = \frac{\lambda^k}{k!} e^{-\lambda}, \qquad (1)$$

where X denotes the number of events and λ is the mean number of events which occur in the time interval ΔT. Assuming that the ΔT = 19 s and $\lambda = \Delta$T × background count rate in α-event region = 19 s × 1.2 × 10^{-3} s^{-1}= 0.0228, $P_{1,\alpha}$ ($X \geq 1$) = 1 − $P_{0,\alpha}$ ($X = 0$) = 0.0225. Noise (N) in the detection of α-α correlation is defined by multiplying the

probability, $P_{1,\alpha}$ ($X \geq 1$) by the background count rate in α- event region, C_{BGD} (α). The S/N values for the detection of α-α, α-SF correlation from [262]Db and [258]Lr, and single SF from [262]Db in this experiment are given in Table 3-7. These values indicate that background count rates are relatively high against the detection rates of α-α and α-SF correlation, and SF originating from [262]Db. Further reduction of background count rates in α- and SF-event regions is necessary by adding the more polyethylene blocks around the detection chambers or by moving the detection chambers to another site where the less fast neutrons come. According to Ref. [35], a water, which can be approximately replaced by polyethylene in terms of neutron shielding, of approximately 40 cm thickness is required in order to decrease transmission of fast neutrons to one tenth.

Signal-to-noise ratio for the detection of the decay chains from [261]Rf, [262]Db, [265]Sg[a] and [265]Sg[b] are estimated by using the background count rates of the blank sample under the beam off condition, which are given in Table 3-8, 3-9, 3-10, 3-11, respectively. The values of the detection rates of [261]Rf, [262]Db, [265]Sg[a] and [265]Sg[b] are referred from the estimation in chapter 2-7.

Table 3-6. Summary of count rates in measurement of the blank samples and the reaction products.

Sample	Beam	Count rate in α-event region [10^{-3} cps]	Count rate in β-event region [cps]	Count rate in SF-event region [10^{-3}cps]
Blank	off	0.13 ± 0.02	0.055 ± 0.001	0.014 ± 0.007
Blank	on	1.2 ± 0.1	0.40 ± 0.01	0.40 ± 0.04
Reaction products	on	1.2 ± 0.2	0.38 ± 0.01	0.46 ± 0.11

Table 3-7. Signal-to-noise ratio for the detection of α-α, α-SF, SF events of ^{262}Db in this experiment.

	α-α from ^{262}Db→^{258}Lr	α-SF from ^{262}Db→^{258}Lr	SF from ^{262}Db
Signal (S) [h^{-1}]	0.166	0.0125	0.230
Noise (N) [h^{-1}]	$C_{BGD}(\alpha) \times P_{1,\alpha}(X \geq 1)$	$C_{BGD}(\alpha) \times P_{1,SF}(X \geq 1)$	$C_{BGD}(SF)$
	0.0974	0.0376	1.66
S/N	1.7	0.3	0.1

Table 3-8. Estimation of signal-to-noise ratio for the detection of the decay chains from [261]Rf under the beam off condition.

	Total Det. Rates of [261]Rf[a] [events/d]	α-α [261]Rf[a]→[257]No→ [events/d]
Signal (S)	171	171
Noise (N)		$C_{BGD}(α) × P_{1,α}(X ≥ 1)$
		0.18
S/N		947

Table 3-9. Estimation of signal-to-noise ratio for the detection of the decay chains from [262]Db under the beam off condition.

	Total Det. Rates of [262]Db [events/d]	α-α [262]Db→[258]Lr→ [events/d]	SF [262]Db→ [events/d]	α-SF [262]Db→[258]Lr→ [events/d]
Signal (S)	24	10	13	0.45
Noise (N)		$C_{BGD}(α) × P_{1,α}(X ≥ 1)$	$C_{BGD}(SF)$	$C_{BGD}(α) × P_{1,SF}(X ≥ 1)$
		0.028	1.2	0.0030
S/N		375	11	151

Table 3-10. Estimation of signal-to-noise ratio for the detection of the decay chains from [265]Sg[a] under the beam off condition.

	Total Det. Rates of [265]Sg[a] [events/d]	α-α-α [265]Sg[a]→[261]Rf[a]→[257]No→ [events/d]	α-SF [265]Sg[a]→[261]Rf[b]→ [events/d]	α-α-α [265]Sg[a]→[261]Rf[b]→[257]No→ [events/d]
Signal (S)	0.73	0.66	0.054	0.012
Noise (N)		$C_{BGD}(α) × P_{1,α}(X ≥ 1) × P_{1,α}(X ≥ 1)$	$C_{BGD}(α) × P_{1,SF}(X ≥ 1)$	$C_{BGD}(α) × P_{1,α}(X ≥ 1) × P_{1,α}(X ≥ 1)$
		0.0078	0.0020	0.00031
S/N		84	26	38

Table 3-10. Estimation of signal-to-noise ratio for the detection of the decay chains from [265]Sg[b] under the beam off condition.

	Total Det. Rates of [265]Sg[b] [events/d]	α-SF [265]Sg[b]→[261]Rf[b]→ [events/d]	α-α-α [265]Sg[b]→[261]Rf[a]→[257]No→ [events/d]	α-α-α [265]Sg[b]→[261]Rf[b]→[257]No→ [events/d]
Signal (S)	1.8	1.2	0.36	0.26
Noise (N)		$C_{BGD}(α) × P_{1,SF}(X ≥ 1)$	$C_{BGD}(α) × P_{1,α}(X ≥ 1) × P_{1,α}(X ≥ 1)$	$C_{BGD}(α) × P_{1,α}(X ≥ 1) × P_{1,α}(X ≥ 1)$
		0.0020	0.0078	0.00031
S/N		579	46	850

3-4. Conclusion

On-line liquid scintillation measurement of ^{262}Db produced in the ^{248}Cm(^{19}F,5n)^{262}Db reaction and preseparated with the GARIS gas-jet system was performed to evaluate the background count rate for the detection of time-correlated α-α events from ^{262}Db and the daughter nuclide ^{258}Lr. The count rates under the beam on condition were larger than those under the beam off condition. The increase of count rates in α- and SF-event regions is attributed to fast neutrons. The increase of count rate in β-event region is attributed to γ rays. The count rates in the measurement of the reaction products are comparable to those of the blank samples under the beam on condition, indicating that α, β, and γ-emitting by-products were suppressed by the GARIS gas-jet system. From the expected detection rates of the time-correlated α-α and α-SF events and background count rates in α- and SF-event regions, S/N values for the detection of time-correlated α-α and α-SF events were estimated to be 1.7 and 0.3, respectively. Further reduction of background count rates in α- and SF-event regions is necessary by adding the more polyethylene blocks around the detection chambers or by moving the detection chambers to another site where the less fast neutrons come.

Chapter 4

Extraction of Mo and W by Aliquat 336
from HF and HCl solutions

4-1. Introduction

We are aiming at the extraction chromatography experiment of element 106, seaborgium (Sg) with a liquid chromatography apparatus, ARCA [13] to elucidate its complex formation properties with some ligands such as fluoride and chloride ions. We have selected methyl-tricaprylyl ammonium chloride (Aliquat 336) as an extractant for anionic species in aqueous solution. Generally, experimental conditions applicable to Sg are investigated using its lighter homologues, molybdenum (Mo) and tungsten (W). It is known that Mo and W form polynuclear species such as $[Mo_7O_{24}]^{6-}$ and $[W_{12}O_{39}]^{6-}$ in solution [31]. On the other hand, Sg cannot form the polynuclear species due to its low production rates and short half-lives. In this study, carrier-free radioisotopes ^{93m}Mo ($T_{1/2}$ = 6.9 h), ^{90}Mo ($T_{1/2}$ = 5.7 h), ^{181}W ($T_{1/2}$ = 121.2 d), and ^{173}W ($T_{1/2}$ = 7.6 m) were used to avoid the polymerization of Mo and W. Extraction behavior of Mo and W onto Aliquat 336-loaded resin (Aliquat 336/CHP20Y resin) from HF and HCl solutions was investigated. Distribution coefficients (K_d) of ^{90}Mo, ^{93m}Mo, ^{173}W and ^{181}W were obtained as functions of HF and HCl concentrations by a batch method. In the experiments of Sg, fast reaction kinetics is required because half-lives of the isotopes ^{265}Sg^a and ^{265}Sg^b are as short as 8.5 and 14 s, respectively. Therefore, reaction kinetics of ^{90}Mo and ^{173}W was also investigated by varying the shaking time in batch extraction. Finally, the on-line extraction chromatography of ^{90}Mo and ^{173}W in HCl solution was performed with ARCA.

4-2. Experimental

4-2-1. Preparation of Aliquat 336-loaded Resin

An Aliquat 336-loaded resin was prepared as follows, with referring to Ref. [36]. A support material for the reversed-phase extraction chromatography was MCI GEL CHP20Y, supplied by Mitsubishi Chemical Corporation, a styrene-divinylbenzene copolymer with a particle size of about 30 μm. The resin was washed several times by stirring alternately with methanol and acetone, and was dried at 80 ℃ in a vacuum oven. The resin was suspended in methanol in a glass vial and then Aliquat 336 was added. After continuously stirring in a covered glass vial for 12 h, the mixture was evaporated to dryness at room temperature, and was dried at 80 ℃.

4-2-2. Extraction of Mo and W by Batch Method

4-2-2-1. Production and Radiotracer Preparation of ^{181}W, ^{93m}Mo, ^{90}Mo and ^{173}W

(a) ^{181}W

The radioisotope ^{181}W ($T_{1/2}$ = 121.2 d) was produced in the ^{181}Ta(p, n)^{181}W reaction. A metallic Ta foil of 83 mg cm^{-2} thickness was irradiated by 14-MeV proton beam delivered from the AVF cyclotron of Research Center for Nuclear Physics (RCNP), Osaka University. The irradiated Ta foil was dissolved with 2 mL of 5 M HNO$_3$/10 M HF solution in a polytetrafluoroethylene (PTFE) beaker. After evaporated to dryness of

the solution, the residue was dissolved with 2 mL of 7 M HCl/2 M HF solution and the sample was then pipetted to a polypropylene (PP) tube. The Ta target was extracted from this solution into the same volume of methyl isobutyl ketone (MIBK), by shaking the mixture for 10 min. After centrifugation, the aqueous solution was pipetted in another PP tube. The above solvent extraction procedure was performed twice to thoroughly remove the Ta target. The aqueous solution was thereafter evaporated to dryness in a PTFE beaker, and the residue was dissolved with 4 mL of 1 M HF/5 M HCl solution. Then, the solution was fed onto a column (2.5 mm i.d. $\times$ 50 mm long) filled with anion-exchange resin (Muromac 1 $\times$ 8, 200–400 mesh, Cl$^-$ form). The ^{181}W species was then eluted from the column with 9 mL of 1 M HF/5 M HCl. After evaporation of the effluent containing ^{181}W, the residue was dissolved with 3 mL of 8 M HCl solution, and 124 mg of H_3BO_3 was added to the solution sample. After that, the solution was fed onto another column (2.5 mm i.d. $\times$ 50 mm long) filled with anion-exchange resin (Muromac 1 $\times$ 8, 200–400 mesh, Cl$^-$ form). The fluoride ions were removed from the column by feeding 7 mL of 8 M HCl solution. The ^{181}W species were then eluted with 20 mL of 1 M HCl. The purified ^{181}W radiotracer fraction was then evaporated to dryness in a PTFE beaker and the residue was dissolved in 1 M HCl as stock solution in a PP tube.

(b) ^{93m}Mo

The radioisotope ^{93m}Mo ($T_{1/2} = 6.9$ h) was produced in the ^{93}Nb(d, $2n$)^{93m}Mo reaction. A metallic ^{93}Nb foil of 856 μg cm^{-2} thickness was irradiated by 24-MeV deuteron beam delivered from the RIKEN K70 AVF cyclotron. Reaction products recoiling out of the

targets were transported with a He/KCl gas-jet from the target chamber to a chemistry laboratory. The transported reaction products were collected on a Naflon sheet or on a PET film for 2–10 min and were then dissolved in 100-200 μL of various concentrations of HF (or HCl) solutions used in the following batch extractions.

(c) ^{90}Mo and ^{173}W

The short-lived isotopes ^{90}Mo ($T_{1/2}$ = 5.7 h) and ^{173}W ($T_{1/2}$ = 7.6 min) were simultaneously produced in the ^{nat}Ge(^{22}Ne, xn) and ^{nat}Gd(^{22}Ne, xn) reactions, respectively, using Gd/Ge mixed targets. A ^{nat}Gd of approximately 0.3 mg cm^{-2} thickness was electrodeposited on a 1.9 mg cm^{-2} beryllium foil, and then 0.3 mg cm^{-2} ^{nat}Ge was deposited on the ^{nat}Gd target by vacuum evaporation. The 140-MeV ^{22}Ne beam, delivered from the RIKEN K70 AVF cyclotron, passed through a beryllium vacuum window, the helium cooling gas, the beryllium target backing, and finally entered the target materials at the energy of 118 MeV. The typical beam intensity was approximately 300 particle nA. Reaction products recoiling out of the targets were stopped in helium gas, attached to KCl aerosols generated by sublimation of KCl powder at 620 ºC, and continuously transported through a Teflon capillary (2.0 mm i.d. × 10 m length) to the chemistry laboratory. The flow rate of the helium gas was 1.8 L min^{-1}. The transported reaction products were deposited on a Naflon sheet for 1 or 5 min. The collected reaction products were dissolved in 240 μL of 1–10 M HF (0.1–10 M HCl) solutions used in the following batch extractions.

4-2-2-2. Extraction of ^{181}W, ^{93m}Mo, ^{90}Mo and ^{173}W in HF and HCl Solutions

A 5–20 mg of 51.9-wt.% Aliquat 336/CHP20Y resin and 500 μL of 1–14 M HF (or

0.1–10 M HCl) solution containing the ^{181}W, ^{93m}Mo, or ^{90}Mo/^{173}W radiotracers were

mixed in a PP tube. These samples were shaken for a certain time at 25 ºC. Standard

samples of ^{181}W, ^{93m}Mo, or ^{90}Mo/^{173}W without resin were also prepared. They were

shaken together with the resin-containing samples. After centrifuging, the aqueous

phase was pipetted into another PP tube and was then subjected to γ-ray spectrometry

using a Ge detector. In the extraction of ^{90}Mo/^{173}W, reaction kinetics was investigated

by varying the shaking time to be 10 s, 5 min, and 10 min in 4 M HF and 2, 6, and 10 M

HCl solutions. In other experiments using the ^{181}W or ^{93m}Mo radiotracers, the shaking

time was fixed to be 50 min and 30 min, respectively.

4-2-3. On-line Extraction Chromatography of Mo and W with ARCA

4-2-3-1. Production of ^{90}Mo and ^{173}W

The short-lived isotopes ^{90}Mo ($T_{1/2}$ = 5.7 h) and ^{173}W ($T_{1/2}$ = 7.6 min) were

simultaneously produced in the ^{nat}Ge(^{22}Ne, xn) and ^{nat}Gd(^{22}Ne, xn) reactions,

respectively, using Gd/Ge mixed targets. A ^{nat}Gd of approximately 0.3 mg cm^{-2}

thickness was electrodeposited on a 1.9 mg cm^{-2} beryllium foil, and then 0.3 mg cm^{-2}

^{nat}Ge was deposited on the ^{nat}Gd target by vacuum evaporation. The 140-MeV ^{22}Ne

beam, delivered from the RIKEN K70 AVF cyclotron, passed through a beryllium

vacuum window, the helium cooling gas, the beryllium target backing, and finally

entered the target materials at the energy of 118 MeV. The typical beam intensity was approximately 300 particle nA. Reaction products recoiling out of the targets were stopped in helium gas, attached to KCl aerosols generated by sublimation of KCl powder at 620 ºC, and continuously transported through a Teflon capillary (2.0 mm i.d. × 10 m length) to the chemistry laboratory. The flow rate of the helium gas was 1.8 L min^{-1}.

4-2-3-2.   Extraction Chromatography of ^{90}Mo and ^{173}W in HCl Solution

The on-line extraction chromatography of ^{90}Mo and ^{173}W was performed with ARCA. A schematic of ARCA is given in Fig. 4-1. The 52.9-wt.% Aliquat 336/CHP20Y resin was filled into the 1.0 mm i.d. × 3.5 mm microcolumn of ARCA. The bottom of the microcolumn was plugged with a glass filter of approximately 1 mm thickness.

Reaction products transported by the He/KCl gas-jet system were deposited on the collection site of ARCA. After collection for 5 min, the reaction products attached to the KCl aerosols were dissolved in HCl solution and were subsequently fed into the column at a flow rate of 1 mL min^{-1}. The effluents were collected in PP tubes for every 50 or 80 µL. Then, the remaining ^{90}Mo and ^{173}W in the column were eluted with 400–500 µL of 6 M HNO_3/0.01 M HF solution and were collected in another PP tube. These fractions of the effluents were assayed by γ-ray spectrometry with Ge detectors to determine radioactivity of ^{90}Mo and ^{173}W with 257 keV and 458 keV γ rays, respectively. The volume of each fraction was determined with the weight of the effluents and the density of the solutions.
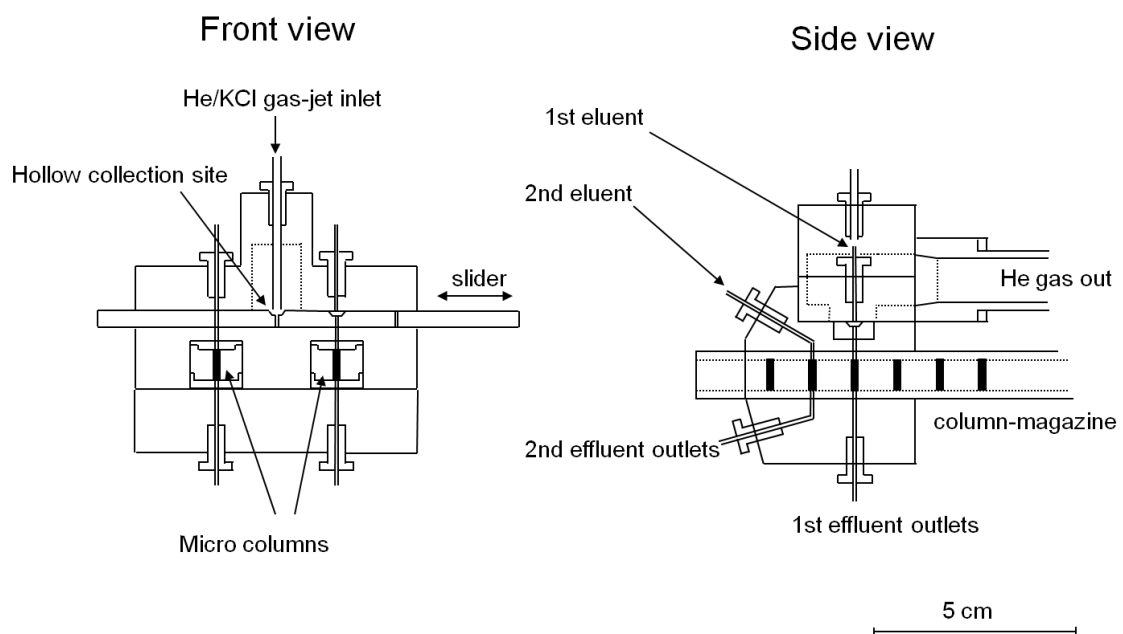
Fig. 4-1. A schematic of ARCA.

4-3.   Results and Discussion

4-3-1.   Extraction of Mo and W by Batch Method

The distribution coefficient (K_d) was obtained by the following equation:

$$K_d = \frac{A_r V_s}{A_s m_r},$$ (1)

where A_r and A_s are the radioactivities on the resin and in the solution, respectively, V_s is the volume of the aqueous solution (mL), and W_r is the mass of the dry resin (g). Variations of the K_d values of ^{90}Mo and ^{173}W in 4 M HF, and 2, 6, and 10 M HCl solutions are shown in Figs. 4-2 (a–d), respectively, as a function of shaking time. It was found that extraction reaction reaches equilibrium state within 10 s under these conditions except for ^{173}W in 2 M HCl solution where the K_d value is low and with large error.

Variations of the K_d values of ^{90}Mo, ^{93m}Mo, ^{173}W, and ^{181}W are shown as functions of HF and HCl concentrations in Fig. 4-3 and Fig. 4-4, respectively. These results are in good agreement with the anion-exchange behavior of Mo and W in HF [37] and HCl [38, 39] solutions. Therefore, it is considered that the vaiarions of the K_d values on the Aliquat 336/CHP20Y resin in HF and HCl solutions reflects formation of anionic fluoride and chloride complexes of Mo(VI) and W(VI), respectively, in addition to anionic hydrolyzed species. In the HF solution, the K_d values of Mo and W decreased with increasing HF concentration. It is explained as the displacement of the metal complex of Mo and W from the binding sites of the resin with $[HF_2]^-$ which is the main anionic species in the solution [23]. The K_d values of Mo were almost the same as those of W, indicating that fluoride complexing strength of Mo is comparable to that of W.

According to the theoretical calculations [40], anionic oxofluoro complexes $[MO_2F_3]^-$, $[MO_2F_4]^{2-}$, and $[MOF_5]^-$ (M = Mo and W) are expected to be consecutively formed with increasing HF concentration over 0.1 M. On the other hand, in the HCl solution, the K_d values of Mo and W increase with increaseing HCl concentration from 1 M to 6 M. In HCl concentration below 1 M, anionic hydrolyzed species such as $[MO_3(OH)]^-$ [41–43] is considered to be extracted by Aliquat 336. Cationic and neutral species such as $[MO(OH)_3]^+$ and $[MO_2(OH)_2]$ are also expected to be existed.Then neutral and anionic oxochloro complexes such as $[MO_2Cl_2]$ and $[MO_2Cl_3]^-$ are considered to be consecutively formed with increasing HCl concentration. The increase of the K_d values is due to the increase of formation of the anionic oxochloro complex $[MO_2Cl_3]^-$. The K_d values of Mo were higher than those of W, which indicates that the chloride complexing strength of Mo is larger than that of W.

From these results, experimental conditions studied in this work are expected to be applicable for Sg experiments in terms of reaction kinetics and variations of the K_d values against HF and HCl concentrations. To study the extraction behavior of Sg on the Aliquat 336/CHP20Y resin in various concentrations of HF and HCl solutions would provide us some findings on formation of oxofluoro and oxochloro complexes of Sg and on difference in those of Mo and W.

4-3-2.   On-line Extraction Chromatography of Mo and W with ARCA

An example of elution curve of [90]Mo and [173]W in 4 M HCl is shown in Fig. 4-3. It was observed that W species were eluted from the column without adsorption on the

resin while approximately 40% of Mo species were adsorbed on the resin. The K_d value by the column method is described as

$$K_d = \frac{V}{m} , \qquad (2)$$

where V and m are the peak volume which is corrected for the dead volume of the apparatus and weight of the dry resin, respectively. In this experiment, the dead volume of the apparatus is considered to be small enough to be approximated as 0. The expected peak volume evaluated from the K_d values of Mo and W in 4 M HCl solution is approximately 1200 μL and 9 μL, respectively. A portion of Mo species were eluted from the column although almost all Mo species were expected to be adsorbed on the resin. This is considered because anionic chloride complex formation or extraction reaction of Mo and W didn't reach equilibrium state during a few seconds of dissolution of Mo and W with HCl solution and subsequent passing through the column.

The percent extraction (%Ext) on the resin was defined as follows:

$$\%Ext = \frac{100A_2}{A_1 + A_2} , \qquad (3)$$

where A_1 and A_2 are radioactivities in first 200 μL and in over 200 μL of the effluents, respectively. Variation of the %Ext values of ^{90}Mo and ^{173}W is shown in Fig. 4-5 as a function of HCl concentration. The order of the %Ext values was Mo > W, which is consistent with the of order of the K_d values obtained in the batch experiment in HCl solution. It is expected that difference in %Ext among Mo, W, and Sg would be observed in these experimental conditions.

Plots of the %Ext values of ^{90}Mo and ^{173}W against the K_d values of ^{90}Mo, ^{93m}Mo, ^{173}W, and ^{181}W are presented in Fig. 4-7. Correlation between the %Ext values and the K_d values were given in the following equation with the free parameters a, b, and c [44],

$$\%Ext = 100 \exp[-a \exp\{-b(K_\mathrm{d} - c)\}]. \tag{4}$$

The fitting curve with the equation (4) is shown by a solid line in Fig. 4-7. The experimental data shows qualitative agreement with the tendency predicted from the equation (4). It suggests that the of order of the K_d values among Mo, W, and Sg could be assumed from the $\%Ext$ values in the chromatography experiment with ARCA by the correlation presented in Fig. 4-7.
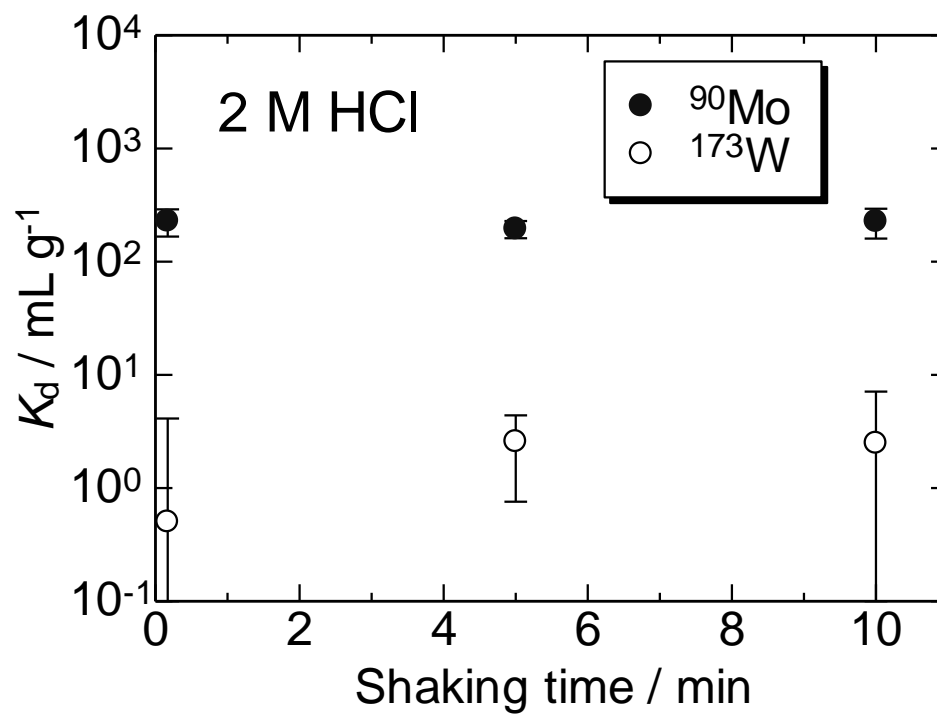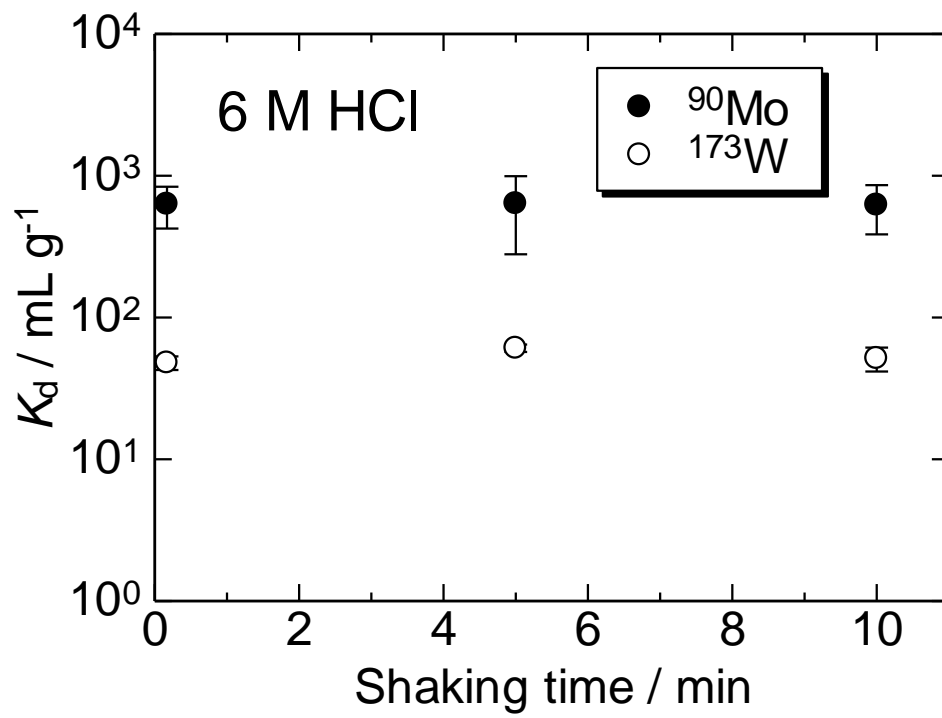
(a)
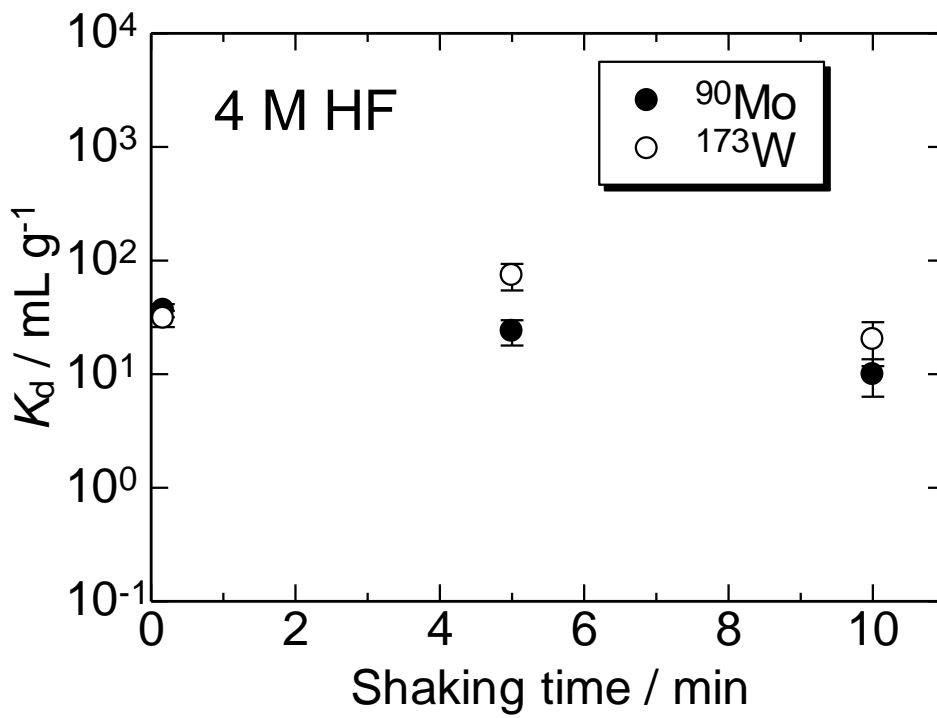
(b)

Fig. 4-2. Extraction kinetics of ^{90}Mo and ^{173}W in (a) 4 M HF and (b) 2 M HCl solutions.
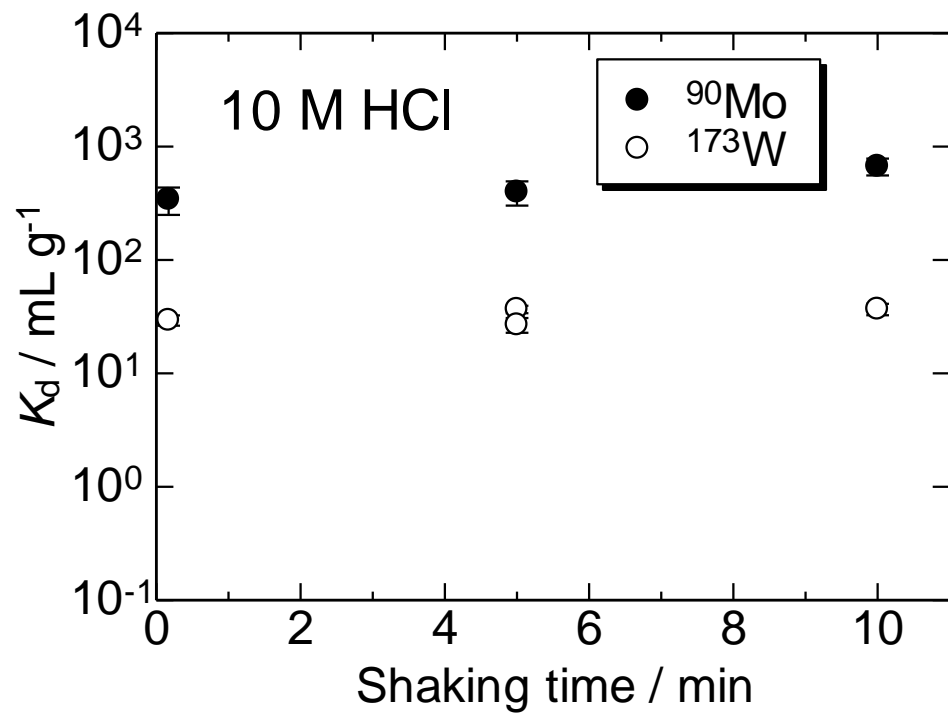
(c)

(d)

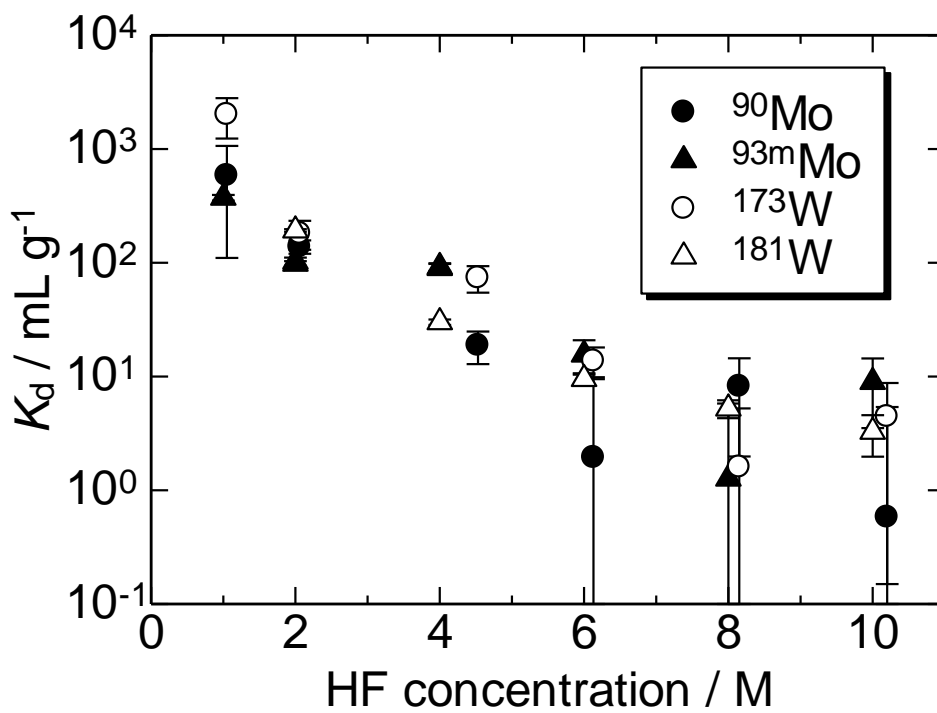Fig. 4-2. Extraction kinetics of ^{90}Mo and ^{173}W in (c) 6 M and (d) 10 M HCl solutions.

Fig. 4-3. Variations of K_d values of ^{90}Mo, ^{93m}Mo, ^{173}W, and ^{181}W on the 51.9-wt.% Aliquat 336/CHP20Y resin as a function of HF concentration.

Fig. 4-4. Variations of K_d values of ^{90}Mo, ^{93m}Mo, ^{173}W, and ^{181}W on the 51.9-wt.% Aliquat 336/CHP20Y resin as a function of HCl concentration.

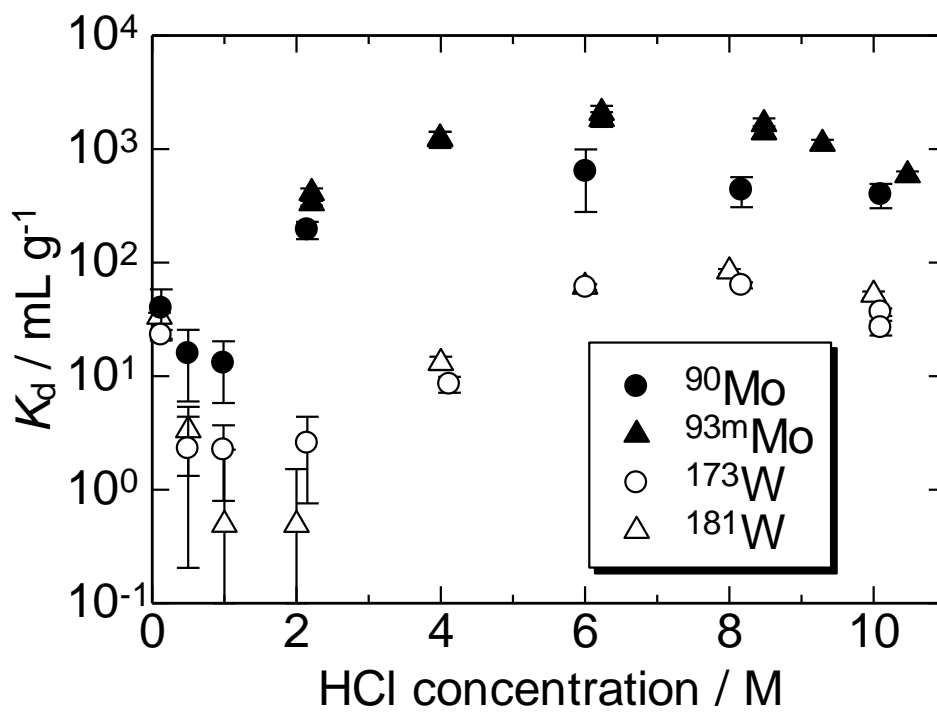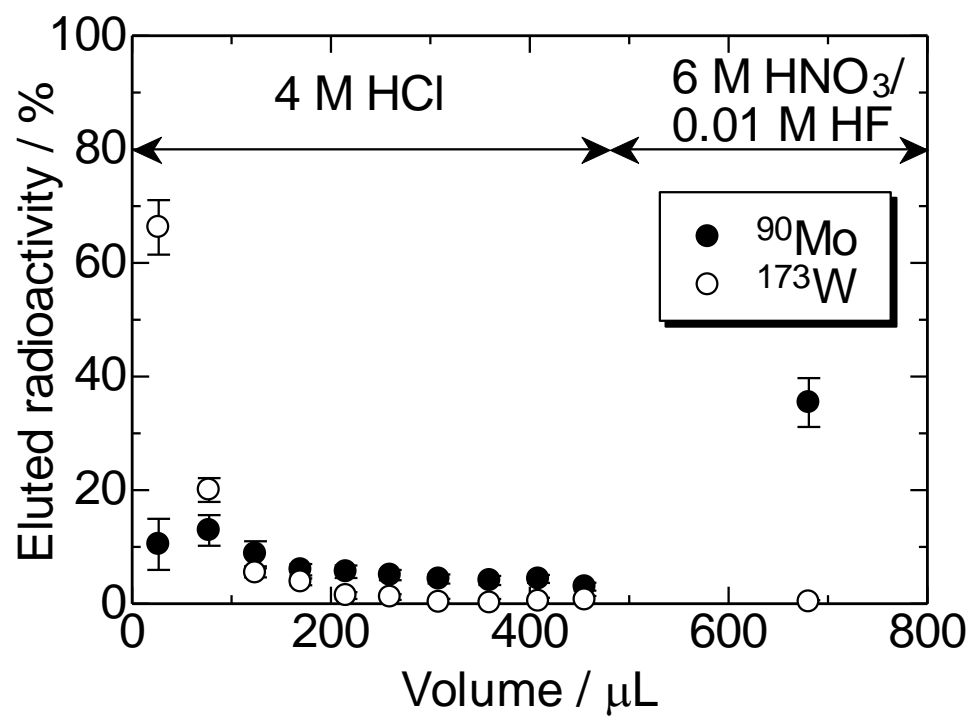Fig. 4-5. An example of elution curve of [90]Mo and [173]W in 4 M HCl.

Fig. 4-6. Variation of %*Ext* values of ^{90}Mo and ^{173}W on the 51.9-wt. % Aliquat 336/CHP20Y column (1.0 mm i.d. $\times$ 3.5 mm) as a function of HCl concentration.
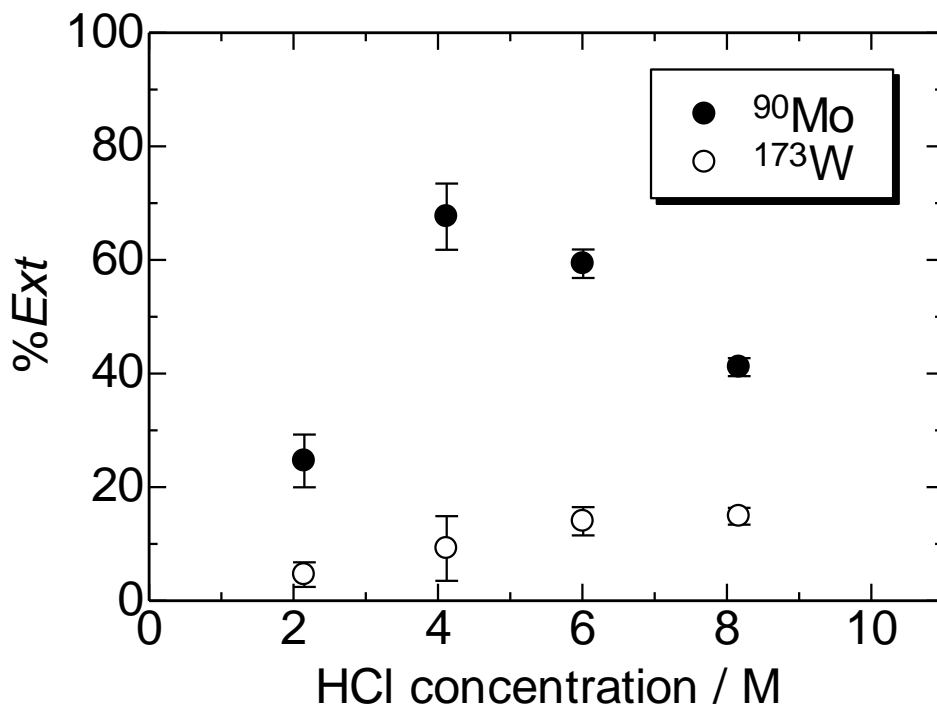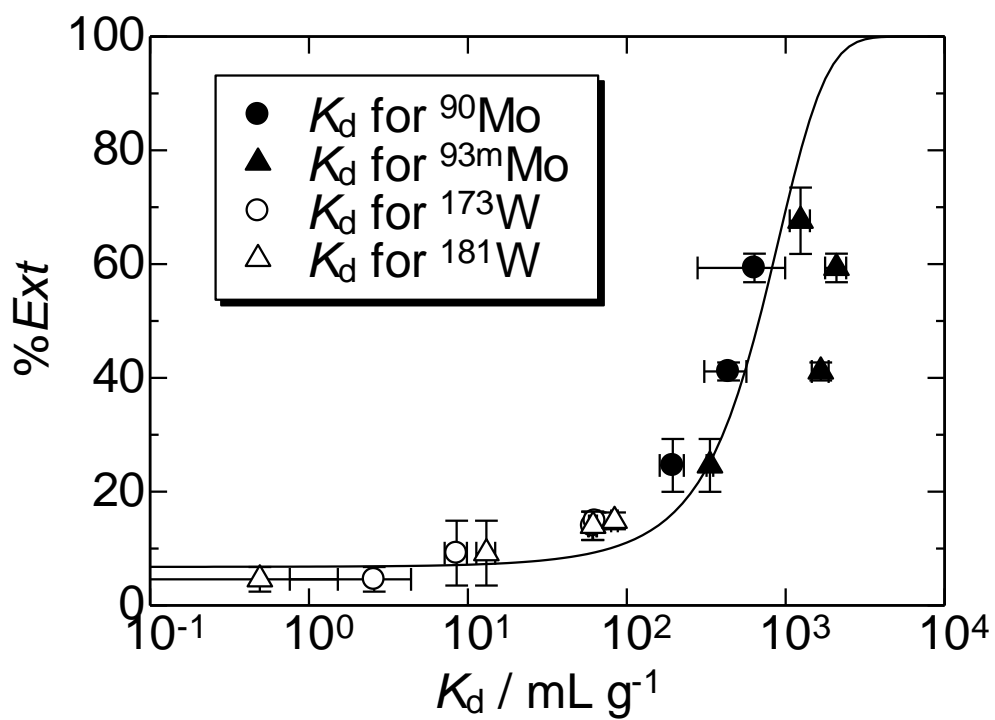
Fig. 4-7. Variation of %*Ext* values of ^{90}Mo and ^{173}W on the 51.9-wt. % Aliquat 336/CHP20Y column (1.0 mm i.d. $\times$ 3.5 mm) as a function of K_d values. The solid line indicates the fitting curve with the equation (4).

131

4-4. Conclusion

Extraction behavior of carrier-free radiotracers Mo and W on Aliquat 336/CHP20Y resin in HF and HCl solutions was investigated. In the batch experiment, it was found that extraction kinetics in both HF and HCl solutions was as fast as to be applicable to ^{265}Sg^{a,b} ($T_{1/2}$ = 8.5 s/14.4 s). The K_d values of Mo and W decreased with increasing HF concentration and the K_d values of Mo were almost the same as those of W. On the other hand, in HCl system, the K_d values of Mo and W increase with increaseing HCl concentration from 1 M to 6 M. The K_d values of Mo were higher than those of W. In the extraction chromatography with ARCA, the order of extraction was Mo > W in 2–8 M HCl solution, which is consistent with the of order of the K_d values obtained in the batch experiment in HCl system. It was suggested that the of order of the K_d values among Mo, W, and Sg could be assumed from the %Ext values in the chromatographic experiment with ARCA by the correlation between the %Ext values and the K_d values.

Chapter 5
Concluding Remarks

An on-line liquid scintillation detection system with α/β discrimination capability has been developed for aqueous chemical studies of the transactinide elements, Rf, Db, and Sg. The presented system allows to detect α particles and SF fragments in aqueous solution sample with almost 100% detection efficiency. The aqueous solution sample can be subjected to α/SF spectrometry in a few seconds after the end of the chemical separation. In the on-line measurement of the isotope ^{213}Fr ($T_{1/2}$ = 34.6 s) with the detection system coupled to ARCA, procedures of the collection, dissolution into the aqueous solution, mixing with the liquid scintillator and liquid scintillation detection were automatically repeated with good stability. Start of the measurement of the reaction products was approximately 15 s after the end of collection. The developed system would be used in column chromatography or liquid-liquid extraction experiments of Rf, Db, and Sg by using the GARIS gas-jet system as a preseparator.

On-line liquid scintillation measurement of ^{262}Db produced in the ^{248}Cm(^{19}F,5n)^{262}Db reaction and preseparated with the GARIS gas-jet system was performed to evaluate the background count rate for the detection of time-correlated α-α events from ^{262}Db and the daughter nuclide ^{258}Lr. The count rates under the beam on condition were larger than those under the beam off condition. The increase of count rates in α- and SF-event regions is attributed to fast neutrons. The increase of count rate in β-event region is attributed to γ rays. The count rates in the measurement of the reaction products are comparable to those of the blank samples under the beam on condition, indicating that α, β, and γ-emitting by-products were suppressed by the GARIS gas-jet system. From the expected detection rates of the time-correlated α-α and α-SF events and background count rates in α- and SF-event regions, S/N values for the detection of time-correlated α-α and α-SF events were estimated to be 1.7 and 0.3, respectively. Further reduction of

background count rates in α- and SF-event regions are necessary by adding the more polyethylene blocks around the detection chambers or by moving the detection chambers to another site where the less fast neutrons come.

In this study, experimental conditions applicable for extraction chromatography experiment of Sg were also investigated using the lighter homologues, Mo and W. We have selected methyl-tricaprylyl ammonium chloride (Aliquat 336) as an extractant for anionic species in aqueous solution. Extraction behavior of Mo and W onto Aliquat 336-loaded resin from HF and HCl solutions was investigated. Extraction behavior of carrier-free radiotracers Mo and W on Aliquat 336/CHP20Y resin in HF and HCl solutions was investigated. In the batch expriment, it was found that extraction kinetics in both HF and HCl solutions was as fast as to be applicable to ^{265}Sg[a,b] ($T_{1/2}$ = 8.5 s/14.4 s). The K_d values of Mo and W decreased with increasing HF concentration and the K_d values of Mo were almost the same as those of W. On the other hand, in HCl system, the K_d values of Mo and W increase with increaseing HCl concentration from 1 M to 6 M. The K_d values of Mo were higher than those of W. In the extraction chromatography with ARCA, the order of extraction was Mo > W, which is consistent with the of order of the K_d values obtained in the batch experiment in HCl solution. It was suggested that the of order of the K_d values among Mo, W, and Sg could be assumed from the %*Ext* values in the chromatographic experiment with ARCA by the correlation between the %*Ext* values and the K_d values.

References

[1] G. V. Flerov, Yu. Os. Oganessian, Yu. V. Lobanov, V. I. Kuznetsov, V. A. Druin, V. P. Perelygin, K. A. Gavrilov, S. P. Tretiakova and V. M. Plotko, Phys. Lett. **13**, 73 (1964).

[2] *The Chemistry of Superheavy Elements*, edited by M. Scädel, Kluwer Academic Publishers, Dordrecht, 2003.

[3] M. Schädel, Angew. Chem. Int. Ed. **45**, 368 (2006).

[4] R. Guillaumont, J. P. Adloff, and A. Peneloux, Radiochim. Acta **46**, 169 (1989).

[5] R. Guillaumont, J. P. Adloff, A. Peneloux, and P. Delamoye, Radiochim. Acta **54**, 1 (1991).

[6] E. Stender, N. Trautmann and G. Herrman, Radiochem. Radioanal. Lett. **42**, 291 (1980).

[7] C. E. Düllmann, Eur. Phys. J. D **45**, 75 (2007).

[8] J. P. Omtvedt, J. Alstad, H. Breivik, J. E. Dyve, K. Eberhardt, C. M. Folden III, T. Ginter, K. E. Gregorich, E. A. Hult, M. Johansson, U. W. Kirbach, D. M. Lee, M. Mendel, A. Nähler, V. Ninov, L. A. Omtvedt, J. B. Patin, G. Skarnemark, L. Stavsetra, R. Sudowe, N. Wiehl, B. Wierczinski, P. A. Wilk, P. M. Zielinski, J. V. Kratz, N. Trautmann, H. Nitsche, and D. C. Hoffman, J. Nucl. Radiochem. Sci. **3**, 121 (2002).

[9] H. Haba, D. Kaji, H. Kikunaga, T. Akiyama, N. Sato, K. Morimoto, A. Yoneda, K. Morita, T. Takabe, and A. Shinohara, J. Nucl. Radiochem. Sci. **8**, 55 (2007).

[10] H. Haba, D. Kaji, Y. Komori, Y. Kudou, K. Moromoto, K. Morita, K. Ooe, K. Ozeki, N. Sato, A. Shinohara, and A. Yoneda, Chem. Lett. **38**, 426 (2009).

[11] H. Haba, D. Kaji, Y. Kudou, K. Morimoto, K. Morita, K. Ozeki, R. Sakai, T.

Sumita, A. Yoneda, Y. Kasamatsu, Y. Komori, A. Shinohara, H. Kikunaga, H. Kudo, K. Nishio, K. Ooe, N. Sato, and K. Tsukada, Phys. Rev. C **85**, 024611 (2012).

[12] H. Haba, K. Ozeki, D. Kaji, J. Kanaya, Y. Kudou, R. Sakai, T. Sumita, K. Morita, K. Morimoto, A. Yoneda, Y. Kasamatsu, Y. Kikutani, Y. Komori, A. Shinohara, H. Kikunaga, H. Kudo, M. Murakami, A. Toyoshima, and K. Nishio, The 56th Symposium on Radiochemistry, 2B05, Tokyo, October (2012).

[13] M. Schädel, W. Brüchle, E. Jäger, E. Schimpf, J. V. Kratz, U. W. Scherer, and H. P. Zimmermann, Radiochim. Acta **48**, 171 (1989).

[14] H. Haba, K. Tsukada, M. Asai, I. Nishinaka, M. Sakama, S. Goto, M. Hirata, S. Ichikawa, Y. Nagame, T. Kaneko, H. Kudo, A. Toyoshima, Y. Shoji, A. Yokoyama, A. Shinohara, Y. Oura, K. Sueki, H. Nakahara, M. Schädel, J. V. Kratz, A. Türler, and H. W. Gäggeler, Radiochim. Acta **89**, 733 (2001).

[15] Y. Nagame, H. Haba, K. Tsukada, M. Asai, K. Akiyama, M. Hirata, I. Nishinaka, S. Ichikawa, H. Nakahara, S. Goto, T. Kaneko, H. Kudo, A. Toyoshima, A. Shinohara, M. Schädel, J. V. Kratz, H. W. Gäggler, and A. Türler, Czech. J. Phys. Suppl. A **53**, 299 (2003).

[16] J. P. Omtvedt, J. Alstad, K. Eberhardt, K. Fure, R. Malmbeck, M. Mendel, A. Nähler, G. Skarnemark, N. Trautmann, N. Wiehl, and B. Wierczinski, J. Alloys Comp. **271**, 303 (1998).

[17] B. Wierczinski, K. Eberhardt, G. Herrmann, J. V. Kratz, M. Mendel, A. Nähler, F. Rocker, U. Tharun, N. Trautmann, K. Weiner, N, Wiehl, J. Alstad, and G. Skarnemark, Nucl. Instrum. Meth. A **370**, 532 (1996).

[18] L. Stavsetra and J. P. Omtvedt, *LSC 2001, Advances in Liquid Scintillation Spectrometry*, edited by S. Möbius, J. E. Noakes, and F. Schönhofer, Radiocarbon,

Tucson, 2002, p. 25.

[19] L. Stavsetra, K. E. Gregorich, J. Alstad, H. Breivik, K. Eberhardt, C. M. Folden III, T. N. Ginter, M. Johansson, U. W. Kirbach, D. M. Lee, M. Mendel, L. A. Omtvedt, J. B. Patin, G. Skarnemark, R. Sudowe, P. A. Wilk, P. M. Zielinski, H. Nitsche, D. C. Hoffman, and J. P. Omtvedt, Nucl. Instrum. Meth. A **543**, 509 (2005).

[20] L. Stavsetra, E. A. Hult, and J. P. Omtvedt, Nucl. Instrum. Meth. A **551**, 323 (2005).

[21] J. P. Omtvedt, J. Alstad, T. Bjørnstad, C. E. Düllmann, K. E. Gregorich, D. C. Hoffman, H. Nitsche, K. Opel, D. Polakova, F. Samadani, F. Schulz, G. Skarnemark, L. Stavsetra, R. Sudowe, and L. Zheng, Eur. Phys. J. D **45**, 91 (2007).

[22] Y. Nagame, M. Asai, H. Haba, S. Goto, K. Tsukada, I. Nishinaka, K. Nishio, S. Ichikawa, A. Toyoshima, K. Akiyama, H. Nakahara, M. Sakama, M. Schädel, J. V. Kratz, H. W. Gäggeler, and A. Türler, J. Nucl. Radiochem. Sci. **3**, 85 (2002).

[23] H. Haba, K. Tsukada, M. Asai, A. Toyoshima, K. Akiyama, I. Nishinaka, M. Hirata, T. Yaita, S. Ichikawa, Y. Nagame, K. Yasuda, Y. Miyamoto, T. Kaneko, S. Goto, S. Ono, T. Hirai, H. Kudo, M. Shigekawa, A. Shinohara, Y. Oura, H. Nakahara, K. Sueki, H. Kikunaga, N. Kinoshita, N. Tsuruga, A. Yokoyama, M. Sakama, S. Enomoto, M. Schädel, W. Brüchle, and J. V. Kratz, J. Am. Chem. Soc. **126**, 5219 (2004).

[24] H. Haba, K. Tsukada, M. Asai, S. Goto, A. Toyoshima, I. Nishinaka, K. Akiyama, M. Hirata, S. Ichikawa, Y. Nagame, Y. Shoji, M. Shigekawa, T. Koike, M. Iwasaki, A. Shinohara, T. Kaneko, T. Maruyama, S. Ono, H. Kudo, Y. Oura, K. Sueki, H. Nakahara, M. Sakama, A. Yokoyama, J. V. Kratz, M. Schädel, and W. Brüchle, J. Nucl. Radiochem. Sci. **3**, 143 (2002).

[25] A. Toyoshima, H. Haba, K. Tsukada, M. Asai, K. Akiyama, S. Goto, Y. Ishii, I. Nishinaka, T. K. Sato, Y. Nagame, W. Sato, Y. Tani, H. Hasegawa, K. Matsuo, D. Saika, Y. Kitamoto, A. Shinohara, M. Ito, J. Saito, H. Kudo, A. Yokoyama, M. Sakama, K. Sueki, Y. Oura, H. Nakahara, M. Schädel, W. Brüchle, and J. V. Kratz, Radiochim. Acta **96**, 125 (2008).

[26] Z. J. Li, A. Toyoshima, M. Asai, K. Tsukada, T. K. Sato, N. Sato, T. Kikuchi, Y. Nagame, M. Schädel, V. Pershina, X. H. Liang, Y. Kasamatsu, Y. Komori, K. Ooe, A. Shinohara, S. Goto, H. Murayama, M. Murakami, H. Kudo, H. Haba, Y. Takeda, M. Nishikawa, A. Yokoyama, S. Ikarashi, K. Sueki. K. Akiyama, and J. V Kratz, Radiochim. Acta **100**, 157 (2012).

[27] K. Tsukada, H. Haba, M. Asai, A. Toyoshima, K. Akiyama, Y. Kasamatsu, I. Nishinaka, S. Ichikawa, K. Yasuda, Y. Miyamoto, K. Hashimoto, Y. Nagame, S. Goto, H. Kudo, W. Sato, A. Shinohara, Y. Oura, K. Sueki, H. Kikunaga, N. Kinoshita, A. Yokoyama, M. Schädel, W. Brüchle, and J. V. Kratz, Radiochim. Acta **97**, 83 (2009).

[28] Y. Kasamatsu, A. Toyoshima, M. Asai, K. Tsukada, Z. J. Li, Y. Ishii, H. Toume, T. K. Sato, T. Kikuchi, I. Nishinaka, Y. Nagame, H. Haba, H. Kikunaga, Y. Kudou, Y. Oura, K. Akiyama, W. Sato, K. Ooe, H. Fujisawa, A. Shinohara, S. Goto, T. Hasegawa, H. Kudo, T. Nanti, M. Araki, N. Kinoshita, A. Yokoyama, F. Fan, Z. Qin, C. E. Düllmann, M. Schädel, and J. V. Kratz, Chem. Lett. **38**, 1084 (2009).

[29] M. Schädel, W. Brüchle, B. Schausten, E. Schimpf, E. Jäger, G. Wirth, R. Günther, J. V. Kratz, W. Paulus, A. Seibet, P. Thörle, N. Trautmann, S. Zauner, D. Schumann, M. Andrassy, R. Misiak, K. E. Gregorich, D. C. Hoffman, D. M. Lee, D. E. R. Sylwester, Y. Nagame, and Y. Oura, Radiochim. Acta **77**, 149 (1997).

[30] M. Schädel, W. Brüchle, E. Jäger, B. Schausten, G. Wirth, W. Paulus, R. Günther, K. Eberhardt, J. V. Kratz, A. Seibet, P. Thörle, N. Trautmann, A. Waldek, S. Zauner, D. Schumann, U. Kirbach, B. Kubica, R. Misiak, Y. Nagame, and K. E. Gregorich, Radiochim. Acta **83**, 163 (1998).

[31] C. F. Baes, and R. E. Mesmer, *The Hydrolysis of Cations*, John Wiley, New York (1976).

[32] K. Ooe, Y. Tashiro, D. Saika, Y. Kitamoto, K. Matsuo, T. Takabe, T. Kuribayashi, N. Takahashi, T. Yoshimura, W. Sato, K. Takahisa, and A. Shinohara, J. Nucl. Radiochem. Sci. **8**, 59 (2007).

[33] W. J. McDowell and B. L. McDowell, *Liquid Scintillation Alpha Spectrometry*, CRC Press, Boca Raton, 1994.

[34] A. Ruden, T. E. Hoagland, R. Forx, P. L. Kerr, G. Montermann, and R. Schneider, 2007.

[35] Annuals of the ICRP/ICRP publication 21, 60 (1973).

[36] H. Haba, K. Tsukada, M. Asai, A. Toyoshima, Y. Ishii, H. Toume, T. Sato, I. Nishinaka, T. Ichikawa, S. Ichikawa, Y. Nagame, W. Sato, K. Matsuo, Y. Kitamoto, Y. Tashiro, A. Shinohara, J. Saito, M. Ito, T. Ikezawa, M. Sakamaki, S. Goto, H. Kudo, H. Kikunaga, M. Arai, S. Kamataki, A. Yokoyama, K. Akiyama, K. Sueki, Y. Oura, M. Schädel, W. Brüchle and J. V. Kratz, Radiochim. Acta **95**, 1 (2007).

[37] J. P. Faris, Anal. Chem. **32**, 520 (1960).

[38] R. Caletka and V. Krivan, J. Radioanal. Nucl. Chem **142**, 373 (1990).

[39] E. H. Huffman, R. L. Oswalt, L. A. Williams, J. Inorg. Nucl. Chem. **3**, 49 (1956).

[40] V. Persina, Radiochim. Acta **92**, 455, (2004).

[41] E. F. C. H. Rohwer and J. J. Cruywagen, J. South Afr. Chem. Inst. **19**, 11 (1966).

[42] T. Sato and K. Sato, Hydrometallurgy **37**, 253 (1995).

[43] K. A. Kraus, F. Nelson and G. E. Moore, J. Am. Chem. Soc **77**, 1972 (1955).

[44] A. Toyoshima, Ph. D. thesis: *Fluoride Complex Formation of Transactinide Element, Rutherfordium, $_{104}Rf$*, Department of Chemistry, Graduate School of Science, Osaka University, 2004.

Acknowledgements

Appendix A. Suppression of β-particle Events Using a Capillary Tube in Liquid Scintillation α Spectrometry

1. Introduction

A problem in α-particle detection by liquid scintillation is interference from β particles because β particles produce approximately ten times more photons per unit energy deposition in the liquid scintillator than α particles. Due to the larger value of the specific energy loss, α particles produce more ionized molecules which act as quenching agents than β particles (Birks, 1951); for example, events for 5-MeV α particles and 0.5-MeV β particles appear in almost the same region of the energy spectrum. Therefore, in some cases, α events are buried in a continuous β component in the energy spectrum in the presence of excess β activity.

To address this problem, we have focused on the difference between the ranges of α and β particles. The range of 5-MeV α particles in toluene is calculated to be approximately 40 μm, whereas that of 0.5- MeV electrons is calculated to be approximately 2 mm (Berger et al., 2005). If liquid scintillation counting is performed with a detection cell with an inner diameter (i.d.) of hundreds of micrometers, β particles will exit the cell before full-energy deposition, while α particles will stop within it. As a result, the amount of light emission caused by β particles will decrease, and it is expected that continuous β components overlapping with the α peak will be located at the lower-energy region in the energy spectrum. Two study groups of solid scintillation flow-cell detectors for α counting, namely a thin layer of solid scintillator (Wenzel et al., 1999) and CsI:Tl granules (Tan et al., 2000; Tan and DeVol, 2002),

reported the suppression effect of the geometrical cell dimension for β events. In contrast to these previous studies, our method is based on liquid scintillation counting, and thus, better energy resolution and higher detection efficiency of α particles would be available.

In this study, we demonstrate that the β component is located at the lower-energy region in the energy spectrum by using a capillary tube as a detection cell. Liquid scintillation counting of ^{241}Am and ^{152}Eu was performed with 200, 300, and 500 μm i.d. PFA tubes. Events generated by α and β particles were discriminated from each other by a two-dimensional analysis of energy versus fluorescence lifetime. The results from using the PFA tubes were compared with those using a standard cell of 8.35 mm i.d. with regard to the shape of the energy spectrum, energy resolution and detection efficiency of α particles, and count ratio of α events to β events (α/β count ratio) in the ^{241}Am energy region, which is an indication of α/β discrimination. Additionally, a simple Monte Carlo calculation was performed to explain the decrease of detection efficiency of α particles due to decreasing the i.d. of the detection cell.

2. Experimental

The nuclides ^{241}Am and ^{152}Eu were used as α and β source, respectively. The nuclide ^{241}Am emits 5.486-MeV α particles and 59.5-keV γ rays. The nuclide ^{152}Eu emits β particles of 1.475 MeV at the maximum energy and a wide energy range of γ rays (Firestone et al., 1996). Standard solutions of ^{241}Am and ^{152}Eu were obtained from Amersham plc. A liquid scintillation cocktail, Ultima Gold AB$^{®}$, was purchased from PerkinElmer, Inc. Glass tubes of φ10 mm (8.35 mm i.d.) × 75 mm length and PFA tubes

of 200 μm, 300 μm, and 500 μm i.d. with wall thicknesses of 100 μm were supplied from AS ONE Co. The glass tubes were used as standard cells in liquid scintillation measurement.

Stock solutions of ^{241}Am and ^{152}Eu were prepared by evaporating the ^{241}Am and ^{152}Eu standard solutions and then dissolving it in an aqueous HCl solution at pH 3. A sample solution for liquid scintillation counting was prepared by mixing the stock solutions of ^{241}Am and ^{152}Eu with the Ultima Gold AB$^®$. The ratio of stock solution to Ultima Gold AB$^®$ was 1:4 (v/v). Radioactive concentrations of ^{241}Am and ^{152}Eu in the sample solutions were 0.9 kBq mL^{-1} and 60 kBq mL^{-1}, respectively.

The sample solution was injected into the PFA tubes with 200, 300, and 500 μm i.d. and with lengths of 4 cm; both ends of the PFA tubes were sealed. Each PFA tube sample was bent into a U-shape and set in the bottom of the standard cell, filled with a silicone oil (Shin-Etsu Chemical Co., Ltd., KF-96-50CS). A reference sample was prepared by the following procedures. A 15 μL aliquot of the sample solution was pipetted into the standard cell, and then the total volume of the solution was adjusted to 1 mL by adding the mixture of an aqueous HCl solution at pH 3 and Ultima Gold AB$^®$ in a 1:4 ratio (v/v). The scintillation liquid levels of the PFA-tube sample and the standard-cell sample were adjusted to the same height to lessen the geometrical effect. A photograph of the samples of the standard cell and of the PFA tubes is given in Fig. 1. Three samples were prepared for each type of detection cell. These samples were measured with a PERALS$^®$ spectrometer (ORDELA, Inc., Model 8100AB-HV) (McDowell et al., 1994), which is equipped with PSD. Pulses from the PULSE HEIGHT output and the PULSE SHAPE output of the PERALS$^®$ spectrometer were connected to an analog-to-digital converter (AMETEK, Inc., ORTEC model 800). The

pulse-height (energy) and the pulse-shape (fluorescence lifetime) spectra were recorded as a two-dimensional plot of energy versus time with a resolution of 1024×1024 channels by using a Multiparameter System (FAST ComTec GmbH, MPA-3). Measurements were performed until 20000 α counts were accumulated.

3. Results and discussion

Fig. 2 (a)-(d) shows the two-dimensional plot of energy versus fluorescence lifetime measured with the standard cell and with the PFA tube of 500, 300, 200 μm i.d, respectively. In the measurement with the standard cell, the β component spreads over a wide energy range. On the other hand, in the measurement with the 500, 300, 200 μm i.d. PFA tube, the β component in high energy region decreases and the endpoint of the β spectrum is located at lower-energy region as the i.d. of the PFA tubes decrease. It is observed that the difference in fluorescence lifetime between α and β particles is approximately the same whether the detection cell is the PFA tubes or the standard cell; therefore, events from α and β particles are discriminated in the same manner that α and β events are separated from each other by fluorescence lifetime.

The energy spectra from the standard cell and the PFA tubes are given in Fig. 3 (a)-(d). The solid lines indicate the total energy spectra, including α and β components. The dashed and dashed-dotted lines indicate α and β components discriminated by the difference in fluorescence lifetime, respectively. These spectra are smoothed by taking a moving average over a width of five adjacent points. In the measurement using the standard cell, the energy peak of [241]Am is highly overlapped with the continuous β component. Note that the β component is gradually located at lower-energy region as

148

the i.d. of the PFA tubes decrease. This is because the amount of deposited energy by electrons in the scintillation solution becomes smaller as the i.d. of the PFA tubes decrease, except for electrons with a much shorter range than the i.d. of the PFA tubes. As a result, the energy peak of ^{241}Am is clearly recognizable even in the one-dimensional energy spectra from the 200, 300, and 500 μm i.d. PFA tubes. We have evaluated the effects of decreasing the i.d. of the detection cells on energy resolution and detection efficiency of α particles, as well as, the ratio of the counts of α events to β events (α/β count ratio) in the area of the ^{241}Am energy peak. The region of interest (ROI) of the ^{241}Am energy peaks has been defined as ±1.5 full width at half maximum (FWHM) around the center of the energy peak of the α component, which is shown with a gray band in Fig. 3. Net counts of the α events have been determined by subtracting counts in the baseline areas of the ROI. The counts of β events have also been determined in the same ROI. The obtained values for the FWHM, the detection efficiency of α particles, and the α/β count ratio are given in Table 1. The FWHM values are expressed as a percentage of the FWHM of the ^{241}Am peak to the ^{241}Am peak position from the zero-point channel (channel at 0-MeV α-particle energy). The zero-point channel was derived by measuring a sample which was prepared by extracting the nuclide ^{226}Ra into a toluene-based scintillation cocktail. The values of the detection efficiency obtained with PFA tubes are shown as "Relative efficiency", taking those obtained with the standard cell as 100. The "Relative efficiency" is almost the same as absolute value because the detection efficiency of α particles in the standard cell is almost 100%. For the α/β count ratio, both absolute and relative values (taking the values obtained with the standard cell as 1) are given. Table 1 shows the mean

values and standard errors obtained by performing a total of three trials for each configuration.

The FWHM values measured with the PFA tubes are larger than those obtained with the standard cell. The variance of FWHM values among 200, 300, and 500 μm i.d. of the PFA tubes is within 1 σ of the standard error. The degradation of the FWHM values relative to the standard cell is approximately 18%. In Fig. 3, the shoulder-like distortions are observed in the low-energy region of the [241]Am peak in measurements with PFA tubes. Although the reason for the distortion of the peak shape is unclear, it seems that the distortions which cause the degradation of the energy resolution increase as the i.d. of the PFA tubes decrease.

The detection efficiencies of α particles with the PFA tubes are 72% for 200 μm i.d., 84% for 300 μm i.d., and 92% for 500 μm i.d. It seems that the decreasing i.d. of the PFA tubes caused the decrease of the detection efficiencies, and at the same time, resulted in increasing continuous components in the low-energy region of the [241]Am energy peak (shown in the dashed lines in Fig. 3). This is because the proportion of α particles that stop at the wall of the PFA tubes without losing their full energy in the scintillation solution increases as the i.d. of the PFA tubes decrease. However, the decrease in the detection efficiency of α particles is much smaller than that of β particles. The α/β count ratio in Table 1 increases with decreasing i.d. of the PFA tubes. This is due to the decrease of the β event counts in the ROI of the [241]Am energy peak. The variation of the α/β count ratio indicates that α/β discrimination in the energy spectrum becomes better with decreasing i.d. of the PFA tubes.

In order to verify the detection efficiency of α particles, a simple Monte Carlo calculation was performed by taking into account the range of α particles from the

150

^{241}Am in the scintillation cocktail and the i.d. of the detection cell. A cylinder with a diameter r was assumed as a detection cell (r = 8350, 500, 300, 200 μm) and a distribution of the flight distances of α particles in the cell was calculated. The length of the cylinder is sufficiently larger than the diameter r. A cross-section of the cylinder (a circle with a diameter r) is a source plane and 10^6 particles with a range R are randomly emitted from there. If the endpoint of the α particles with the range R is within the cell, the flight distance is equal to R. Otherwise, the flight distance is a distance between the emitted point on the source plane and the endpoint on the wall of the cylinder. The range R of 5.486-MeV α particles in the scintillation solution was calculated to be 43 μm.

Next, each bin of the flight distance was converted to deposited energy of α particles within the cell by multiplying 5.486 MeV/43 μm by the flight distance obtained by the Monte Carlo calculation described above, and then assuming a Gaussian distribution using the FWHM value obtained from the corresponding experiment. The energy of α particles was assumed to be proportional to the flight distance. In addition, energy loss per unit length of α particles in the scintillation solution was assumed to be constant. The ROI is set and subsequently the net counts are determined in a fashion similarly to that used to determine the experimentally-obtained energy peak of ^{241}Am. The calculated detection efficiencies are also shown in Table 1. The calculated efficiencies are in good agreement with experimental results. The decrease of detection efficiency with decreasing i.d. of the PFA tubes could be explained to be due to the effects of increasing the proportion of α particles which stop at the wall of the PFA tubes.

4. Conclusion

This work presents a method to decrease photons produced by β particles by using a capillary tube with an i.d. of hundreds of micrometers as a detection cell in liquid scintillation α spectrometry. The capillary tube allows β particles to exit the tube without depositing their full energy in the scintillation solution, while retaining α particles within the tube. Liquid scintillation counting of ^{241}Am and ^{152}Eu was performed with 200, 300, and 500 μm i.d. PFA tubes, and the results were compared with those in the standard cell. It was observed that the β spectrum was shifted to the lower-energy region by decreasing the i.d. of the PFA tube, and as a result, the α peak of ^{241}Am was separated from the β component in the energy spectrum. This method reduces the β component overlapping with the α peak while keeping a certain level of energy resolution and high detection efficiency of α particles, which enables the determination of α activity in the one-dimensional energy spectrum even in the presence of a large amount of β activity.

This method discriminates α events from β events by decreasing the amount of light emission derived from β particles, while the commonly used pulse shape discrimination (PSD) method utilizes the difference in scintillation lifetimes between the α and β particles. Therefore, this method can be used as a simple α/β discrimination technique for α spectrometry either in a commercial liquid scintillation counter, which is not equipped with PSD, or in combination with PSD for better signal-to-noise ratio. In the future, a detection cell which is composed of coiled or bundled capillary tube will be made for expansion of the detection volume.
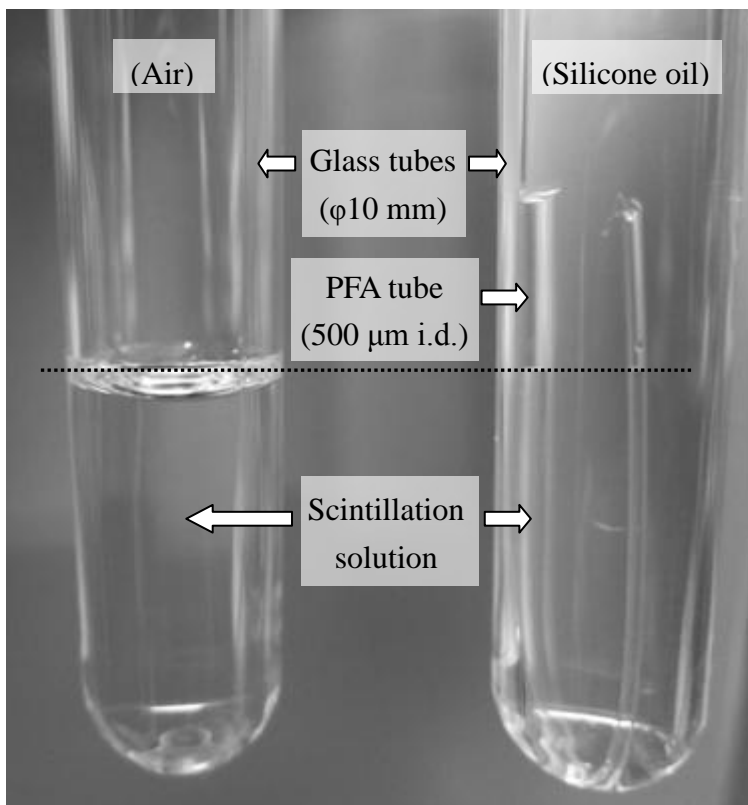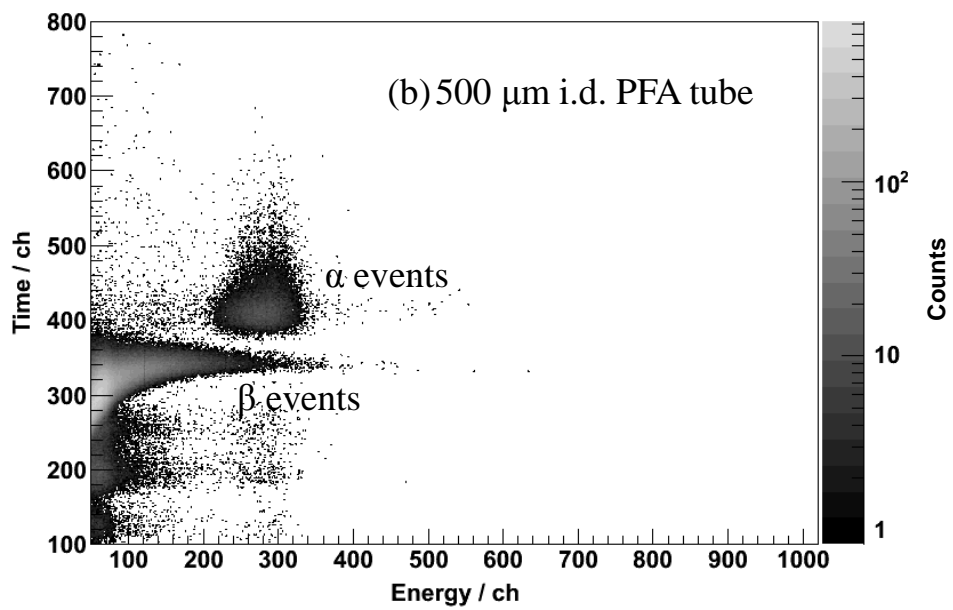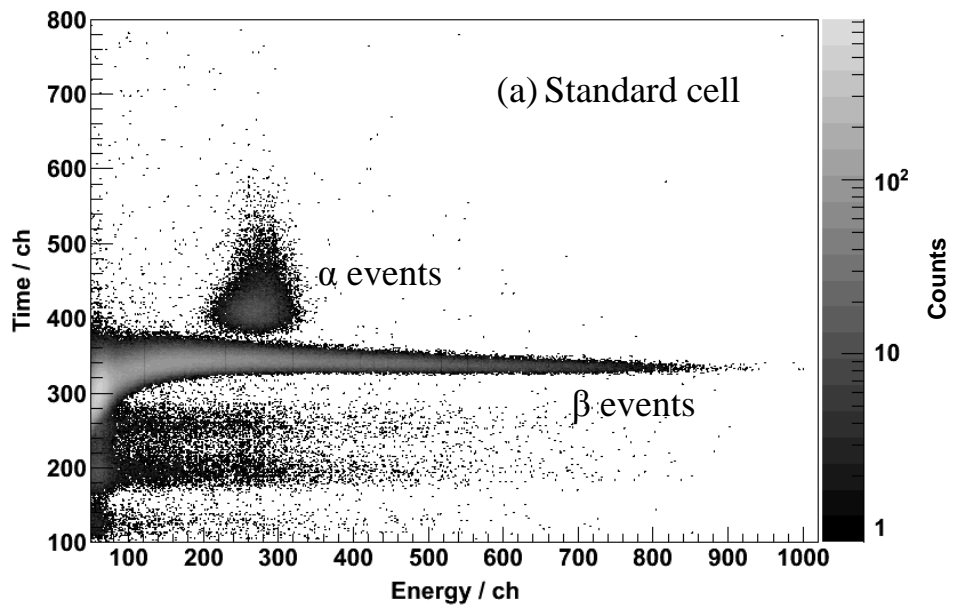
Fig. 1. A photograph of the samples of the standard cell (left) and of the PFA tube (right). The PFA tube, which contains scintillation solution, is bent into a U-shape and set in the bottom of the standard cell filled with silicon oil. Scintillation liquid levels (indicated by the dotted line) of both samples were adjusted to the same height to lessen the geometrical effect.
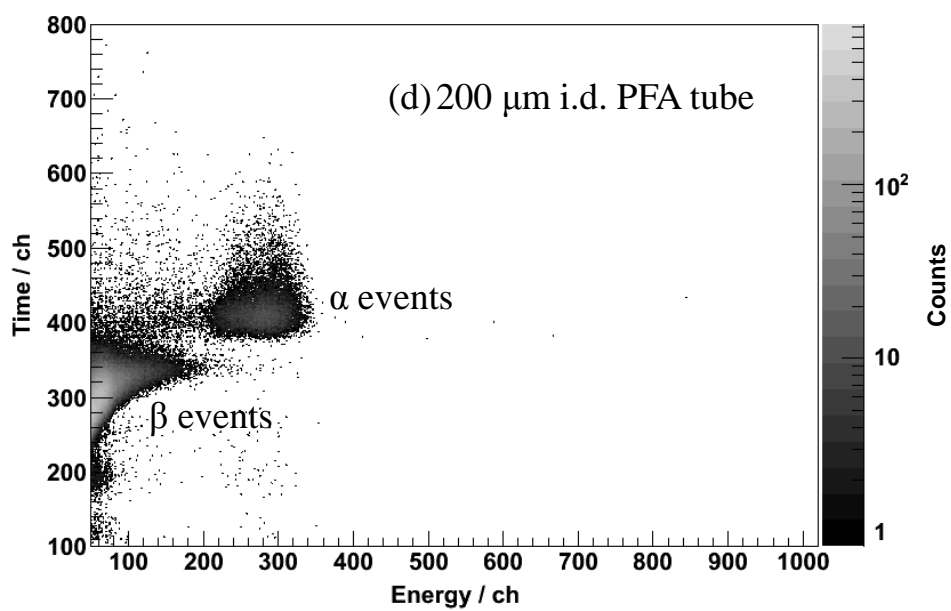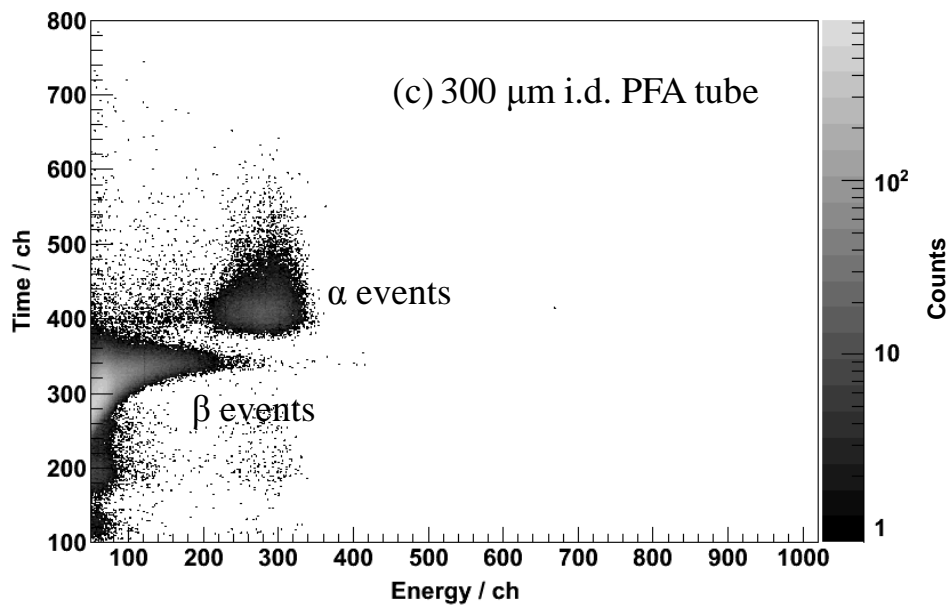
Fig. 2. Two-dimensional plot of energy versus fluorescence lifetime in (a) the standard cell of 8.35 mm i.d. and the PFA tube of (b) 500, (c) 300, (d) 200 μm i.d.
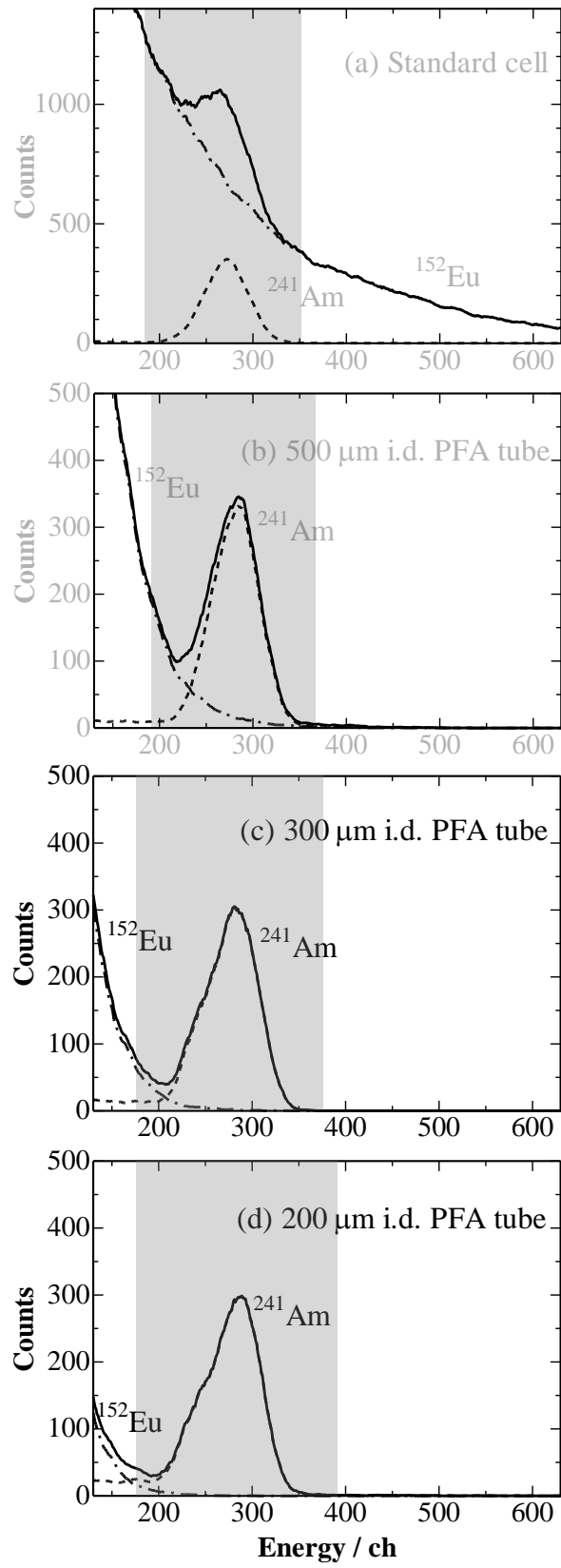
Fig. 3. Energy spectra in (a) the standard cell and the PFA tube of (b) 500, (c) 300, and (d) 200 μm i.d. The solid lines are the total energy spectra including α and β components. The dashed and dash-dotted lines are single α and β components discriminated by the difference of fluorescence lifetimes, respectively. These spectra are smoothed by taking a moving average over a width of five adjacent points. The ROI is shown with a gray band.

Table 1

FWHM, relative efficiency, calculated efficiency, and α/β count ratio in the ROI of the α spectrum of ^{241}Am in the standard cell and in the PFA tubes of 500, 300, and 200 μm i.d. The values within parentheses show relative values, taking those obtained with the standard cell as 1.

Detection cell	n	FWHM [%]			Relative efficiency [%]			Calculated efficiency [%]	α/β count ratio			
Standard cell	3	8.3	±	0.1	100			99	0.15	±	0.01	(1)
500 μm i.d. PFA tube	3	9.4	±	0.3	92	±	2	91	2.5	±	0.3	(16)
300 μm i.d. PFA tube	3	9.9	±	0.2	84	±	3	85	11.5	±	0.5	(74)
200 μm i.d. PFA tube	3	9.8	±	0.4	72	±	4	79	42	±	2	(271)

Appendix B. Pulse Shape Discrimination of α and SF Events from β Events with MPD-4 and A3200

1. Introduction

The capability to discriminate α/β and SF/β events on the basis of pulse shape was investigated using two types of pulse shape discrimination method. One is MPD-4 (Mesytec GmbH & Co. KG) which is a 4-channel neutron/gamma discriminator module [34] based on the zero-crossing method. The other is A3200 (Niki Glass Co., Ltd) which is a 16-channel VME-QDC module and it is applicable to pulse shape discrimination by digital charge comparison method.

2. Experimental

The isotope ^{252}Cf was used as an α and SF source. A sample for liquid scintillation counting was prepared by mixing 200 μL of stock solution of Cf (which contains 6% ^{249}Cf, 58% ^{250}Cf, and 36% ^{252}Cf in activity) dissolved in 5×10^{-3} M HF/0.1 M HNO$_3$ solution with 4 mL of the Ultima Gold AB$^{®}$. The sample was transferred to a glass cell and measured with our self-made liquid scintillation detector for the on-line chemistry experiments of Sg (see chapter 2). The detector consists of a photomultiplier tube R331-05 (Hamamatsu Photonics K.K.) and the glass cell set in a reflector. A silicone oil (Shin-Etsu Chemical Co., Ltd., KF-96-50CS) is filled between the cell and the photomultiplier tube as an optical coupling. The cell has a cylindrical shape of 28 mm in diameter and 19 mm in height.

The block diagram of the electronics for pulse shape discrimination using MPD-4 is shown in Fig. 2. The voltage of the photomultiplier tube was +1300 V. The anode signal of the photomultiplier tube was deliverd to the input of MPD-4. Both the amplitude (energy) and the time-to-amplitude converter (TAC) outputs of MPD-4 were digitized with A3100 (Niki Glass Co., Ltd) which is a 16-channel VME-ADC module. A proper condition for discrimination of α and SF events from β events was examined by varying gain value of the amplitude and walk value. Conversion gains of the A3100 for the energy and the TAC signal outputs were both 8192 ch.

The block diagram of the electronics for pulse shape discrimination using A3200 is shown in Fig. 3. The voltage of the photomultiplier tube was +1300 V. The anode signal was amplified by a variable-gain fast amp (CAEN, N978) and then divided into three identical signals using a FAN IN/OUT (Hoshin Electronics Co., Ltd., N007). Two of these signals were given different delays and were then sent to A3200 QDC modules to be recorded as "total charge in pulse" and "charge in tail of pulse", respectively. The third signal passed through a constant fraction discriminator (ORTEC, Model 473A) and a quad gate/delay generator (Phillips Scientific, Model 794) to provide the gate signal with the A3200. The relative timing of these signals at the inputs of the A3200 are shown in the lower part of Fig. 3. Width of the gate signal, which is the charge integration interval, was 100 ns. Measurements were performed by varying the time difference between the tail pulse and the total pulse from 6 to 26 ns. Conversion gains of the A3200 for the tolal charge in pulse and the charge in tail of pulse were both 8192 ch.

3. Results and discussion

Two-dimensional plot of TAC (y-axis) versus energy (x-axis) in the measurement with MPD-4 is presented in Fig. 4 (a) and (b). Fig. 4 (a) is a whole spectrum which contains both α and SF events, and (b) is an extended figure of α-event region. It is very similar to the two-dimensional plots presented in Ref. [10] which is obtained in the measurement of ^{252}Cf using the extractive scintillator. It was found that α and SF events were well discriminated from β events even with the emulsier scintillator which contains a dilute nitric acid solution.

Two-dimensional plot of charge in tail of pulse (y-axis) versus total charge in pulse (x-axis) in the measurement with A3200 is presented in Fig. 5 (a) and (b). Fig. 5 (a) is a whole spectrum which contains both α and SF events, and (b) is an extended figure of α-event region. Through the investigated time difference between the tail pulse and the total pulse of 6 to 26 ns, it was found that α and SF events were well discriminated from β events as with MPD-4.

In measurement with MPD-4, the degree of discrimination of α events from β events is the same as that of SF events from β events. In measurement with A3200, the better pulse shape discrimination is obtained with increasing values of the integration charge of the total pulse. Thus SF events are more separated from β events than α events from β events. In both measurements with MPD-4 and A3200, SF events are observed in the wide energy region of the two-dimensional plots. In addition, pulse shape characteristics of fission fragments seem to be similar to those of α particles. This is probably because that scintillation light produced by fission fragments would be more quenched than that produced by α particles due to higher value of the specific energy loss of fission

fragments, though greater specific energy loss would generate more excited triplet states which form a slow component of the scintillation light, as described in Ref. [8].

Count rate of α and SF events obtained in measurements with the MPD-4 was 36.5 ± 0.1 cps and 0.43 ± 0.01 cps, respectively. That obtained with the A3200 was 36.2 ± 0.1 cps and 0.42 ± 0.01 cps, respectively. Since the isotope ratio of ^{252}Cf is 36%, a disintegration ratio of α/SF of ^{252}Cf is 30.7 ± 0.3 for MPD-4 and 30.8 ± 0.7 for A3200, respectively. These values are consistent with the value of 31.0 ± 0.5 reported by Horrocks [8] and branching ratio of ^{252}Cf for α/SF [12] which corresponds to 31.3.

4. Conclusion

We have performed liquid scintillation measurement of ^{252}Cf using two types of electronics. One is MPD-4 based on the zero-crossing method and the other is A3200 based on the digital charge comparison method. In both measurements with MPD-4 and A3200, it has been shown that α and SF events are clearly separated from β events and that pulse shape characteristics of fission fragments are similar to those of α particles. Especially in case of using MPD-4, arrangement of the electronic modules for pulse shape discrimination is more simple compared to that in case of using A3200 or pulse-shape and timing single-channel analyzer (ORTEC model 552) which is shown in Fig. 2-5 in chapter 2.
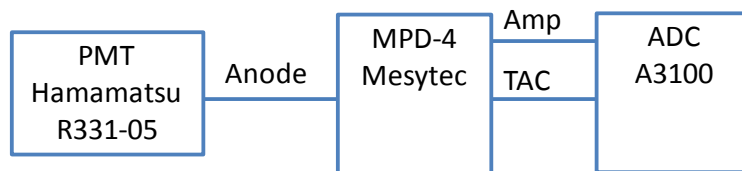
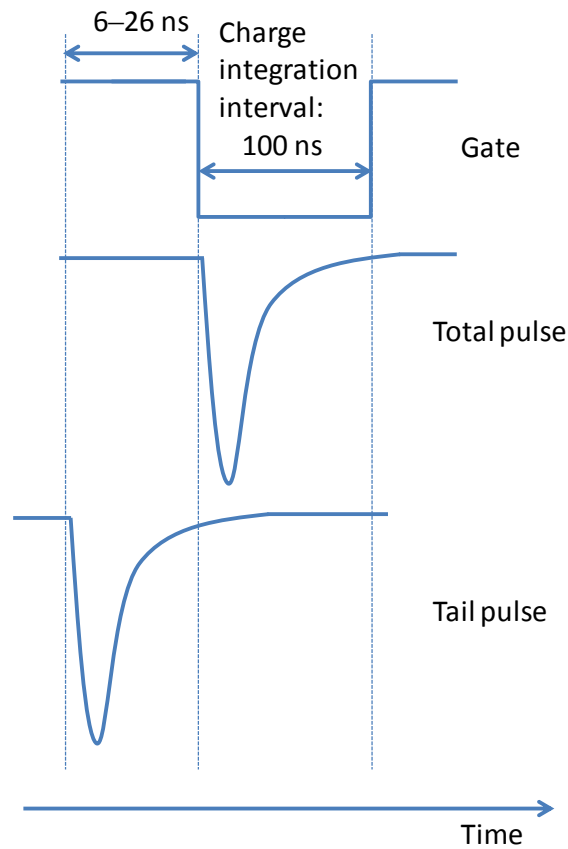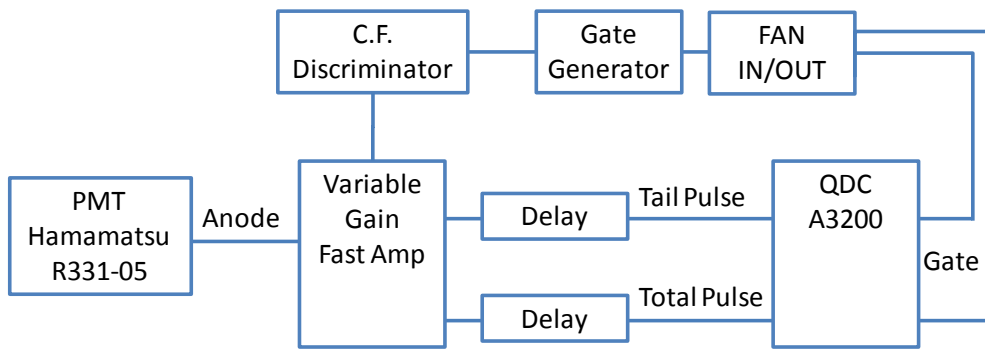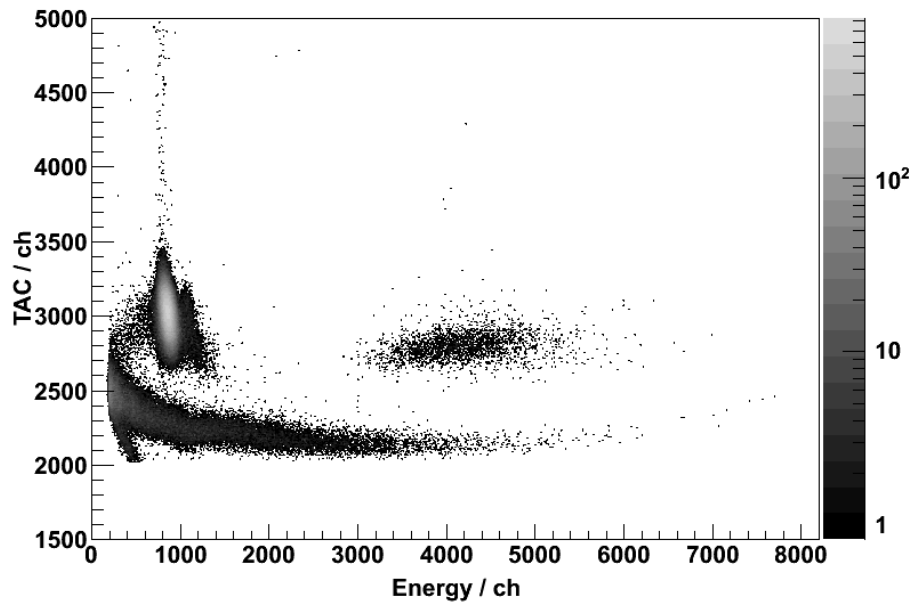Fig. 2. The block diagram of electronics for pulse shape discrimination by the zero-crossing method using MPD-4.

Fig. 3. The block diagram of electronics for pulse shape discrimination by the digital charge comparison method using A3200. The lower part indicates relative arrival timing of the signals at the inputs of A3200.
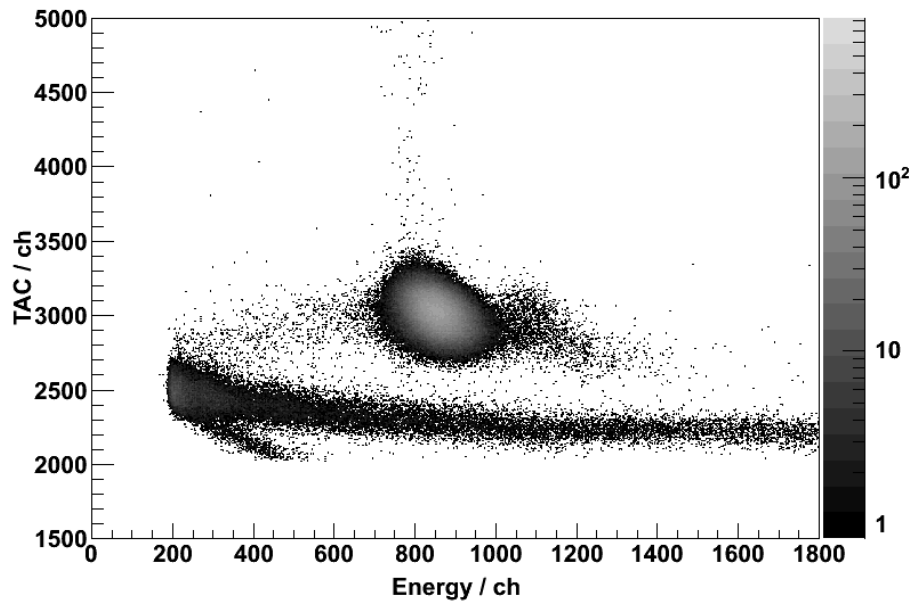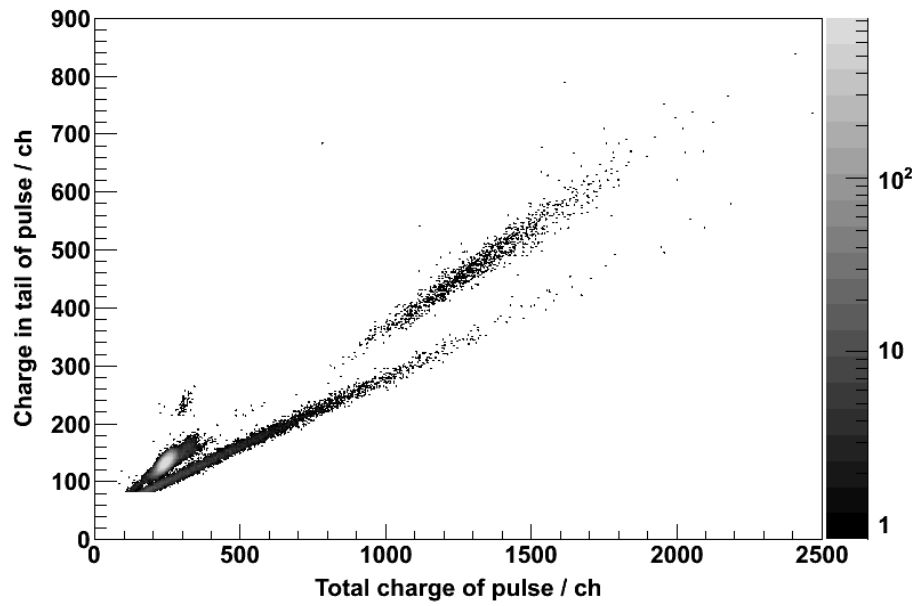
(a)

(b)

Fig. 4. Two-dimensional spectrum of energy versus TAC measured with MPD-4. Gain value of the amplitude was 0 and walk value was 70. (a) shows both α and SF events. (b) is an extended figure of α events.
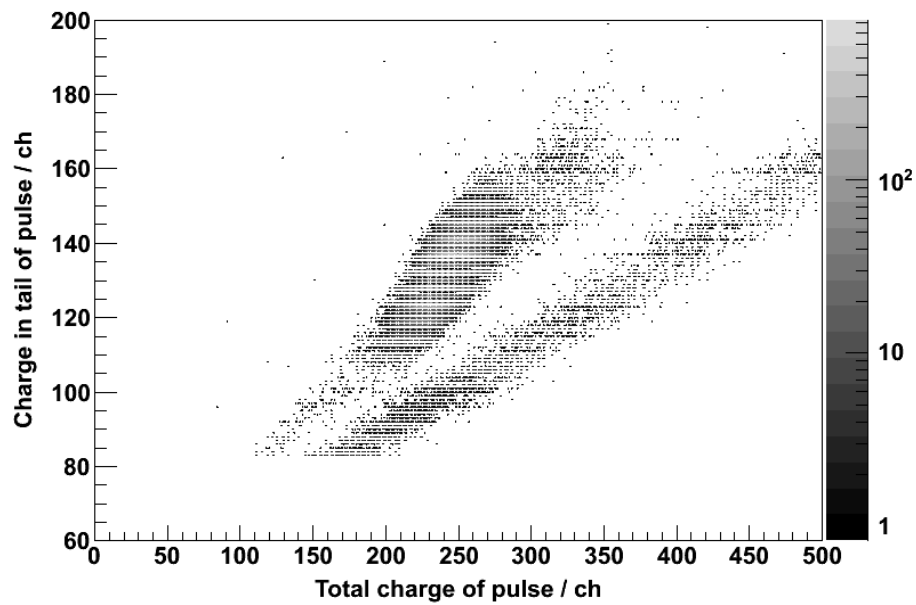
(a)

(b)

Fig. 5. Two-dimensional spectrum of total charge versus charge in tail of pulse in measurement with the QDC system. The time difference between the tail pulse and the total pulse was 20 ns. (a) shows both α and SF events. (b) is an extended figure of α events.

166

List of Publications

1. **Suppression of β-particle events using a capillary tube in liquid scintillation α spectrometry**

   Y. Komori, H. Kikunaga, T. Yoshimura, A. Shinohara

   Appl. Radiat. Isot. **72**, 195 (2013).

2. **Production of ^{265}Sg in the ^{248}Cm(^{22}Ne,5n)^{265}Sg reaction and decay properties of two isomeric states in ^{265}Sg**

   H. Haba, D. Kaji, Y. Kudou, K. Morimoto, K. Morita, K. Ozeki, R. Sakai, T. Sumita, A. Yoneda, Y. Kasamatsu, Y. Komori, A. Shinohara, H. Kikunaga, H. Kudo, K. Nishio, K, Ooe, N. Sato, K. Tsukada

   Phys. Rev. C **85**, 024611 (2012).

3. **Sulfate complexation of element 104, Rf, in H_2SO_4/HNO_3 mixed solution**

   Z. J. Li, A. Toyoshima, M. Asai, K. Tsukada, T. K. Sato, N. Sato, T. Kikuchi, Y. Nagame, M. Scädel, V. Pershina, X. H. Liang, Y. Kasamatsu, Y. Komori, K. Ooe, A. Shinohara, S. Goto, H. Murayama, M. Murakami, H. Kudo, H. Haba, T. Takeda, M. Nishikawa, A. Yokoyama, S. Ikarashi, K. Sueki, K. Akiyama, J. V. Kratz

   Radiochim. Acta **100**, 157 (2012).

4. **Production and decay properties of the 1.9-s isomeric state in ^{261}Rf**

   H. Haba, D. Kaji, H. Kikunaga, Y. Kudou, K. Morimoto, K. Morita, K. Ozeki, T. Sumita, A. Yoneda, Y. Kasamatsu, Y. Komori, K, Ooe, A. Shinohara

Phys. Rev. C **83**, 034602 (2011).

5. **Extraction behavior of carrier-free and macro amounts of molybdenum and tungsten from HCl solution**

   K. Ooe, W. Yahagi, <u>Y. Komori</u>, H. Fujisawa, R. Takayama, H. Kikunaga, T. Yoshimura, N. Takahashi, H. Haba, Y. Kudou, Y. Ezaki, A. Shinohara

   Proc. Radiochim. Acta **1**, 127 (2011).

6. **Solvent Extraction of Trivalent Actinides with Di(2-ethylhexyl)phosphoric Acid**

   R. Takayama, K.Ooe, W. Yahagi, H. Fujisawa, <u>Y. Komori</u>, H. Kikunaga, T. Yoshimura, N. Takahashi, K. Takahisa, H.Haba, Y. Kudou, Y. Ezaki, A. Toyoshima, M.Asai, Y. Nagame, T. Saito, T. Mitsugashira and A. Shinohara

   Proc. Radiochim. Acta **1**, 157 (2011).

7. **Superheavy Element Nuclear Chemistry at RIKEN**

   H. Haba, D. Kaji, Y. Kasamatsu, H. Kikunaga, <u>Y. Komori</u>, Y. Kudou, K. Morimoto, K. Morita, K. Ooe, K. Ozeki, N. Sato, A. Shinohara, A. Toyoshima, A. Yokoyama, A. Yoneda, and T. Yoshimura

   AIP Conf. Proc. **1235**, 356 (2010).

8. **RIKEN Gas-filled Recoil Ion Separator (GARIS) as a Promising Interface for Superheavy Element Chemistry—Production of Element 104, ^{261}Rf, Using the GARIS/Gas-jet System—**

   H. Haba, D. Kaji, <u>Y. Komori</u>, Y. Kudou, K. Morimoto, K. Morita, K. Ooe, K. Ozeki,

N. Sato, A. Shinohara, and A. Yoneda

Chem. Lett. **38**, 426 (2009).

9. **Decay Properties of ^{266}Bh and ^{262}Db Produced in the ^{248}Cm + ^{23}Na Reaction**

K. Morita, K. Morimoto, D. Kaji, H. Haba, K. Ozeki, Y. Kudou, N. Sato, T. Sumita,

A. Yoneda, T. Ichikawa, Y. Fujimori, S. Goto, E Ideguchi, Y. Kasamatsu, K. Katori,

Y. Komori, H. Koura, H. Kudo, K. Ooe, A. Ozawa, F. Tokanai, K. Tsukada, T.

Yamaguchi, and A. Yoshida

J. Phys. Soc. Jpn. **78**, 064201 (2009).